Theses and Dissertations

2015

Iridium – Bismuth Carbonyl Cluster Complexes: New Directions for Chemistry and Selective Oxidation Catalysis

Gaya R. Elpitiya
University of South Carolina

IRIDIUM – BISMUTH CARBONYL CLUSTER COMPLEXES: NEW DIRECTIONS FOR CHEMISTRY
AND SELECTIVE OXIDATION CATALYSIS

by

Gaya R Elpitiya

Bachelor of Science
University of Colombo, 2009

_____

Submitted in Partial Fulfillment of the Requirements

For the Degree of Doctor of Philosophy in

Chemistry

College of Arts and Sciences

University of South Carolina

2015

Accepted by:

Richard D. Adams, Major Professor

Daniel L. Reger, Committee Member

Sheryl L. Wiskur, Committee Member

Oleg Alexeev, Committee Member

Lacy Ford, Senior Vice Provost and Dean of Graduate Studies

ACKNOWLEDGEMENTS

A PhD is a struggle, a challenge and a bright light at the end of the tunnel. The past five years had lots of ups and downs which I didn't take an elevator to climb up where I am now. I had to take stairs and each time I fell, I got back on my feet with even more strength thanks to so many nice and kind people around me. So this is the moment to be grateful to all the awesome people around me because I wouldn't have accomplished any of these without any of you.

First and foremost I would like to thank Professor Richard D Adams, my advisor for being such a wonderful mentor. Your enormous passion and knowledge about chemistry together with tremendous mentoring skills helped me grow into an Inorganic-Organometallic synthetic and a structural chemist after five challenging years. I didn't just learn chemistry from you, I learned about career and about life which helped me to shape up my life and grow up as to what I am now. I'm more than glad that I had you as my PhD mentor and would like to make this an opportunity to express my heartfelt thanks to you for being such a great advisor, and an extremely supportive figure who always pushed me towards success.

My heartfelt gratitude goes to the members of my research committee; Professors Daniel Reger, Sheryl Wiskur and Oleg Alexeev. Your suggestions and comments always helped me to succeed in my research. Thank you very much for spending your valuable time on my comprehensive exams, seminars and dissertation defense. I would like to

ii

thank Dr. Perry Pellechia, Dr. William Cotham and Dr. Mike Walla for assisting me with NMR and MS measurements. Thank you very much Dr. Mark Smith for helping me with difficult to solve crystal structures and always filling me with your enormous knowledge on crystallography. I would like to thank Dr. Robert Raja and Dr.Mathew Potter from University of Southampton, UK for being great collaborators helping me with the catalyst testings. Without your support, I wouldn't have completed any of my catalysis work which formed much of my second chapter.

I would like to take a moment to thank my past lab members, Dr. Qiang Zhang, Dr. Yuwei Kan, Dr. Mingwei Chen, Dr. Onn Wong, and also to my current lab members Joseph Kiprotich, Jonathan Tedder, Zhongwen Luo, Poonam Dhull and Morteza Maleki. Joseph, Jonathan, Zhongwen, Poonam and Morteza thanks a lot for all the good time we spent together and good luck with your PhD. Special thanks goes to Dr. Qiang Zhang and Dr.Yuwei Kan for being great friends and always supportive in every possible way. Dr. Qiang Zhang, I would like to call you a second mentor in my career because I learned so much from you. Thank you so much for the delicious Chinese food you both cooked for me and my husband and for being good friends. Dr. Yuwei Kan, thank you so much for your priceless friendship, for all the motivation you keep giving me even you are not here in Columbia right now.

My deepest appreciation goes to my beloved parents for your unconditional love and support. I can't thank you enough for the blessings, motivation and courage you have given me throughout the years and continuously giving me. I don't think I have enough words to express what I feel about all you have done for me, my dear mother and father. All I know is, you wanted to see your only daughter growing in to a successful figure, a

person valuable to the society and I think I made your dream come true. PhD was OUR dream , and I reached it because of you mother and father, and I love both of you endlessly for making me into a strong person with lots of skills. I owe you both forever for holding up this ladder so securely helping me climb up and up, till I touch the sky.

Last, but not least, I need to express my greatest thanks to my ever loving husband Prasanna Malinda Witharana who gave up a successful career in Sri Lanka and accompanied me to US to make my dream come true and also to my adorable little daughter Aurora Ariana Witharana for making me a mom. Every moment I have spent with both of you have being awesome and I wouldn't have accomplished any of these without both of you. Prasanna, you are a great husband and a great father and you played the role of a mother as well taking care of our little Aurora helping me focus on my research. You have done so many things for me which I could write an entire book about you. With limited space here I would like to say Thank you very much my dear husband, for being my shadow, for holding my hands throughout this difficult journey and for not letting me down. You are the best and I love you till I die. I love you my dear daughter for making our lives complete and happy. You bring priceless joy to my life each day and you are the most precious gift I have ever got in my life. You may not know right now, but this is for you to know one day when you grow up and read your mother's thesis, that you played a huge role unknowingly to make me into a strong and a motivated person. Thank you all for everything you have done and continuously doing for me.

ABSTRACT

CHAPTER 2

The reaction of $Ir_3(CO)_9(\mu_3\text{-}Bi)$, **2.1**, with $BiPh_3$ has yielded a iridium−bismuth cluster complex $Ir_5(CO)_{10}(\mu_3\text{-}Bi)_2(\mu_4\text{-}Bi)$, **2.2**. The first examples of bimetallic iridium−bismuth nanoparticles have been subsequently synthesized from **2.1** and **2.2**, and these have been securely anchored onto the inner walls of mesoporous silica. These isolated, bimetallic iridium−bismuth nanoparticles display a superior catalytic performance, when compared to their analogous monometallic counterparts and equivalent physical mixtures, in the C−H activation of 3-picoline to yield niacin.

CHAPTER 3

The reaction of $Ir_3(CO)_9(\mu_3\text{-}Bi)$ with Ph_3GeH yielded the compound $Ir_3(CO)_6(GePh_3)_3(\mu_3\text{-}Bi)(\mu\text{-}H)_3$ **3.1** When **3.1** was heated to reflux in hexane, it was transformed into the compound $Ir_3(CO)_6(\mu\text{-}GePh_2)_3(\mu_3\text{-}Bi)$ **3.2**, which contains three bridging $GePh_2$ ligands by loss of 3 equiv of benzene. The reaction of $Ir_3(CO)_9(\mu_3\text{-}Bi)$ with Ph_3SnH yielded the compounds $Ir_3(CO)_6(SnPh_3)_3(\mu_3\text{-}Bi)(\mu\text{-}H)_3$ **3.3** and $Ir_3(CO)_6\text{-}(\mu\text{-}SnPh_2)_3(\mu_3\text{-}Bi)$ **3.4**, respectively. Compounds **3.1**−**3.4** were characterized crystallographically. Compounds **3.1** and **3.3** each have three terminally coordinated EPh_3 (E = Ge, Sn) ligands in equatorial coordination sites, one on each of the iridium

atoms. In solution compounds **3.1** and **3.3** exist as two isomers. The major isomer has the structure found in the solid state. The two isomers interconvert rapidly on the NMR time scale by tripodal, trigonal-twist rearrangement mechanisms: for **3.1**, $\Delta H^{\ddagger} = 66.6$ kJ/mol and $\Delta S^{\ddagger} = 1.58$ J/(K mol), and for **3.3**, $\Delta H^{\ddagger} = 65.6$ kJ/mol and $\Delta S^{\ddagger} = -1.4$ J/(K mol). The molecular orbitals and UV−vis spectra of **3.2** were calculated and analyzed by ADF DFT computational treatments. The visible spectrum is dominated by transitions from the Ir−Bi bonding orbitals HOMO-3 and HOMO-4 to an Ir−Ir antibonding orbital, the LUMO, in the Ir3 core of the complex.

CHAPTER 4

$Ir_3(CO)_9(\mu_3\text{-Bi})$ was found to react with PhAu(NHC) by losing one CO ligand and then oxidatively adding the Au − C bond to the phenyl ligand of the PhAu(NHC) to one of the iridium atoms to yield the compound **4.2** that contains a σ-phenyl coordinated ligand and an Au(NHC) group bridging one of the Ir − Bi bonds of the cluster. Based on the structural analysis and the MO and QTAIM calculations, the Au − Bi interaction is substantial and is comparable in character to the Ir − Bi and Ir − Ir bonds in this cluster. We have shown previously that $Ir_3(CO)_9(\mu_3\text{-Bi})$ reacts with $HSnPh_3$ by adding three equivalents of $HSnPh_3$ to yield the compound $Ir_3(CO)_6(SnPh_3)_3(\mu_3\text{-Bi})(\mu\text{-H})_3$, (Figure 4.2).[5] Compound **4.2** will add only two equivalents of $HSnPh_3$ to yield **4.3**. It is possible that the bridging Au(NHC) group with the bulky NHC ligand inhibits a third addition of $HSnPh_3$ by producing a blocking effect proximate to the third Ir atom. Finally, we observed that water can facilitate the cleavage of phenyl groups from the $SnPh_3$ ligands in **4.3** presumably with the formation of some benzene and the formation of an OH

grouping bridging the two tin atoms to yield the compound **4.4**. The O-bridged linking of

tin and germanium ligands could lead to design and synthesis of interesting new chelating

ligands in polynuclear metal complexes in the future.

CHAPTER 5

Compound **5.1** readily loses CO upon heating and condenses to form the

hexairidium product **5.2**. Years ago, Adams et al. showed that bridging sulfido ligands

could facilitate condensation and self-condensation reactions of osmium and ruthenium

carbonyl cluster complexes to produce higher nuclearity complexes [16 − 19]. The lone pair

of electrons on the sulfido ligands clearly played a key role in the formation of new bonds

between the condensing species [17-19]. The bridging bismuth ligand in **5.1** formally

contains a lone pair of electrons and these electrons may also serve to facilitate the self-

condensation of **5.1** to form the hexairidium complex **5.2** even though no intermediates

were isolated that would confirm that such interactions did in fact occur in the course of

the formation of **5.2**. Because of its facile elimination of CO, it was easy to prepare the

PPh$_3$ derivatives **5.3** - **5.5** of **5.1** by reactions between **5.1** and PPh$_3$. Compound **5.3**

eliminated CO and PPh$_3$ to yield **5.6** , the PPh$_3$ derivative of **5.2** by a condensation

reaction, but **5.6** could be obtained in an even better yield by treatment of **5.2** with PPh$_3$.

Pyrolysis of **5.3** also yielded a pentairidum complex **5.8** having a square pyramidal

cluster of metal atoms in a very low yield by a combination of cluster and ligand

degradation and reassembly. Compound **5.8** has an interesting structure and ligands.

Unfortunately, we have not yet been able to synthesize compound **5.8** in a systematic

way. Pyrolysis of **5.4** did not yield any higher nuclearity metal compounds, but did yield

the complex **5.7**, an o-metallated PPh$_3$ derivative of **5.4** in a high yield. Complex **5.7** was also obtained in a low yield from the pyrolysis of **5.3**. The condensation of **5.1** with Ru$_3$(CO)$_{10}$(NCMe)$_2$ yielded compounds **5.9** and **5.10**, (Scheme 5.2) , the first examples of iridium-ruthenium carbonyl complexes containing bismuth ligands. We have not been able to establish the mechanisms of the formation of **5.9** and **5.10** in this work, but we suspect that the Bi ligand in **5.1** probably played a role in the condensation processes leading to these products.

CHAPTER 6

The synthesis and chemistry of heavy atom metallaheterocycles remained largely unexplored until Adams et al[1,2,3]. and Leong et al.[4,5] started synthesizing unusual new metallaheterocycles by linking heavy transition metal groupings with heavy atom bridging ligands, such as diphenylbismuth and diphenylantimony. A novel Iridium - Bismuth metallaheterocycle, **6.1** has been synthesized by the reaction of [HIr$_4$(CO)$_{11}$]$^-$ and Ph$_2$BiCl in methylene chloride solvent at 0°C for 10 mintues. The compound, **6.1** is formed by a simple salt elimination and a self dimerzation process while eliminating CO from the electron rich monomeric Ir$_4$(CO)$_{11}$(μ-BiPh$_2$)(μ-H) (62 valence electrons) to form [Ir$_4$(CO)$_{10}$(μ-BiPh$_2$)(μ-H)]$_2$ dimer.

TABLE OF CONTENTS

LIST OF TABLES

LIST OF FIGURES

LIST OF SCHEMES

CHAPTER 1

INTRODUCTION

Catalysis is a science and technology of influencing rates and thus selectivity of chemical reactions. It is the molecular process by which reactants are transformed into products under mild conditions without the catalyst itself being expended.[1,2] Use of catalysts in chemical reactions has been practiced for centuries and the use of transition metal clusters and main group metals in this context has attracted considerable attention among chemists for the last five decades. In this regard the synthesis and chemistry of transition metal clusters combined with main group elements has become an area of great interest.[3] There are three major purposes for combining a main group element with a transition metal core: (1) to polarize bonding within the cluster core, leading to different reaction chemistry; (2) to act as centre for stabilizing the cluster core towards the varying conditions of temperature and pressure needed in catalytic reactions; and (3) to participate in bifunctional chemical transformations. Transition metal carbonyl cluster chemistry which emerged about four decades ago is of enormous value in the rational design and synthesis of bi- and multi-metallic nano catalysts, and the introduction of certain main group metal atoms into these metal cluster complexes has been found to enhance the catalytic properties of the metal core resulting in higher conversions and improved selectivities in industrially important chemical reactions.[4–6] Furthermore,

capping CO ligands on these metal carbonyl clusters impose an added advantage of producing well isolated, well defined and spatially uniform active sites on the catalyst upon thermal removal of the CO ligands under vacuum, which is important in suppressing undesired side reactions resulting in improved selectivities.

1.1 Selective Oxidation catalysis

Selective oxidations are one of the widely discussed and extensively studied catalytic reactions in recent decades. It has not only attracted great interest in industrial research but has also influenced many areas of basic research. Selective oxidation provides promising pathways for the production of higher value chemicals or oxyfunctionalized chemicals such as methanol, acetic acid, acrylic acid and phenol etc. starting from cheaper and more abundant starting materials like light alkanes[2]. The global abundance of light alkanes, especially methane being a major component of shale and natural gas and the huge economic incentives for converting methane into expensive and highly desirable petrochemical feedstocks, has attracted a great deal of research to find new examples of selective oxidation catalysis.[7–9] Although selective oxidation appears to be a promising attempt and a viable approach to higher value chemicals, its applications are limited mostly to research laboratories due to few major governing factors to this process, which inhibits new processes from becoming commercial realities. A widely discussed and well-known factor is reflected by the other name for alkanes known as "paraffins" meaning not enough affinity. Alkanes are known for their relative unreactivity except for reactions like combustion which produce complete oxidations. Their chemical

2

inertness arises from their strong C-C and C-H bonds.[10] Another problem is the over oxidation of alkanes which give rise to undesired low value oxygenates such as carbon monoxides and carbon dioxides during the alkane oxidation process. Therefore addressing these two major problems, namely C-H bond activation and controlled or selective incorporation of oxygen into these activated C-H bonds are of paramount importance in utilizing selective oxidation as a viable alternative on the commercial scale. Solutions to these problems have become major targets for numerous fundamental researches these days. The work in this thesis is an attempt to address these two major problems through the careful selection of suitable metal atoms and the design and synthesis of a new class of compounds: Iridium-Bismuth carbonyl cluster complexes and modifying them by incorporating other catalytically important transition metals like gold and ruthenium and main group elements like tin and germanium which are also known to be valuable modifiers for heterogeneous catalysts, and then transforming these new bi- and multi-metallic cluster compounds into bi- and multi-metallic nanoparticles which could eventually serve as new catalysts for selective oxidation reactions.

1.2 Bismuth in Selective Oxidation catalysis

Transition metal clusters with Bi as a main group metal component are of particular interest due to the rich chemistry of bismuth in oxidation reactions, and also due to its low cost and high abundance.[11] Bismuth stands out from other heavy metal elements such as mercury, thallium and lead due to its relatively non toxic character.[12] Bismuth has been successfully used in mixed metal oxide catalyst systems, known as

3

bismuth molybdates for the large scale industrial production of acrolein and acrylonitrile by selective oxidation and ammoxidation (eq.1,2)[13–16].

$$\text{propylene} + O_2 \xrightarrow{\text{catalyst}} \text{acrolein} + H_2O \qquad \text{(eq.1)}$$

$$\text{propylene} + 3/2\, O_2 + NH_3 \xrightarrow{\text{catalyst}} \text{acrylonitrile} + 3\, H_2O \qquad \text{(eq.2)}$$
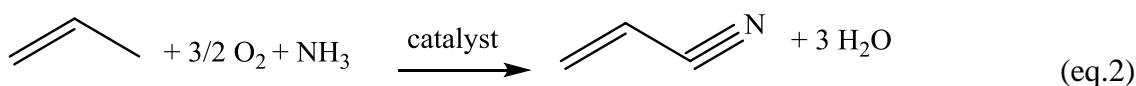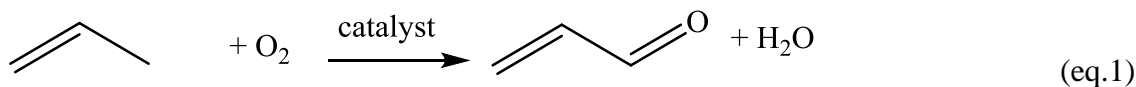
This process was first developed by the Standard Oil of Ohio company (SOHIO) in 1959-1962[16] and the selective oxidation and ammoxidation of propylene has been used to make acrolein and acrylonitrile ever since. The selective oxidation of propane has been widely studied in order to try to obtain acrolein from this lower cost feedstock. It has been found that Bi plays an important role as a cocatalyst by providing site isolation and by increasing the amounts of surface active oxygen during the catalytic cycle. It also promotes H abstraction and the activation of oxygen[17,18]. Adams et al. have used Bi as an oxophile in ReBi and FeBi bimetallic catalyst systems which were derived from ReBi and FeBi carbonyl cluster complexes, respectively. They have shown the catalytic properties of ReBi and FeBi nanoparticles for the selective conversion of 3-picoline to niacin and in the ammoxidation of propane to acrylonitrile, respectively.[4,19] The ability of bismuth (an oxophile) to interact favorably with the mesoporous silica support, through covalent - bond formation between the oxophilic metal and pendant silanol groups, renders this nanoparticle catalysts amenable for oxidation reactions[20].

4

1.3 Iridium as a C-H activating agent

The use of transition metals to activate unreactive C-H bonds goes back to 1970s when Shilov first discovered that certain platinum compounds could perform this conversion to make alkyl halides and acetates from alkanes.[21] C-H activation by iridium attracted great interest after Crabtree reported the first examples of dehydrogenation of cyclopentane by a soluble iridium complex in 1979.[22] Use of iridium as a C-H bond activating agent was exhibited again in 1982 by Bergman and W. A. G. Graham during a direct photochemical reaction of an iridium metal complex with alkanes to produce hydridoiridium alkyl complexes where an intermolecular C-H activation was observed (eq.3).[23,24]

(eq.3)
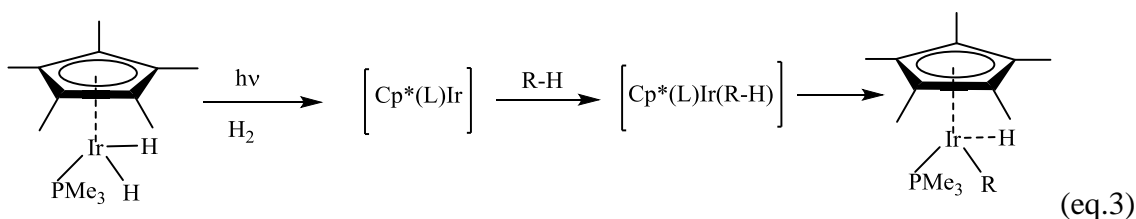
Recently Bergman et al. discovered a series of higher valent methyliridium(III) complexes that are efficient for C-H bond activation in saturated hydrocarbons (eq.4). [25]

(eq.4)
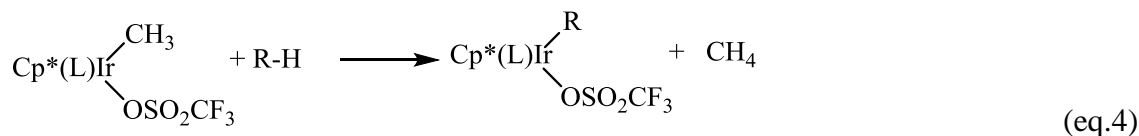
There are numerous other examples of iridium exhibiting high degrees of reactivity and selectivity toward C-H bond activations.[26–28] This area of research on C-H bond activation performed by iridium is further broadened by the new discoveries like iridium mediated catalytic alkane dehydrogenation, catalytic methane oxidation and

catalytic H/D exchange.[29] Although most iridium assisted catalysts are of a homogeneous type[30,31], it has been shown that iridium carbonyl cluster complexes can be precursors for highly active heterogeneous nanocluster catalysts for the hydrogenation of aromatics and olefins.[32,33]

Intrigued by the catalytic properties of iridium and bismuth as C-H activating agents and as oxophiles, respectively, we have created an intimate connection between the two metals at molecular level by synthesizing iridium-bismuth carbonyl cluster complexes to utilize their individual catalytic properties synergistically. Synthesis of iridium and bismuth carbonyl clusters is an opening for a new area in bimetallic transition metal - main group metal chemistry and this will open doors for the design of new bi- and multi-metallic catalysts which could perform new selective oxidation catalysis.

1.4 Synthesis of Transition metal-Bismuth carbonyl clusters

The first known transition metal - main group element clusters were synthesized in 1950s by Hieber and co-workers (eq.5)[34].

$$Fe(CO)_5 + 3\ KOH_{aq} \longrightarrow K^+[HFe(CO)_4] + K_2CO_3 + H_2O$$

Main group oxides or
Oxo complexes

Iron-main group metal
cluster anions

(eq.5)
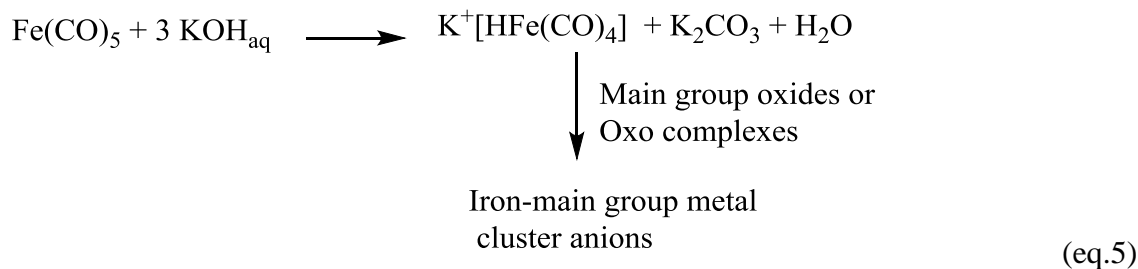
The chemistry of transition metal -main group elements grew slowly at first. In 1980s a major growth in the chemistry of transition metal clusters with heaviest metals of the main group such as bismuth was observed.

1.41 Chromium, Cobalt and Tungsten carbonyl clusters with Bismuth

Malisch et al. and N.C. Norman made chromium, cobalt and tungsten carbonyl clusters with bismuth and the synthetic strategies were based on simple salt elimination by reaction of the metal carbonyl anion with bismuth halides (eq.6).[35]

$$Na[CpM(CO)_3] + Me_2BiBr \longrightarrow [CpM(CO)_3]_2Bi\ Me + [CpM(CO)_3]_2Bi\ Me + BiMe_3$$
$$(M=Cr,Mo,W)$$

(eq.6)
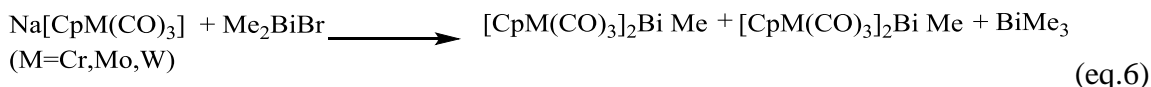
1.42 Rhenium and Manganese carbonyl clusters with Bismuth

Bismuth containing clusters of rhenium and manganese transition metals have been reported as well. The first ReBi compound known dates back to 1960s and it was prepared by reacting $Na[Re(CO)_5]$ and Ph_2BiCl (eq.7). It wasn't well characterized at the time, but later discoveries revealed that it has a structure analogous to the manganese compound $Mn(CO)_5BiPh_2$ which was synthesized in 1991.[36]

$$Na[M(CO)_5] + Ph_2BiCl \longrightarrow M(CO)_5BiPh_2$$
$$M= Re,Mn$$

(eq.7)
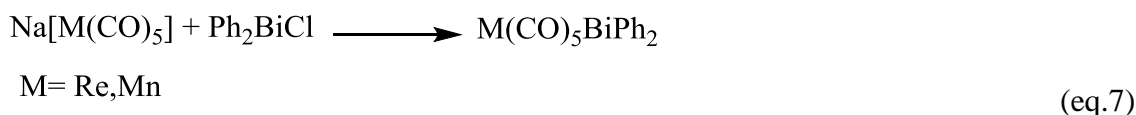
Recently, various other ReBi clusters were reported by Adams et al. by reacting $Re_2(CO)_8[\mu\text{-}\eta^2\text{-}C(H)=C(H)Bu^n](\mu\text{-}H)$ with Ph_3Bi in refluxing heptane (eq.8).[37] The products from this reaction, $Re_2(CO)_8(\mu\text{-}BiPh_2)_2$ and $Re_3(CO)_{12}(\mu\text{-}BiPh_2)_3$ were pyrolyzed in toluene and octane respectively and have given rise to three new products $Re_2(CO)_8(\mu\text{-}BiPh)_2$ (eq.9) and cis-$Re_4(CO)_{16}(\mu\text{-}BiPh_2)_2\text{-}(\mu_4\text{-}BiPhBiPh)$, trans-$Re_4(CO)_{16}(\mu\text{-}BiPh_2)_2(\mu_4\text{-}Bi\text{-}PhBiPh)$, respectively (eq.10).

$$+Ph_3Bi \quad 97\,°C \qquad \qquad \text{(eq.8)}$$

$$110\,°C \qquad \qquad \text{(eq.9)}$$

$$125\,°C \qquad \qquad \text{(eq.10)}$$
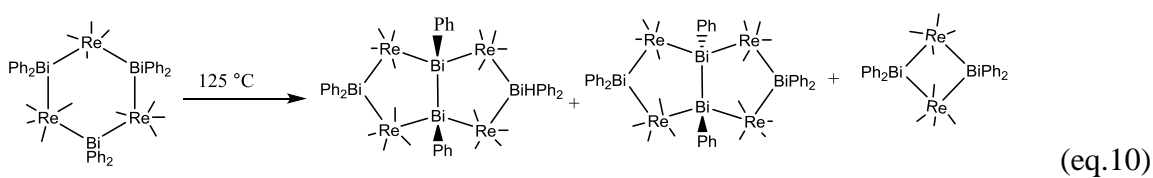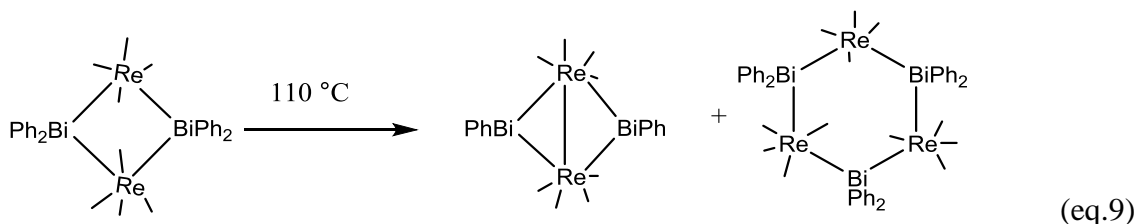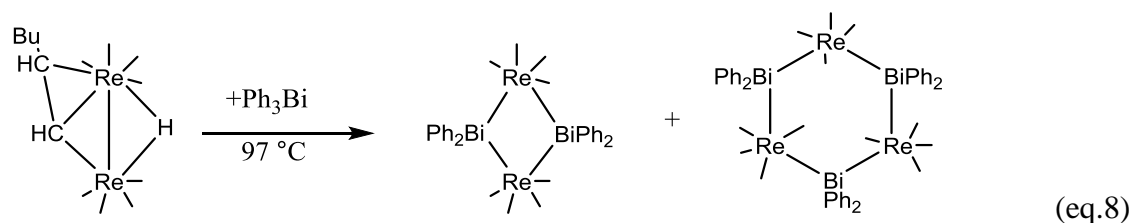
1.43 Iron, Ruthenium and Osmium carbonyl clusters with Bismuth

Whitmire et al. began developing transition metal-bismuth chemistry by re-examining Hieber's work and they were able to synthesize the first closo clusters of bismuth and a first row transition metal namely, $Bi_2Fe_3(CO)_9$ and $H_3BiFe_3(CO)_9$. These compounds were synthesized by the treatment of a methanolic solution of $Fe(CO)_5$/KOH with $NaBiO_3$[38,39]. When $Fe(CO)_5$ was treated with KOH in methanol a green solution was observed and Whitmire was able to isolate this green compound $[Bi\{Fe(CO)_4\}_4]^{3-}$ in 80% yield by adding a bulky cation, $[PPN]^+$ or $[Et_4N]^+$ into the green solution. The x-ray structure of the green compound showed that the highly charged anion is a regular tetrahedrally bonded Bi atom coordinated to four trigonal bipyramidal $Fe(CO)_4$ fragments. Another new FeBi cluster $[Bi_2Fe_4(CO)_{13}]^{2-}$ was synthesized in high yield by

8

reacting $Bi_2Fe_3(CO)_9$ with $[Fe(CO)_4]^{2-}$. It had a square pyramidal core made with $[Bi_2Fe_3(CO)_9]^{2-}$ fragment with the $Fe(CO)_4$ fragment attached to the lone pair of one of the Bi atoms (eq.11).

$$Bi_2Fe_3(CO)_9 + [Fe(CO)_4]^{2-} \longrightarrow [Bi_2Fe_4(CO)_{13}]^{2-} \qquad \text{(eq.11)}$$

A methanol solution of the mixture of $NaBiO_3$ and $Fe(CO)_5$ under refluxing conditions (without any base being added) gave rise to a different metal carbonyl cluster anion, $[BiFe_3(CO)_9(\mu_3\text{-}CO)]^-$, which has a triply bridging carbonyl group. This new cluster anion led to a comparison of the basicities of the Bi atom and the oxygen atom of the bridging carbonyl group. It was found that the treatment of this cluster anion with methyl triflate resulted in alkylation of the oxygen atom of the triply bridging carbonyl group evidencing the poor basicity of the lone pair on the Bi atom (eq.12,13).

$$NaBiO_3 + 3Fe(CO)_5 \longrightarrow Na[BiFe_3(CO)_9(\mu_3\text{-}CO)]^- + 3CO_2 + 2CO \qquad \text{(eq.12)}$$

$$Na[BiFe_3(CO)_9(\mu_3\text{-}CO)]^- + CF_3SO_3Me \longrightarrow$$

(eq.13)
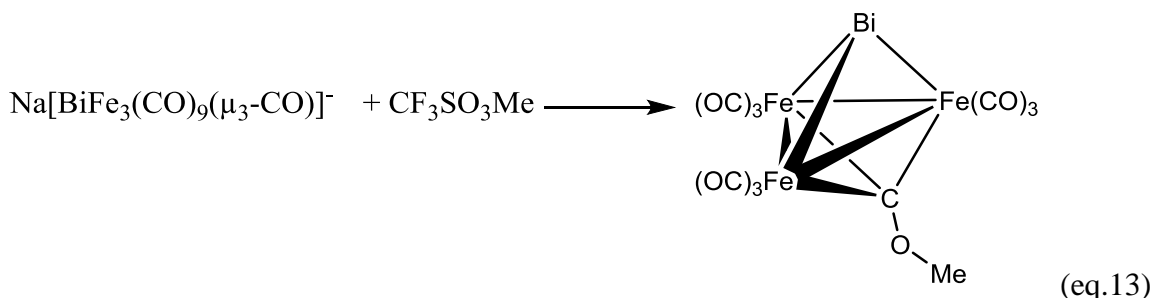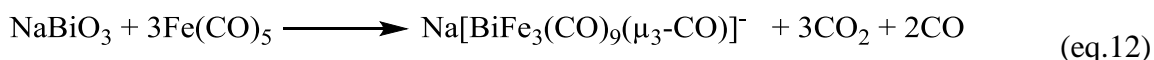
One of the most interesting clusters synthesized in this family, $[Et_4N]_2[Bi_4Fe_4(CO)_{13}]$ was obtained by the treatment of $[BiFe_3(CO)_9(\mu_3\text{-}CO)]^-$ with CO in CH_2Cl_2. The uniqueness of this compound lies in its tetrahedral Bi_4 which contains three faces capped by $Fe(CO)_3$ groups and another $Fe(CO)_4$ group attached to one of the

9

Bi atoms. This novel cluster compound did not possess any Fe-Fe bonds and contained only Bi-Bi bonds.

Several clusters with heavier transition metals which are isostructural to some of the FeBi clusters have been reported, namely $H_3Ru_3(CO)_9Bi$, $Bi_2Ru_3(CO)_9$ and $H_3Os_3(CO)_9Bi$. All of them have been synthesized either by the treatment of the respective anion solution or by a metal carbonyl cluster with $NaBiO_3$ or $Bi(NO_3)_3.5H_2O$.[3,40] Another very interesting structural isomerism was observed for Ru and Os compounds of formula $Bi_2M_4(CO)_{12}$ where M = Ru or Os. Crystal structure analyses of both of the compounds showed octahedral clusters, but the positions of the two Bi atoms showed some differences, in particular the bismuth atoms occupied trans vertices in the Ru cluster and cis vertices in the Os cluster.

1.44 Cobalt carbonyl clusters with Bismuth

Carbonyl clusters of Co and Bi have been reported and the first well characterized BiCo complex $Bi[Co(CO)_4]_3$ was synthesized by a simple metathesis reaction of $BiCl_3$ with $Na[Co(CO)_4]$ in an aqueous solution. This compound did not show any bonding between the cobalt atoms. When this compound was heated to reflux in hexane or tetrahydrofuran solvents, it was converted to the closed complex, $BiCo_3(CO)_9$ by elimination of some of the CO ligands (eq.14,15).[41] Furthermore, it is found that the Bi atom on the $Bi[Co(CO)_4]_3$ can act as a Lewis acidic site by adding yet another $[Co(CO)_4]^-$ to form the tetrahedral $[Bi\{Co(CO)_4\}_4]^-$ anion. In this compound the Bi-Co distances are unusually long, 2.906 Å due to the spatial crowding and also due to the presence of an extra pair of electrons on Bi.[42,43]

10

$$BiCl_3 + 3Na[Co(CO)_4] \longrightarrow \text{[structure]} + 3NaCl \qquad (eq.14)$$

$$\text{[structure]} \xrightarrow[\text{THF or hexane}]{\text{Reflux}} \text{[structure]} + 3CO \qquad (eq.15)$$
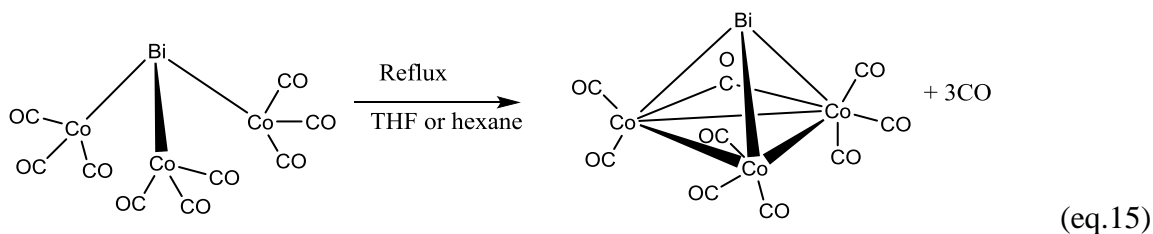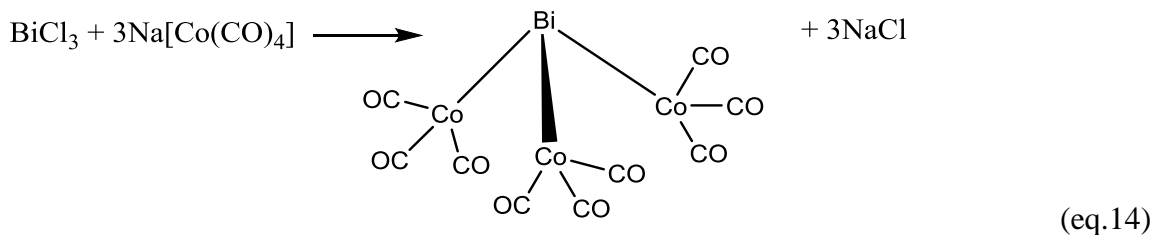
1.45 Iridium carbonyl clusters with Bismuth

The Iridium-Bismuth carbonyl cluster chemistry remained extremely underdeveloped since recently. This is proven by the existence of only one Iridium-Bismuth carbonyl cluster for the past thirty years which was synthesized in 1982 by a group of German scientists by treating a tetrahydrofuran solution of Na[Ir(CO)$_4$] with BiCl$_3$ at -20 ºC to obtain the compound, Ir$_3$(μ_3-Bi)(CO)$_9$ in 22% yield.[44] Since then IrBi cluster synthesis, chemistry and their applications remained unexplored until ideas raised in Adams's group in 2012 to synthesize novel IrBi carbonyl cluster complexes and explore and expand the chemistry of this new family of transition metal-main group metal carbonyl clusters with the hope of using them as catalyst precursors for new selective oxidations.

1.45.1 Facile cleavage of Phenyl groups from BiPh$_3$ adds naked Bismuths on to the Ir$_3$Bi cluster

The cleavage of phenyl groups from triphenylbismuth, Ph$_3$Bi in the synthesis of OsBi and ReBi clusters was demonstrated previously[37,45]. It is well known that Ph$_3$Bi is a poor acceptor ligand compared to PPh$_3$ and contains weak C-Bi bonds which are readily cleaved, assisting in the addition of naked Bi atoms to the transition metal atoms. We have utilized this synthetic strategy in our work to synthesize the higher nuclearity IrBi clusters, Ir$_5$(CO)$_{10}$(μ_3-Bi$_2$)(μ_4-Bi) starting from the previously known IrBi cluster, Ir$_3$(CO)$_9$(μ_3-Bi) by thermally cleaving the phenyl groups from Ph$_3$Bi[20]. The parent compound, Ir$_3$(CO)$_9$(μ_3-Bi), is electronically saturated with 48 valence electrons with average bond distances Ir−Ir $_{av}$ =2.759(2) Å, Ir−Bi $_{av}$ = 2.734(2) Å. The Ir$_5$Bi$_3$ cluster consists of two triply bridging Bi atoms and one quadruply bridging Bi atom, in which each one donates 3 electrons to the metal cluster core forming an electronically saturated square pyramid cluster with 74 valence electrons. The average bond distances are similar to the previously known IrBi cluster complex. More details can be found in chapter 2 of this thesis.

1.45.2 Oxidative addition of Ph$_3$SnH and Ph$_3$GeH expands bimetallic IrBi cluster chemistry into tri -metallic systems.

Germanium and tin are known to be valuable modifiers of heterogeneous catalysts. FTIR studies carried out on CO adsorption/desorption of supported Rh monometallic and RhGe bimetallic catalysts showed the enhancement of the bimetallic catalytic properties through the incorporation of germanium and it was revealed that

germanium has a stabilizing effect on the catalyst.[46] Furthermore, it was shown that the addition of germanium to iridium catalysts lead to increased selectivity towards aromatization reactions and hydrogenation of certain unsaturated hydrocarbons.[47] Selective partial hydrogenation of cyclododecatriene (CDT) for the production of cyclodecene (CDE) is a chemical reaction with high commercial importance. Adams et al. have shown recently that the introduction of tin into the monometallic platinum group metal (PGM) catalyst precursors yields bimetallic catalyst precursors for the aforementioned reaction and greatly improves its selectivity towards catalytic hydrogenation.[4,48] Therefore in our work we have introduced tin and germanium ligands into the IrBi bimetallic catalyst system with the hope of utilizing the merits of tin and germanium towards heterogeneous catalysis. We have used Ph_3SnH and Ph_3GeH as the sources for Sn and Ge respectively in which both of them react through an oxidative addition with the previously known $Ir_3(CO)_9(\mu_3\text{-Bi})$ cluster and the new compound $Ir_3(\mu_3\text{-Bi})(CO)_8(Ph)[\mu\text{-Au(NHC)}]$,(NHC= N-heterocyclic carbene). Products of these reactions further proceed through alpha phenyl cleavage from EPh_3 (E=Sn or Ge) ligands, giving rise to IrBi and IrBiAu adducts with bridging EPh_2 or $Ph_2E(OH)EPh_2$ ligands subsequently eliminating benzene.[49] The latter phenyl cleavage is facilitated by the presence of water to generate a bridging OH ligand between the two EPh_2 ligands. It has recently been shown by a computational analysis that the alpha cleavage of a phenyl group from a $GePh_3$ ligand in the transformation of the triiridium complex $Ir_3(CO)_6(\mu\text{-CO})(\mu\text{-GePh}_2)_2(GePh_3)_3$ into the complex $Ir_3(CO)_6(\eta^1\text{-Ph})(\mu\text{-GePh}_2)_3(GePh_3)_2$ occurs at a single iridium atom[50]. The IrBiSn, IrBiGe and IrBiAuSn clusters synthesized this way and loaded on to catalyst supports could be potential tri and tetrametallic catalyst

13

precursors upon thermal removal of phenyl groups. More details of this work can be found in chapter 3 of this thesis.

1.45.3 Oxidative addition of PhAu(NHC) on to bimetallic IrBi cluster

Various studies have demonstrated gold's ability to act as an oxidation catalyst, specifically for the oxidation of CO and for the conversion of propylene to propylene oxide in which TiO_2 supported gold particles exhibit extraordinary catalytic performance compared to TiO_2 or Au used alone[51,52,53]. There have been very few reports on Iridium and Gold carbonyl complexes[54,55] until Adams et al. started exploring IrAu carbonyl chemistry recently[56]. $PhAuPPh_3$ is known to add oxidatively to substitutionally active metal carbonyl cluster complexes under mild conditions to yield transition metal – gold complexes containing phenyl ligands[57,58]. Due to the instability of Au-P bond in $PhAuPPh_3$, we have used PhAu(NHC), NHC = N-heterocyclic carbene ligand, in our work to add Au atoms into the IrBi bimetallic system, with the hope of enhancing the catalytic properties of the IrBi bimetallic system towards selective oxidation reactions even further. This work revealed the first Au-Bi bond in a carbonyl cluster complex and the shortest Au-Bi bond known so far. The Au – Bi interaction was determined to be substantial and is comparable in character to the Ir – Bi and Ir – Ir bonds in this new IrBiAu cluster complex. Further details are available in chapter 4 of this thesis.

14

1.45.4 Addition of Ruthenium on to bimetallic Ir$_3$Bi cluster and thermal condensation of Ir$_3$Bi clusters to produce higher nuclear IrBi clusters

Supported ruthenium and iridium catalysts are well known to produce C$_2$ oxygenated compounds such as ethanol, acetaldehyde and acetic acids from syngas[59]. Furthermore ruthenium combined with iridium is well known to catalyze oxygen evolution reactions (OER) [60] as well. We have used the moderately stable, 48 electron complex Ru$_3$(CO)$_{10}$(NCMe)$_2$ in our work to introduce Ru into the previously known Ir$_3$(CO)$_9$(μ_3-Bi) complex. This reaction proceeds through the elimination of the labile ligand, NCMe on the Ru cluster and the elimination of the CO ligands from the Ir$_3$Bi cluster and also through fragmentation and rearrangement of the metal clusters to produce higher nuclearity IrRuBi metal cluster complexs. Thermal condensation of smaller carbonyl clusters to produce higher nuclear clusters has been practiced for years and in our work we have utilized this strategy to synthesize various IrBi cluster complexes with and without phosphine ligands to create higher nuclearity IrBi clusters. The thermal condensation of the previously known Ir$_3$(CO)$_9$(μ_3-Bi) cluster and its mono phosphine, PPh$_3$-substituted derivatives both yielded dimeric forms by the loss of CO ligands. The mono phosphine analog of Ir$_3$(CO)$_9$(μ_3-Bi), Ir$_3$(CO)$_8$(PPh$_3$)(μ_3-Bi) has been further reacted with two and three equivalents of PPh$_3$ through CO elimination and ligand addition to yield bis and tris substituted analogs. The bis-phosphine substituted Ir$_3$Bi complex exhibited a intramolecular C-H activation , by activating one of the Phenyl C-H bonds on the PPh$_3$ ligands, which is commonly known as " orthometallation " . Additional details of this work can be found in chapter 5 of this thesis.

Summary

The synthesis of bi-metallic nanoparticles from carbonyl precursors came on the scene about two decades ago when B. F. G. Johnson and coworkers synthesized the first RuPd bimetallic nano particles from PdRu carbonyl complexes[6]. The process could be monitored by using a combination of techniques such as *in situ* FTIR for the CO removal and EXAFS measurements to analyze the covalent bonding between the metal nanoparticles and the catalyst support.[6] In our work, numerous IrBi carbonyl cluster complexes were synthesized and were characterized by using IR, Mass spec and single crystal X-ray diffraction techniques and these bimetallic cluster systems were further extended to tri- and tetra-metallic systems by the careful selection and incorporation of catalytically important metal atoms like Ru, Au, Sn and Ge with the hopes of combining the individual catalytic properties of each metal atom to obtain a synergistic effect towards selective oxidation catalysis. Furthermore, the first catalyst nanoparticles of Ir and Bi were synthesized from their carbonyl precursors and were characterized by using HRSTEM and EDS techniques. These catalyst nano particles were tested for a commercially important reaction, which includes the synthesis of niacin (commonly known as vitamin B_3) from 3-picoline. Niacin is used in food stuffs and cholesterol lowering agents as well. This conversion involves both C-H activation and selective incorporation of oxygen into the activated C-H bond which is essentially know as "selective oxidation ". The catalytic results of the aforementioned conversion exhibited extraordinary efficiency in terms of both conversion and selectivity making IrBi carbonyl cluster complexes promising catalyst precursors for new selective oxidation catalysis.

REFERENCES

(1) Sun, M. Z. *Chem. Rev.* **2014**, *114* (2), 981–1019.

(2) Schlögl, R. *Angew. Chem. Int. Ed.* **2015**, *54* (11), 3465–3520.

(3) Hay, C. M.; Johnson, B. F. G.; Lewis, J.; Raithby, P. R.; Whitton, A. J. *J. Chem. Soc. Dalton Trans.* **1988**, No. 8, 2091–2097.

(4) Adams, R. D.; Blom, D. A.; Captain, B.; Raja, R.; Thomas, J. M.; Trufan, E. *Langmuir* **2008**, *24* (17), 9223–9226.

(5) Adams, R. D.; Boswell, E. M.; Captain, B.; Hungria, A. B.; Midgley, P. A.; Raja, R.; Thomas, J. M. *Angew. Chem. Int. Ed.* **2007**, *46* (43), 8182–8185.

(6) Thomas, J. M.; Adams, R. D.; Boswell, E. M.; Captain, B.; Grönbeck, H.; Raja, R. *Faraday Discuss.* **2008**, *138* (0), 301–315.

(7) Grasselli, R. K.; Lugmair, C. G.; Volpe, A. F.; Andersson, A.; Burrington, J. D. *Catal. Today* **2010**, *157* (1-4), 33–38.

(8) Lin, M. M. *Appl. Catal. Gen.* **2001**, *207* (1-2), 1–16.

(9) Baerns, M.; Buyevskaya, O. *Catal. Today* **1998**, *45* (1-4), 13–22.

(10) Labinger, J. A. ; Bercaw, J. E. *Nature* **2002**, *417* (6888), 507–514.

(11) Braunschweig, H.; Cogswell, P.; Schwab, K. *Coord. Chem. Rev.* **2011**, *255* (1–2), 101–117.

(12) Gaspard-Iloughmane, H.; Le Roux, C. *Eur. J. Org. Chem.* **2004**, *2004* (12), 2517–2532.

(13) Zhai, Z.; Getsoian, A. B; Bell, A. T. *J. Catal.* **2013**, *308*, 25–36.

(14) Moro-Oka, Y.; Ueda, W. In *Advances in Catalysis*; D.D. Eley, H. P. and W. O. H., Ed.; Academic Press, 1994; Vol. 40, pp 233–273.

17

(15) Carson, D.; Coudurier, G.; Forissier, M.; Vedrine, J. C.; Laarif, A.; Theobald, F. *J. Chem. Soc. Faraday Trans. 1 Phys. Chem. Condens. Phases* **1983**, *79* (8), 1921–1929.

(16) Hanna, T. A. *Coord. Chem. Rev.* **2004**, *248* (5–6), 429–440.

(17) He, Y.; Wu, Y.; Yi, X.; Weng, W.; Wan, H. *J. Mol. Catal. Chem.* **2010**, *331* (1–2), 1–6.

(18) Grasselli, R. K. *Top. Catal.* **2001**, *15* (2/4), 93–101.

(19) Adams, R. D.; Elpitiya, G.; Khivantsev, K.; Blom, D.; Alexeev, O. S.; Amiridis, M. D. *Appl. Catal. Gen.* **2015**, *501*, 10–16.

(20) Adams, R. D.; Chen, M.; Elpitiya, G.; Potter, M. E.; Raja, R. *Acs Catal.* **2013**, *3* (12), 3106–3110.

(21) Shilov, A. E. *Activation of Saturated Hydrocarbons by Transition Metal Complexes*; Springer Science & Business Media, 1984.

(22) Crabtree, R. H.; Mihelcic, J. M.; Quirk, J. M. *J. Am. Chem. Soc.* **1979**, *101* (26), 7738–7740.

(23) Bengali, A. A.; Arndtsen, B. A.; Burger, P. M.; Schultz, R. H.; Weiller, B. H.; Kyle, K. R.; Moore, C. B.; Bergman, R. G. *Pure Appl. Chem.* **1995**, *67* (2).

(24) Bergman, R. G. *Science* **1984**, *223* (4639), 902–908.

(25) a) Klei, S. R.; Tan, K. L.; Golden, J. T.; Yung, C. M.; Thalji, R. K.; Ahrendt, K. A.; Ellman, J. A.; Tilley, T. D.; Bergman, R. G. In *Activation and Functionalization of C—H Bonds*; Goldberg, K. I., Goldman, A. S., Eds.; American Chemical Society: Washington, DC, 2004; Vol. 885, pp 46–55. b) Burger, P.; Bergman, R. G. *J. Am. Chem. Soc.* **1993**, *115* (22), 10462. c) Arndtsen,

18

B. A.; Bergman, R. G.; Mobley, T. A.; Peterson, T. H. *Acc. Chem. Res.* **1995**, *28* (3), 154.

(26) Coetzee, J.; Eastham, G. R.; Slawin, A. M. Z.; Cole-Hamilton, D. J. *Dalton Trans.* **2015**, *44* (4), 1585–1591.

(27) Wang, H.; Xie, F.; Qi, Z.; Li, X. *Org. Lett.* **2015**, *17* (4), 920–923.

(28) Murai, M.; Takami, K.; Takeshima, H.; Takai, K. *Org. Lett.* **2015**, *17* (7), 1798–1801.

(29) Donnelly, K. F.; Lalrempuia, R.; Müller-Bunz, H.; Clot, E.; Albrecht, M. *Organometallics* **2015**, *34* (5), 858–869.

(30) McVicker, G. B.; Daage, M.; Touvelle, M. S.; Hudson, C. W.; Klein, D. P.; Baird Jr., W. C.; Cook, B. R.; Chen, J. G.; Hantzer, S.; Vaughan, D. E. W.; Ellis, E. S.; Feeley, O. C. *J. Catal.* **2002**, *210* (1), 137–148.

(31) Choi, J.; MacArthur, A. H. R.; Brookhart, M.; Goldman, A. S. *Chem. Rev.* **2011**, *111* (3), 1761–1779.

(32) Jones, J. H. *Platin. Met. Rev.* **2000**, *44* (3), 94–105.

(33) Gates, B. C. *Chem. Rev.* **1995**, *95* (3), 511–522.

(34) Whitmire, K. H. *J. Clust. Sci.* **1991**, *2* (4), 231–258.

(35) Panster, P.; Malisch, W. *J. Organomet. Chem.* **1977**, *134* (2), C32–C36.

(36) Cassidy, J. M.; Whitmire, K. H. *Inorg. Chem.* **1991**, *30* (13), 2788–2795.

(37) Adams, R. D.; Pearl, W. C. *Inorg. Chem.* **2009**, *48* (19), 9519–9525.

(38) Churchill, M. R.; Fettinger, J. C.; Whitmire, K. H. *J. Organomet. Chem.* **1985**, *284* (1), 13–23.

19

(39) Whitmire, K. H.; Lagrone, C. B.; Rheingold, A. L. *Inorg. Chem.* **1986**, *25* (14), 2472–2474.

(40) Ang, H. G.; Hay, C. M.; Johnson, B. F. G.; Lewis, J.; Raithby, P. R.; Whitton, A. J. *J. Organomet. Chem.* **1987**, *330* (1–2), C5–C11.

(41) Etzrodt, G.; Und, R. B.; Schmid, G. *Chem. Ber.* **1979**, *112* (7), 2574–2580.

(42) Martinengo, S.; Fumagalli, A.; Ciani, G.; Moret, M. *J. Organomet. Chem.* **1988**, *347* (3), 413–422.

(43) Leigh, J. S.; Whitmire, K. H. *Angew. Chem. Int. Ed. Engl.* **1988**, *27* (3), 396–398.

(44) Kruppa, W.; Blaser, D.; Boese, R.; Schmid, G. *Z. Naturforsch*. 1982, 37B , 209-213

(45) Adams, R. D. ; K. *J. Organomet. Chem.* **2014**, *751*, 475–481.

(46) Lafaye, G.; Mihut, C.; Especel, C.; Marécot, P.; Amiridis, M. D. *Langmuir* **2004**, *20* (24), 10612–10616.

(47) Ekou, T.; Vicente, A.; Lafaye, G.; Especel, C.; Marecot, P. *Appl. Catal. Gen.* **2006**, *314* (1), 73–80.

(48) Adams, R. D.; Boswell, E. M.; Captain, B.; Hungria, A. B.; Midgley, P. A.; Raja, R.; Thomas, J. M. *Angew. Chem. Int. Ed.* **2007**, *46* (43), 8182–8185.

(49) Adams, R. D.; Chen, M.; Elpitiya, G.; Zhang, Q. *Organometallics* **2012**, *31* (20), 7264–7271.

(50) Adams, R. D.; Fang, F.; Zhang, Q.; Hall, M. B.; Trufan, E. *Organometallics* **2012**, *31* (7), 2621–2630.

(51) Haruta, M.; Daté, M. *Appl. Catal. Gen.* **2001**, *222* (1–2), 427–437.

(52) Haruta, M. *Catal. Today* **1997**, *36* (1), 153–166.

20

(53)   Hashmi, A. S. K.; Hutchings, G. J. *Angew. Chem. Int. Ed.* **2006**, *45* (47), 7896–7936.

(54)   Della Pergola, R.; Demartin, F.; Garlaschelli, L.; Manassero, M.; Martinengo, S.; Masciocchi, N.; Sansoni, M. *Organometallics* **1991**, *10* (7), 2239–2247.

(55)   Ceriotti, A.; Della Pergola, R.; Garlaschelli, L.; Manassero, M.; Masciocchi, N. *Organometallics* **1995**, *14* (1), 186–193.

(56)   Adams, R. D.; Chen, M. *Organometallics* **2012**, *31* (17), 6457–6465.

(57)   Adams, R. D.; Rassolov, V.; Zhang, Q. *Organometallics* **2013**, *32* (21), 6368–6378.

(58)   Adams, R. D.; Rassolov, V.; Wong, Y. O. *Angew. Chem. Int. Ed.* **2014**, *53* (41), 11006–11009.

(59)   Hamada, H.; Kuwahara, Y.; Kintaichi, Y.; Ito, T.; Wakabayashi, K.; Iijima, H.; Sano, K. *Chem. Lett.* **1984**, *13* (9), 1611–1612.

(60)   Fuentes, R. E.; Farell, J.; Weidner, J. W. *Electrochem. Solid-State Lett.* **2011**, *14* (3), E5–E7.

CHAPTER 2

IRIDIUM BISMUTH CLUSTER COMPLEXES YIELD BIMETALLIC NANO CATALYSTS FOR THE
DIRECT OXIDATION OF 3-PICOLINE TO NIACIN[1]

---

[1] Adams, R. D.; Chen, M.; Elpitiya, G.; Potter, M. E.; Raja, R. *ACS Catal.* **2013**, *3* (12), 3106–3110.

Introduction

Probing the origins of the catalytic synergy between multimetallic active centers in porous solids, wherein a Platinum Group Metal (PGM) such as Ru, Pt, or Rh, is alloyed with suitable oxophiles such as Sn, Bi, or Mo facilitates the rational design of well-isolated, single-site nanoparticle catalysts, that exhibit enhanced stability and improved catalytic performance.[1,2] Tailoring suitable oxophiles in combination with multimetallic clusters has afforded intrinsic compositional control at the nanoscale, with the added advantage of controlling the morphology, size, and shape of the ensuing naked-metal nanoparticles.[3−5] Such a design approach could be integrated with custom-made support modifications (e.g., tuning the hydrophobicity) to yield both functional and structural synergies facilitating structure−property relationships to be established.[6] The precise controlled synthesis of catalytically active metal nanoparticles has been of great interest in recent years,[7,8] with the ever-expanding target of creating discrete single-sites. With a view to achieving this goal, a number of elegant strategies using inorganic porous supports,[9−11] polymer-stabilized matrixes,[12] and framework extrusion processes[13] have been developed. Despite the intrinsic merits of these approaches,[9−13] the desire to modulate catalytic activity and selectivity at the nanoscale, through the skillful choice of appropriate metal combinations and their concomitant oxophilic analogues, for generating uniform, discrete, well defined, multifunctional single-sites, remains a challenging prospect.

Bismuth on oxide supports has been shown to catalyze the oxidation of certain hydrocarbons heterogeneously. [15] Bismuth molybdate is well-known for its ability to catalyze the ammoxidation of propene.[16] We have recently shown that a bimetallic

rhenium−bismuth catalyst, derived from a rhenium − bismuth complex $Re_2(CO)_8(\mu$-$BiPh_2)_2$, can selectively convert 3-picoline to 3-nicotinonitrile. [2] The ability of the oxophile (bismuth in this case) to interact favorably with the mesoporous silica support, through the covalent-bond formation between the oxophilic metal and pendant silanol groups, renders this nanoparticle catalyst amenable for oxidation reactions.[3,5] Furthermore, the capping of the CO ligands on the nanocluster precursor improves the degree of site-isolation, leading to the creation of the catalytically active nanoparticle catalyst. It has been previously demonstrated[1−5] that the subsequent removal of the CO ligands, generates uniform (<5 nm), well-defined, anchored bimetallic nano-particles, where the bismuth plays a pivotal role in securing the nanoclusters to the support and ensuring its compositional integrity.[3−5] Furthermore, it has also been demonstrated that bismuth plays a key role in enhancing the catalytic efficiency in a range of selective oxidation reactions.[17−19] Most notable is the combination of bismuth with precious metals to form Pd−Bi[17] and Pt−Bi[18] species. While the exact role of bismuth in such catalysts is not conclusive, it has been suggested that the production of 2,5-furandicarboxylic acid (FDCA) from hydroxymethylfurfural (HMF) was appreciably increased owing to the favorable interaction between Bi atoms and π - electrons in the furan ring.[18] There are also other plausibilities attributing the promoter ability of Bi to its oxophilicity, [6,17] which enhances the ability of bismuth to activate molecular oxygen thereby facilitating α -H abstraction.[19]

These unique properties of the bismuth prompted us to devise other bimetallic catalysts, and we report herein, for the first time, the design of two novel iridium − bismuth bimetallic nano- clusters that are derived from new Ir−Bi complexes.

24

Preliminary catalytic studies outlining the performance of these new iridium −bismuth nanoparticle catalysts for the direct oxidation of 3-picoline to niacin (Figure 2.1) are reported, offering a subtle contrast to the previously reported [2] ammoxidation route to nicotinonitrile (precursor to niacin).Until recently, the only example of an iridium−bismuth complex was the compound $Ir_3(CO)_9(\mu_3-Bi)$,**2.1**, that was reported by Schmid et al.[20]

Experimental Details

General Data.

Reagent grade solvents were dried by the standard procedures and were freshly distilled under nitrogen prior to use. Infrared spectra were recorded on a Thermo Nicolet Avatar 360 FT-IR spectrophotometer. Mass spectrometric (MS) measurements were performed by a direct-exposure probe using electron impact ionization (EI) by using a VG 70S instrument. $BiPh_3$ was obtained from STREM CHEMICALS and were used without further purification. $Ir_3(CO)_9(\mu_3-Bi)$, **2.1** was prepared according to a published procedure.[20] Product separations were performed by TLC in air on Analtech 0.25 and 0.5 mm silica gel 60 Å F254 glass plates.

Synthesis of $Ir_5(CO)_{10}(\mu_3-Bi_2)(\mu_4-Bi)$, 2.2

3.0 mg (0.075 mmol) of Ph_3Bi was added to 16.0 mg (0.015 mmol) of $Ir_3(CO)_9(\mu_3-Bi)$, **2.1** that was dissolved in 20 mL of hexane and was heated to reflux for ~4h or until all the $Ir_3(CO)_9(\mu_3-Bi)$ is gone. The solvent was then removed in vacuo, and

25

the product was then isolated by TLC eluting using a 4:1 hexane/methylene chloride solvent mixture. This yielded 15.7 mg of dark red $Ir_5(CO)_{10}(\mu_3\text{-}Bi_2)(\mu_4\text{-}Bi)$, **2.2** (91% yield) as the only product.

Spectral data for **2.2**: IR νCO (cm-1 in CH_2Cl_2): 2095(w), 2032(s), 2022(m), 1990(w). Mass Spec. EI/MS for 2: m/z = 1868, M+. The isotope distribution pattern was consistent with the presence of five iridium atoms and three bismuth atoms.

Crystallographic Analyses

Dark red single crystals of **2.2** suitable for x-ray diffraction analyses were obtained by slow evaporation of solvent from a hexane/methylene chloride solvent mixture at -25 °C. The data crystal was glued onto the end of a thin glass fiber. X-ray intensity data were measured by using a Bruker SMART APEX CCD-based diffractometer using Mo Kα radiation (λ = 0.71073 Å). The raw data frames were integrated with the SAINT+ program by using a narrow-frame integration algorithm.[21] Correction for Lorentz and polarization effects were also applied with SAINT+. An empirical absorption correction based on the multiple measurement of equivalent reflections was applied using the program SADABS. All structures were solved by a combination of direct methods and difference Fourier syntheses, and refined by full-matrix leastsquares on F2, using the SHELXTL software package.[22] All atoms were refined with anisotropic displacement parameters. Crystal data, data collection parameters, and results of the analyses are listed in Table **2.1**. Compound **2.2** crystallized in the orthorhombic crystal system. The space groups Pnma and Pna21 were indicated by

the systematic absences in the data. Pnma was selected and confirmed by the successful solution and refinement for the structure.

Preparation of the catalysts

Three supports were tested in this study; MCM-41, Davison 923 mesopore and silica gel (60, 0.06-0.2mm (70-230 mesh).

1) 37.49 mg of $Ir_3(CO)_9(\mu_3\text{-Bi})$, **2.1** was dissolved in benzene. To this solution, 918 mg of MCM41 support was added and mixture was slurried under nitrogen for 24h. The solvent was then slowly removed under vacuum. The solid catalyst was then preconditioned by heating under vacuum to 200 °C for a period of 2h to remove the CO ligands to yield 0.947 g amount of supported catalyst with 3% metal loading.

2) 35.28 mg amount of **2.2** was dissolved in 30 mL of CH_2Cl_2. To this solution, 970 mg of MCM41 support was added and mixture was slurried under nitrogen for 24h. The solvent was then slowly removed under vacuum. The solid catalyst was then preconditioned by heating under vacuum to 200 °C for a period of 2h to remove the CO ligands to yield 1.00 g of catalyst with 3% metal loading.

3) A pure bismuth catalyst with 3% metal loading was prepared similarly on MCM41 by thermal treatment by using a commercially obtained sample of $BiPh_3$ as the precursor.

4) A pure iridium catalyst with 3% metal loading was prepared similarly by using a commercially obtained sample (STREM) of $Ir_4(CO)_{12}$ as the precursor.

5) Bimetallic IrBi catalysts (physical mixes) in the Ir/Bi 3/1 and 5/3 ratios were also prepared at the 3% metal loading by co-impregnation methods by slurring solutions containing $Ir_4(CO)_{12}$ and $BiPh_3$ in the appropriate ratios, evaporating to dryness and preconditioning by heating to 200 ^{o}C in vacuo for 2h to remove the ligands.

High Resolution Transmission Electron Imaging of the Supported Catalysts

Scanning high resolution transmission electron microscopy (STEM) was performed at the University of South Carolina Electron Microscopy Center by using a JEOL 2100F 200kV FEG STEM/TEM equipped with a CEOS C_s corrector on the illumination system. The geometrical aberrations were measured and controlled to provide less than a $\pi/4$ phase shift of the incoming electron wave over the probe-defining aperture of 17.5 mrad. High angle annular dark-field (HAADF) scanning transmission electron microscopy (STEM) images were acquired on a Fischione Model 3000 HAADF detector with a camera length such that the inner cut-off angle of the detector was 50 mrad. The scanning acquisition was synchronized to the 60 Hz AC electrical power to minimize 60 Hz noise in the images and a pixel dwell time of 15.8 µs was used. HAADF - HRTEM images of Ir_3Bi nanoparticles on MCM-41 before catalysis (on left, pretreated at 200 ^{o}C to remove the ligands) and after use in catalysis (on right, pretreated at 300 ^{o}C to remove the ligands) are shown in Figure **2.2** .

Synthesis and analysis of APB oxidant

APB served as a solid source of oxygen, liberating peroxyacetic acid (PAA) in situ when dissolved in water, it was synthesized by adding 4 mL (36-40% in acetic acid,

Sigma) of peroxyacetic acid (23 mmol) to a glass reactor, preheated to 30 ^{o}C. 2.0 g of ground sodium tetraborate anhydrous (10 mmol, Sigma) was slowly added, yielding a white gel, which stirred for 16 hours. The white powder formed was dried at 50 ^{o}C for 16 hours. The PAA concentration of APB was determined through an iodometric titration. In a standard procedure 0.1 g of APB was dissolved in 10 ml solution of 0.6 M KI. This was then titrated against a 0.1 M solution of $Na_2S_2O_3$. The PAA content was then determined through the following equation 1:

$$\% \text{ PAA} = \frac{\text{Final tire/ml x 0.38}}{\text{Mass of APB/g}} \qquad (eq.1)$$

Catalyst Evaluations

The catalysts were activated through calcination by using a mixture of 5% H_2/N_2 for two hours at the stated temperature, prior to the catalytic tests. The liquid-phase oxidations were performed in a glass reactor at 66 ^{o}C by using 15 mmol of 3-picoline, 3.5 mmol of monoglyme internal standard, the appropriate quantity of acetylperoxyborate (APB) to yield 5 mmol of PAA (3:1 substrate:oxidant ratio), 25 mL of water and 150 mg of catalyst. The reaction mixtures were analyzed by using a Clarus 400 gas chromatogram, employed with a FID detector, using an Elite 5 column; the peak areas were calibrated using authenticated standards to evaluate respective response factors. Mass-balances were determined using the internal standard calibration method and individual response factors (RF) were calculated to establish a material balance and account for handling losses. A typical example (Ir_5Bi_3/MCM-41, calcined at 300°C, 15 minute data point) is shown below.

29

Mass balance

RF for 3-Picoline (relative to Monoglyme)	2.016
RF for Niaicn (relative to Monoglyme)	1.17
Initial Monoglyme area	114612.2
Initial 3-Picoline area	1161982
Intitial Niacin area	0
Initial moles of Monoglyme (added)	0.003329
Initial moles of 3-Picoline (detected)	0.016737
Initial moles of Niacin (detected)	0
Total initial reaction mix moles (detected)	0.016737
15 minutes Monoglyme area	69917.31
15 minutes 3-Picoline area	666737.9
15 minutes Niacin area	25325.5
15 mins moles of Monoglyme (added)	0.003329
15 mins moles of 3-Picoline (detected)	0.015742
15 mins moles of Niacin (detected)	0.001031
Total 15 mins reaction mix moles (detected)	0.016773

Mass balance	100.22
Conversion accounting for mole ratio	18.4
Niaicn selectivity	99.9

The conversions were calculated as the percentage moles of picoline consumed, and these values were normalized relative to the oxidant ratio employed. Selectivity values were calculated from the moles of niacin produced, as a function of the total moles of product formed in mole percent. Turnover numbers (TON) were evaluated from the moles of picoline reacted per mole of the bimetallic catalyst Ir_3Bi or Ir_5Bi_3.

Results and Discussion

We have now found that **2.1** reacts with $BiPh_3$ to yield the new higher nuclearity complex $Ir_5(CO)_{10}(\mu_3\text{-}Bi)_2(\mu_4\text{-}Bi)$, **2.2** in high yield (91%),(Scheme 2.1). Compound **2.2** was characterized crystallographically by single-crystal X-ray diffraction, and an ORTEP[23] diagram of its molecular structure is shown in Figure 2.3. The molecule lies on a reflection plane in the solid state. Compound **2.2** contains five iridium atoms arranged in the form of a square pyramid.

Complex **2.2** contains three bridging bismuth atoms: Atom Bi(1) is a quadruple bridge that spans the base of the Ir5 square pyramid; the other two, Bi(2) and Bi(3), are triply bridging ligands that bridge oppositely positioned triangular faces of the square pyramid. The Ir−Ir and Ir−Bi bond distances, Ir(1)−Ir(2) = 2.7824(7) Å, Ir(1)−Ir(3) = 2.8226(7) Å, Ir(2)−Ir(3) =2.7903(7)Å, Ir(2) −Ir(2′) = 2.8255(9) Å, Ir(3) −Ir(3′)= 2.7796(9) Å, Ir(1)−Bi(3) = 2.8322(9), Ir(1)− Bi(2) = 2.7623(9), Ir(2) − Bi(3) = 2.6868(7),

Ir(2) − Bi(1) = 2.8004(7), Ir(3) −Bi(2) = 2.7002(7), Ir(3)− Bi(1) = 2.8185(7) are similar to those found in **2.1**, (Ir−Ir $_{av}$ =2.759(2) Å), (Ir−Bi $_{av}$ = 2.734(2) Å).[7]

Initial catalytic studies have revealed that two novel iridium − bismuth catalysts (derived from the Ir$_3$Bi and Ir$_5$Bi$_3$ cluster complexes) are indeed active for the direct oxidation of 3-picoline to niacin (Figure 2.1).[2] Niacin is a key component of the NADH/NAD+ system that is known to play a key role in many processes related to human metabolism.[24] Also known as vitamin B$_3$, niacin is an essential food element; deficiencies can lead to the disorder known as Pellagra.[24] Niacin is also known to exhibit benefits for treatments of cholesterol-related problems.[25] Therefore the synthesis of niacin is of great interest, as evidenced by the range of industrial processes employed to produce it, by direct oxidation as well as via its precursor, nicotinamide, that is generated by ammoxidation of 3-picoline followed by hydrolysis. [26−28] Industrially viable routes for niacin production are well-established with solid, metal-oxide catalysts yielding over 87 mol % at 300°C,[27] and microbial biocatalysts (Rhodococcus rhodochrous) producing nictonamide in a continuous fashion, albeit in a multistep fashion.[28] While our previous work with the Re−Bi catalysts achieve C−H activation of 3-picoline via ammoxidation to achieve low yields (<5 mol %) of niacin using an excess of sacrificial NH$_3$,[2] we have adopted a more direct oxidative approach, as a proof-of-concept study, with these novel IrBi catalysts for the single-step oxidation of 3-picoline to niacin. Compounds **2.1** and **2.2** were deposited onto mesoporous (MCM-41) silica supports by the incipient wetness method and then both were converted into bimetallic IrBi nanoparticles by thermal treatments under vacuum. They were subsequently evaluated for their ability to oxidize 3-picoline to niacin catalytically by using acetylperoxyborate (APB) as the oxidant.

32

Representative high angle annular darkfield (HAADF) high resolution transmission electron microscopy images of the Ir_3Bi and Ir_5Bi_3 nanoparticles after use in catalysis are shown in Figure 2.4. As can be seen the particles are uniformly dispersed and are less than 2 nm in diameter. It can also be seen that the porous character of the support was maintained during the calcination/particle formation process. Analysis of their compositions by energy dispersive X-ray emission spectroscopy (EDS) are consistent with the Ir_3Bi and Ir_5Bi_3 compositions of the precursor complexes,(Tables 2.2-2.4). The Ir_3Bi nanoparticles obtained from **2.1** were tested for the direct oxidation of 3-picoline to niacin by using the oxidant APB. APB has been shown to be a useful reagent for selective oxidation reactions under mild conditions, serving as a solid source of active oxygen by liberating peroxyacetic acid (PAA) insitu when dissolved in water.[29] For comparisons, supported forms of pure Ir and pure Bi, 3Ir/1Bi (created from a solution of a mixture of $Ir_4(CO)_{12}$ and $BiPh_3$ combined in the appropriate ratio), Ir_5Bi_3 nanoparticles obtained from compound **2.2** and 5Ir/3Bi particles (created from a solution of a mixture of $Ir_4(CO)_{12}$ and $BiPh_3$ combined in the appropriate ratio) were also tested. The best catalytic results were obtained by preheating the nanoparticles to 300°C for 2 h under vacuum before use. The catalytic tests were performed at 65°C for a period of 45 min. The results of the various tests are shown in the chart in Figure 2.5 where blue represents the conversion of 3-picoline, red represents the selectivity of the conversion to niacin, and purple represents the turnover number (TON) for niacin formation.

Pure Ir and pure Bi are ineffective catalysts as represented by the very low TONs for Niacin. The principal side product is 3-picoline-N-oxide, which is the major product of oxidation with pure Bi on the support. The contrasting catalytic behaviors and catalytic

33

opportunities afforded through the utilization of bimetallic nanoclusters are outlined in Figure 2.6. The monometallic Ir and Bi catalysts display distinctly different catalytic profiles ; while Ir clearly shows an increased selectivity for niacin, it is far less active than its Bi counterpart, which has a greater propensity for the formation of picoline N-oxide. This difference in activity suggests that the monometallic Ir catalysts facilitate a targeted reaction pathway necessary to form niacin from picoline; whereas the monometallic Bi catalysts is far more proficient in activating the oxidant, which evokes a more diverse range of oxidation products. The bimetallic catalysts derived from **2.1** and **2.2** are superior to the bimetallics derived by co-impregnation (the physical mix), and they exhibit the best selectivity and TONs for niacin. The attributes of the two individual metal centers are maximized by combining them to generate intimately mixed bimetallic IrBi nanoclusters, which display vastly enhanced selectivity toward the desired niacin along with a concomitant increase in catalytic efficiency (TON). The differing behavior of the $3Ir:1Bi$ and Ir_3Bi catalysts (the former being a physical mixture prepared using identical moles of monometallic Ir and Bi) strongly suggests that a specific structural integrity of the cluster is fundamental in optimizing the overall selectivity and efficiency of the catalysts in the oxidation reaction. Through careful synthetic design of the bimetallic precursor, one can ensure that the Ir and Bi metals are in close proximity to one another; a feature that cannot be readily controlled or guaranteed with the preparation of the bimetallic physical mixture. By using a cluster-based precursor, where the structural and compositional integrity can be controlled at the molecular level, it is possible to exploit the individual benefits of the two metals to facilitate a synergistic enhancement in overall catalytic behavior resulting in significant improvements in

catalytic turnover. Thus, the Bi atoms are able to readily activate the oxidant, while the adjacent Ir atoms selectively form the niacin via CH activation processes upon the 3-picoline, ultimately creating an effective spillover catalyst. The catalyst derived from the Ir_5Bi_3 cluster exhibited the best activity for both conversion and catalytic efficiency (TON). This may be attributed to the Ir/Bi ratio becoming closer to unity, thereby promoting a more efficient transfer of activated intermediates between the two metal sites. As with the Ir_3Bi, the cluster derived Ir_5Bi_3 catalyst was far superior to the analogous physical mixture catalyst (5Ir:3Bi), further high-lighting the importance of the structural and compositional integrity provided by the cluster precursor.

The effect of mesoporous support was investigated (Figure 2.7) by comparing a range of ordered and disordered mesoporous architectures. It was found that the choice of support has very little effect on the overall activity of the catalyst, though it plays a significant role in the observed niacin selectivity. Given that an analogous synthetic strategy was adopted using the (same) Ir_3Bi cluster and the fact that the pore dimensions of the mesopore are large enough to influence any diffusion restrictions, we can attribute the differences in catalytic selectivity to the surface specific interactions between the cluster and support. The increased selectivity of the MCM-41 matrix makes it the preferred candidate for further optimizing the catalytic potential, due to the favorable catalyst-surface interactions. It is well known[4] that the abundance of pendant silanol groups on the MCM-41 facilitate robust covalent anchoring of the cluster precursor, that leads to the creation of well-isolated single-sites.

The complete removal of CO ligands is paramount to increasing the overall catalytic activity of these catalysts; as this facilities a greater interaction of substrate and

35

oxidant with the individual metal sites. A direct correlation can be observed between calcination temperature and degree of conversion of 3-picoline (Figure 2.8), which can be attributed to the removal of excess ligands and adsorbed molecules via calcination; making the catalytic active sites more readily accessible for oxidants and reactants. The selectivity is also greatly affected by the calcination temperature. Whilst there is very little change between 200-300 $^{\circ}$C, on activation at 400 $^{\circ}$C, the selectivity to niacin is significantly reduced, which strongly indicates that the catalytically active sites undergo sintering and subsequent aggregation at this temperature. It is highly likely that the structural integrity of the cluster is lost on sintering and thus the proximity of the metals is altered, thereby modifying the interaction of the different catalytic pathways.

The structural and compositional integrity and heterogeneous nature of the Ir and Bi bimetallic clusters was confirmed by evaluating their recycle profile (Figure 2.9). Despite multiple reaction cycles, a constant catalytic profile was maintained, thereby confirming the resilience of the anchoring technique employed to anchor the catalysts to the inorganic support. While this confirms the heterogeneous nature of the materials, analysis of the reaction mixture, post catalysis, revealed < 3 ppb of any dissolved metal (Ir and Bi), which further emphasizes the synergistic importance of having isolated single-sites for enhancing the catalytic efficiency.

The effect of substrate:oxidant mole ratio was explored with a view to increasing the overall conversion of 3-picoline and corresponding yield of niacin (Figure 2.10). It was observed that increasing the amount of oxidant saturates the individual metal sites, amplifying the available concentration and quantity of highly active oxidant intermediates with respect to the substrate, which subsequently blocks the 3-picoline

molecules from accessing the active sites. This results in the wasteful decomposition of the oxidant that leads to the formation of the undesired N-oxides, while the pathway to niacin is greatly retarded. Due to the greater availability of the oxidant in the vicinity of the active site, the oxidant decomposition pathway predominates leading to a lower selectivity in the reaction. By limiting the oxidant ratio, the Ir sites are readily available for interaction with the 3-picoline, with the Bi sites preferentially activating and binding to the oxidant, that leads to a synergistic enhancement and concomitant increase in niacin selectivity.

Summary

The first higher nuclearity iridium−bismuth cluster complex **2.2** has been synthesized and structurally characterized. The first examples of bimetallic IrBi nano-particles have been synthesized from the bimetallic IrBi molecular cluster complexes **2.1** and **2.2.**. In a proof-of-concept study, these bimetallic nano particles exhibit superior catalytic activity for the direct oxidation 3-picoline to niacin, compared to their monometallic analogues. By using cluster-based bimetallic precursors, where the compositional integrity can be better controlled at the molecular level, it is possible to produce superior nano catalysts to better exploit the benefits of the individual metals by synergistic complementarity in the overall catalytic behavior. It is believed that these new iridium − bismuth catalysts will exhibit superior catalytic activity for other types of hydrocarbon oxidation reactions and will pave the way to an emerging family of precious metal-heavy main group metal bimetallic catalysts.[2,16,30]
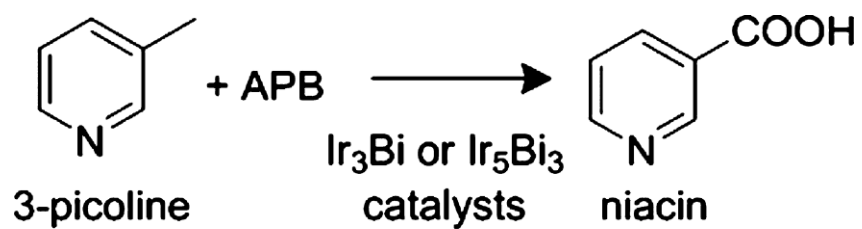
Figure 2.1 Oxidation of 3-picoline to niacin
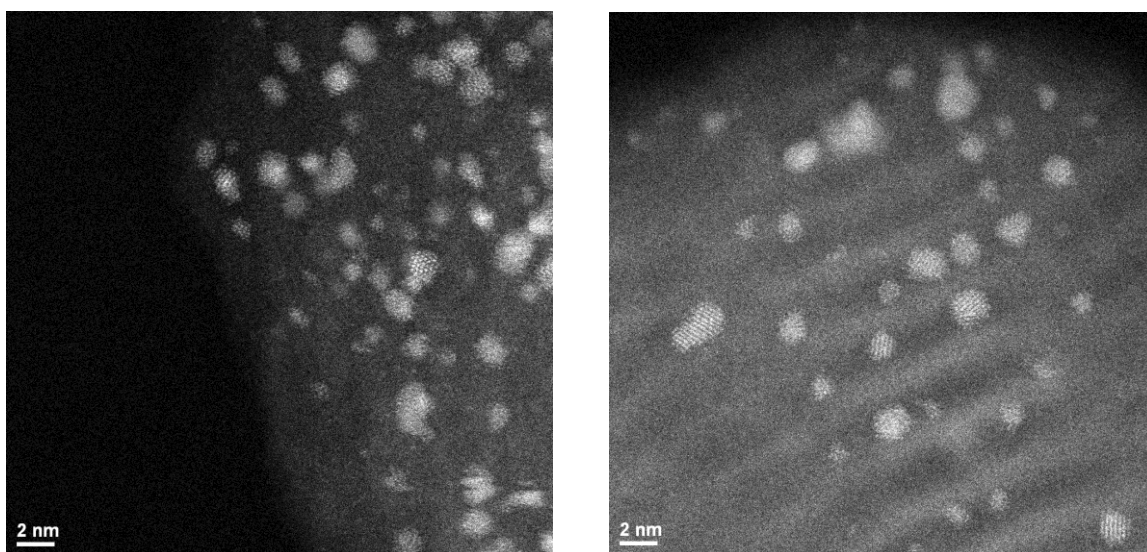
Figure 2.2 HAADF-HRTEM image of Ir$_3$Bi nano particles on MCM-41 before catalysis (on left, pretreated at 200 ℃ to remove the ligands) and after use in catalysis (on right, pretreated at 300 ℃) to remove the ligands.
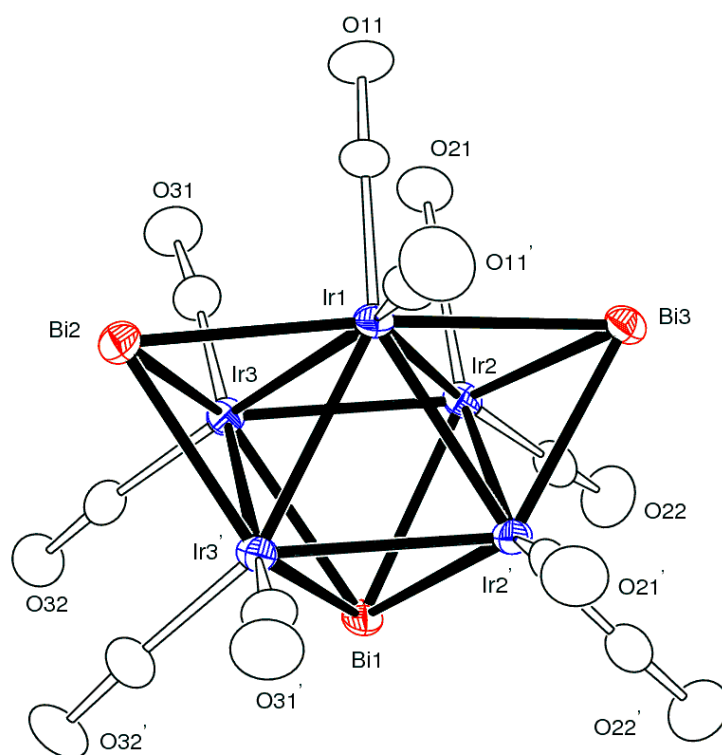
Figure 2.3 An ORTEP diagram of the molecular structure of $Ir_5(CO)_{10}(\mu_3\text{-Bi})_2(\mu_4\text{-Bi})$, **2.2,** showing 30% thermal probability.
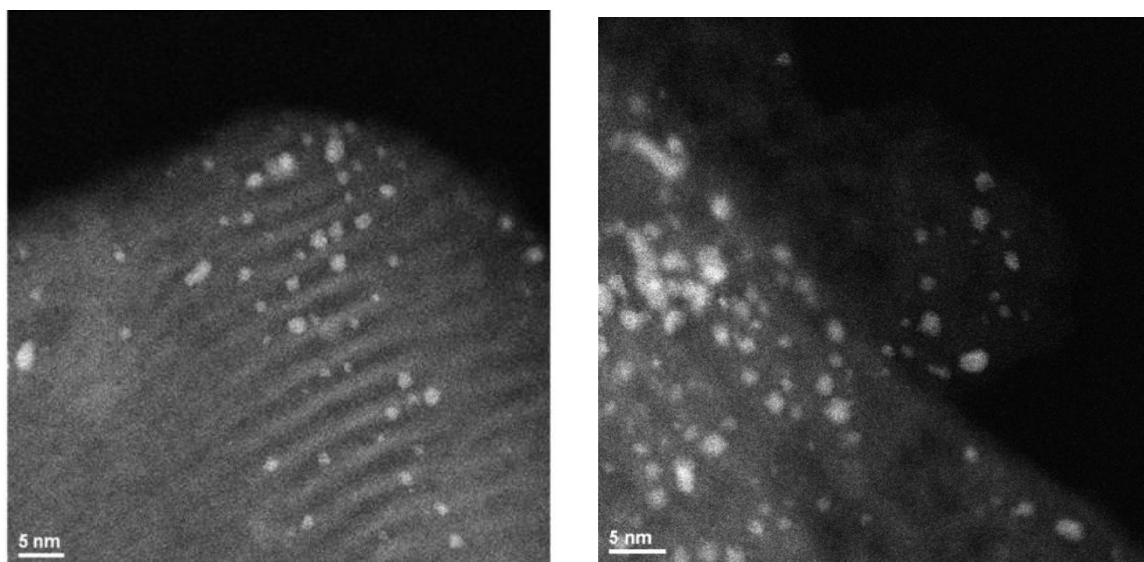
Figure 2.4 HAADF-HRTEM image of Ir_3Bi (on left) and Ir_5Bi_3 (on right) nano particles on MCM-41 after use in catalysis at 65 ºC . The catalysts were preconditioned/activated at 300 ºC for 2h before use.
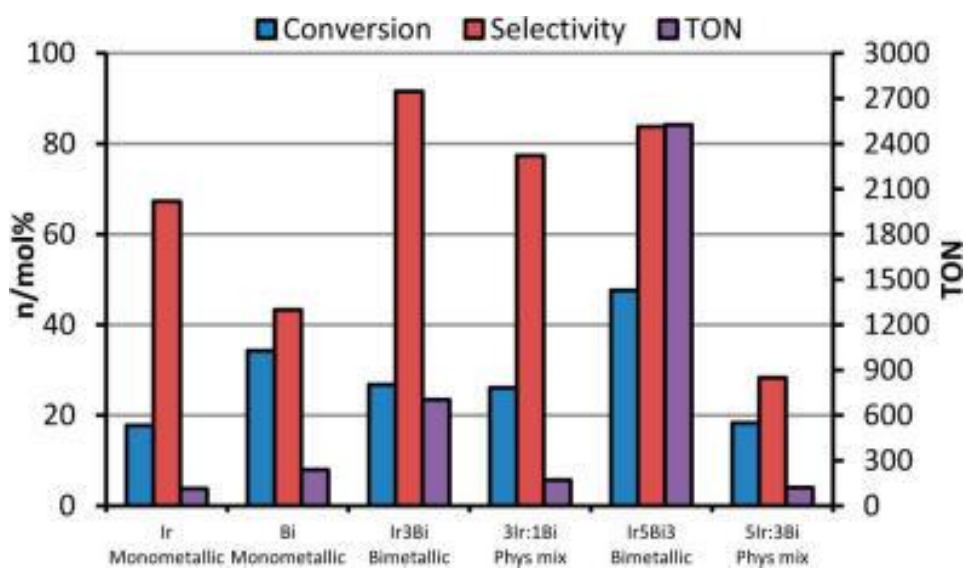
Figure 2.5.Comparisons of catalytic behavior of the monometallic and bimetallic Ir and Bi catalysts on MCM-41
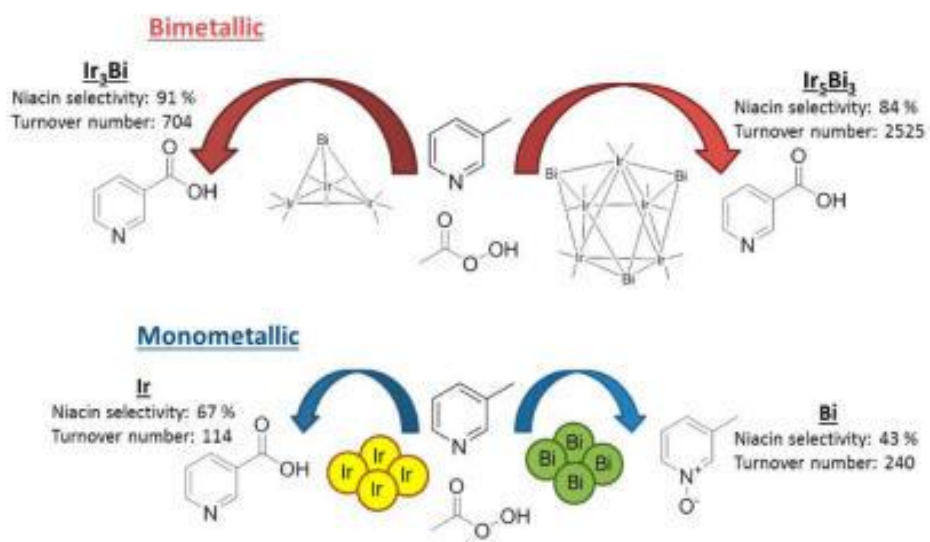
Figure 2.6.Schematic representation of the contrasting catalytic
behaviors afforded by the Ir/Bi containing catalysts

Effect of support - Ir$_3$Bi/MCM-41

◼ Conversion ◼ Selectivity ◼ Yield
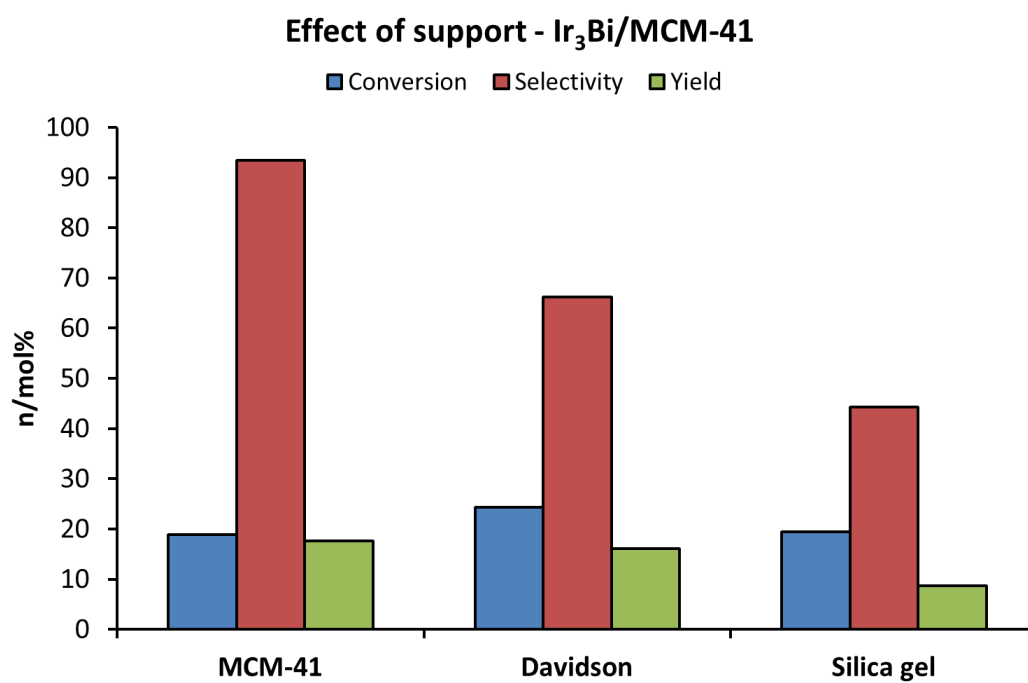
Figure 2.7 The effect of support in the oxidation of 3-picoline with Ir$_3$Bi
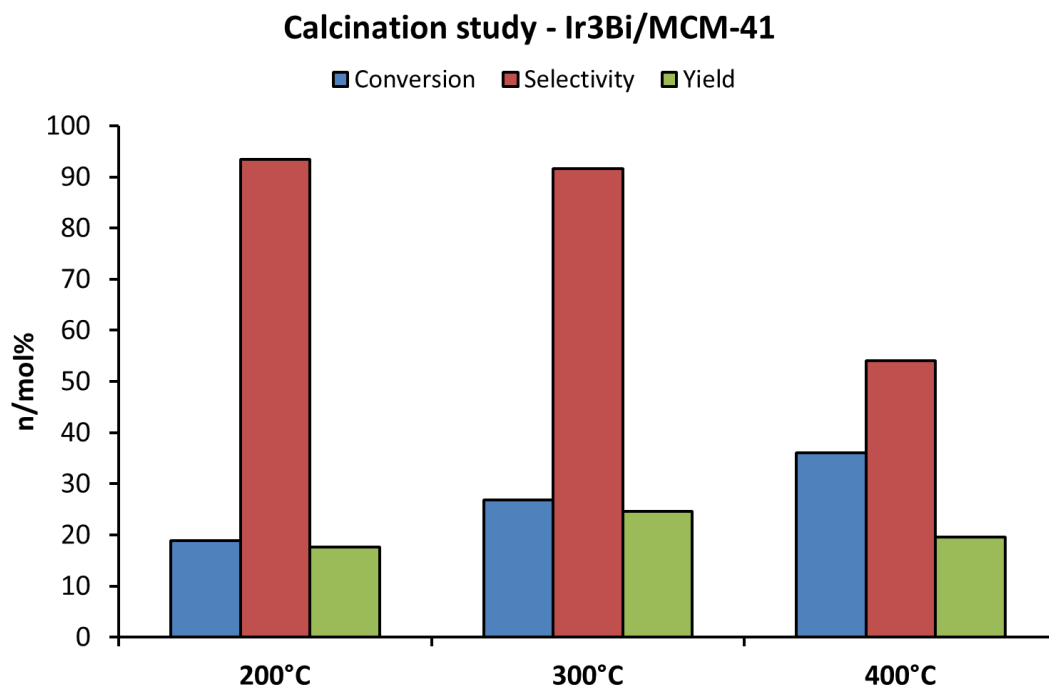
Figure 2.8 The effect of different calcination temperatures on the activity and selectivity of the Ir$_3$Bi/MCM-41 catalyst

Recycle study - Ir_5Bi_3/MCM-41 (300^oC)
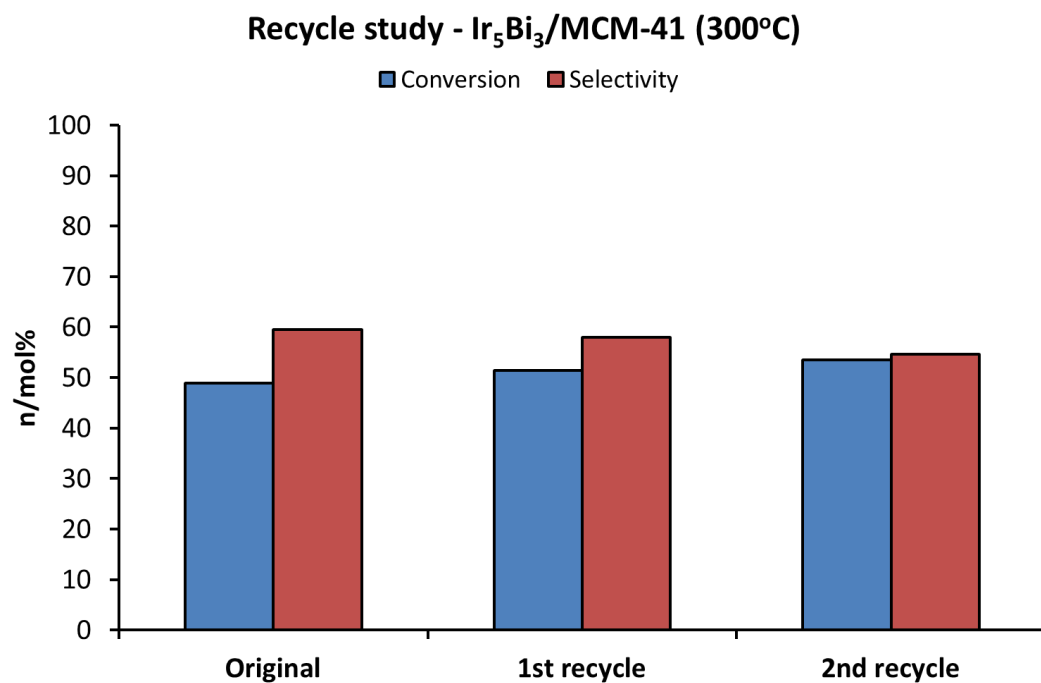
Figure 2.9 Catalyst recycle studies emphasizing the heterogeneous nature and recyclability of the anchored Ir_5Bi_3 catalyst
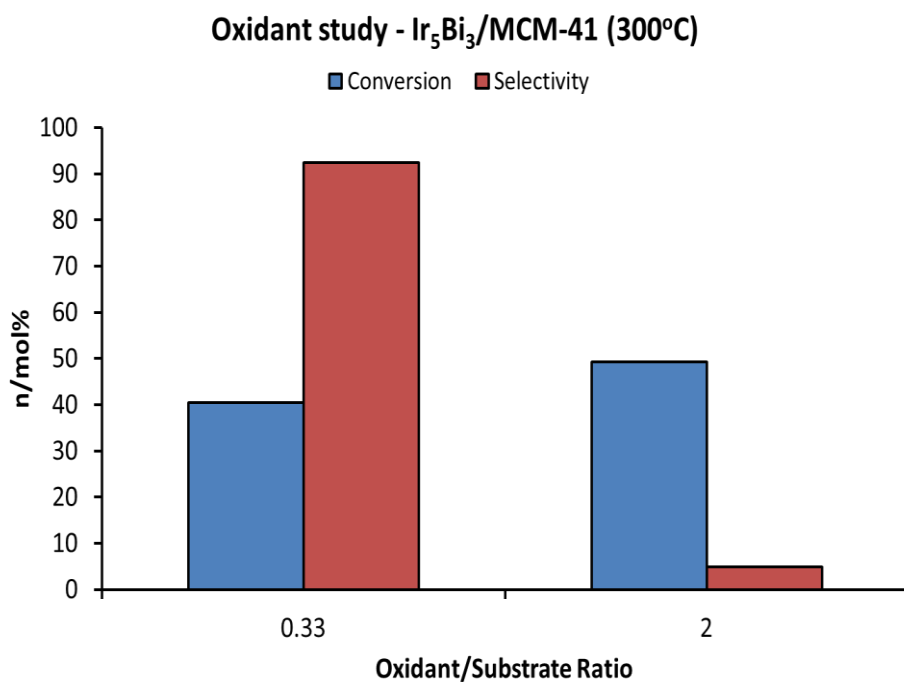
Figure 2.10 The effect of substrate:oxidant mole ratio on the activity and selectivity of the Ir_5Bi_3 catalyst for the oxidation of 3-picoline.

Ir$_3$(CO)$_9$(μ_3-Bi), **2.1**   Ir$_5$(CO)$_{10}$(μ_3-Bi$_2$)(μ_4-Bi) **2.2**
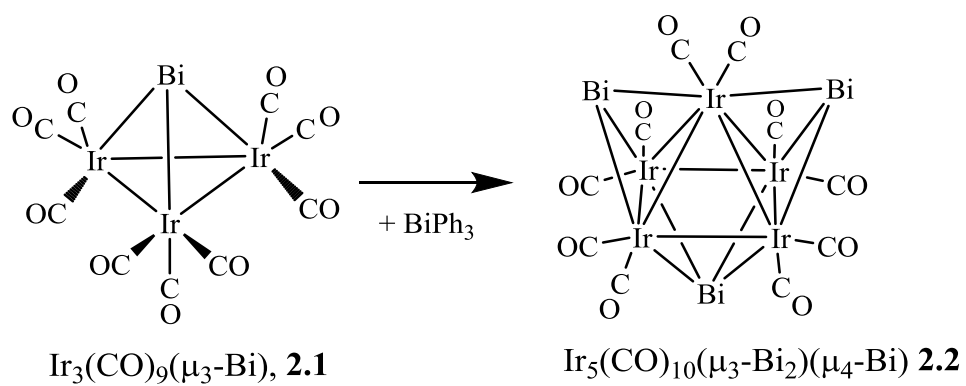
Scheme 2.1 Schematic of the transformation of **2.1** to **2.2** by
reactions with BiPh$_3$ (CO ligands are only shown as lines)

Table 2.1 Crystallographic data for 2.2[a]

Compound	**2.2**
Emperical formula	$Ir_5Bi_3C_{10}O_{10}$
Formula weight	1868.04
Crystal system	Orthorhombic
Lattice parameters	
a (Å)	16.3842(13)
b (Å)	14.3198(11)
c (Å)	9.2009(7)
α (deg)	90.00
β (deg)	90.00
γ (deg)	90.00
V (Å^3)	2158.7(3)
Space group	Pnma
Z value	4
ρ_{calc} (g / cm^3)	5.748
μ (Mo Kα) (mm^{-1})	55.096
Temperature (K)	294(2)
$2\Theta_{max}$ (°)	50.06
No. Obs. ($I > 2\sigma(I)$)	1982
No. Parameters	133
Goodness of fit (GOF)[a]	0.993
Max. shift in cycle	0.000
Residuals:[*] R1; wR2	0.0287; 0.0831
Absorption Correction,	Multi-scan
Max/min	1.000 / 0.315
Largest peak in Final Diff. Map ($e^-/\text{Å}^3$)	1.79

[*] $R1 = \Sigma_{hkl}(||F_{obs}| - |F_{calc}||)/\Sigma_{hkl}|F_{obs}|$; $wR2 = [\Sigma_{hkl}w(|F_{obs}| - |F_{calc}|)^2/\Sigma_{hkl}wF^2_{obs}]^{1/2}$; $w = 1/\sigma^2(F_{obs})$; $GOF = [\Sigma_{hkl}w(|F_{obs}| - |F_{calc}|)^2/(n_{data} - n_{vari})]^{1/2}$.

49

Table 2.2. Seven TEM EDS Composition Anal of the Ir3Bi catalyst on MCM-41 support; before use

Particle	Ir Atomic %	95% confidence	Bi Atomic %	95% confidence
1	78.67	±3.98	21.33	±3.66
2	80.95	±4.08	19.05	±3.76
3	75.24	±3.94	24.76	±3.62
4	75.23	±3.72	24.77	±3.44
5	75.31	±3.72	24.69	±3.42

Table 2.3. Seven TEM EDS Composition Anal of the Ir3Bi catalyst on MCM-41
support; after use

Particle	Ir Atomic %	95% confidence	Bi Atomic %	95% confidence
1	74.78	±8.66	25.22	±7.96
2	91.22	±4.36	8.78	±4.00
3	80.14	±3.24	19.86	±2.98
4	80.20	±2.76	19.80	±2.54
5	78.82	±4.66	21.18	±4.30
6	82.23	±5.80	17.77	±5.34
7	86.35	±4.58	13.65	±4.20

Table 2.4 Four EDS Composition Analyses of Ir_5Bi_3 catalyst after use on MCM-41support

Spectrum	Ir Atomic %	95% confidence	Bi Atomic %	95% confidence
1	62.46	±1.72	37.54	±1.58
2	64.93	±5.1	35.07	±4.68
3	64.38	±5.8	35.62	±5.32
4	75.92	±8.08	24.08	±7.44

Table 2.5 Selected intermolecular angles and bond distances for **2.2** [a]

Atom	Atom	Distance	Atom	Atom	Atom	Angle
Ir1	Ir2	2.7824(7)	Bi2	Ir1	Ir2	117.51(2)
Ir1	Ir3	2.8226(7)	Ir2	Ir1	Ir2	61.03(2)
Ir2	Ir3	2.7903(7)	Bi2	Ir1	Ir3	57.814(18)
Ir2	Ir2'	2.8255(9)	Ir2	Ir1	Ir3	89.74(2)
Ir3	Ir3'	2.7796(9)	Bi2	Ir1	Ir3	57.814(18)
Ir1	Bi3	2.8322(9)	Ir2	Ir1	Ir3	59.704(17)
Ir1	Bi2	2.7623(9)	Bi2	Ir1	Bi3	173.43(3)
Ir2	Bi3	2.6868(7)	Ir3	Ir1	Bi3	116.77(2)
Ir2	Bi1	2.8004(7)	Bi3	Ir2	Ir1	62.35(2)
Ir3	Bi2	2.7002(7)	Ir1	Ir2	Bi1	90.97(2)
Ir3	Bi1	2.8185(7)	Bi2	Ir3	Ir3	59.023(12)

[a] Estimated standard deviations in the least significant figure are given in parenthesis

R<small>EFERENCES</small>

(1) Hermans, S.; Raja, R.; Thomas, J. M.; Johnson, B. F. G.; Sankar,G.; Gleeson, D. *Angew. Chem., Int. Ed.* **2001**, *40*, 1211−1215.

(2) Adams, R. D.; Blom, D. A.; Captain, B.; Raja, R.; Thomas, J. M.;Trufan, E.*Langmuir* **2008**, *24*, 9223−9226.

(3) Adams, R. D.; Boswell, E. M.; Captain, B.; Hungria, A. B.;Midgley, P. A.; Raja, R.; Thomas,J. M.*Angew. Chem., Int. Ed.***2007**, *46*, 8182−8185.

(4) Hungria, A. B.; Raja, R.; Adams, R. D.; Captain, B.; Thomas, J.M.; Midgley, P. A.; Golovko,V.; Johnson, B. F. G.*Angew. Chem., Int.Ed.***2006**, *45*, 4782−4785.

(5) Thomas, J. M.; Adams, R. D.; Boswell, E. M.; Captain, B.;Gronbeck, H.; Raja, R.*FaradayDiscuss.***2008**, *138*, 301−315.

(6) Gianotti, E.; Shetti, V. N.; Manzoli, M.; Blaine, J. A. L.; Pearl, W.C., Jr.; Adams, R. D.; Coluccia, S.; Raja, R.*Chem.Eur. J.***2010**, *16*, 8202−8209.

(7) (a) Humphrey, S. M.; Grass, M. E.; Habas, S. E.; Niesz, K.;Somorjai, G. A.; Tilley, T. D.*Nano Lett.***2007**, *7*, 785−790.(b) Vicente, B. C.; Nelson, R. C.; Singh, J.; Scott, S. L.; van Bokhoven, J. A.*Catal. Today***2011**, *160*, 137−143. (c) Bal, R.; Tada,M.; Sasaki, T.; Iwasawa, Y. *Angew. Chem., Int. Ed.***2006**, *45*, 448−452.

(8) (a) Ide, M. S.; Hao, B.; Neurock, M.; Davis, R. J. *ACS. Catal.***2012**, *2*, 671−683. (b) Lobo-Lapidus, R. J.; McCall, M. J.; Lanuza, M.; Tonnesen, S.; Bare, S. R.; Gates, B. C.*J. Phys. Chem. C* **2008**, *112*, 3383−3391. (c) Boucher, M. B.; Zugic, B.; Cladaras, G.;Kammert,J.;Marcinkowski,M.;Latwon,T.J.;Sykes,E.C.H.;Flytzani Stephanopoulos, M.*Phys. Chem. Chem. Phys.***2013**, *15*, 12187−12196.

(9) Herzing, A. A.; Kiely, C. J.; Carley, A. F.; Landon, P.; Hutchings,G.   *J.Science* **2008**, *321* , 1331−1335.

(10) Ishia, T.; Kinoshita, N.; Okatsu, H.; Akita, T.; Takei, T.; Haruta, M.*Angew. Chem., Int. Ed.***2008**, *47*, 9265−9268.

(11) Corma, A.; Serna, *P.Science* **2006**, *313*, 332−334.

(12) Kesavan, L.; Tiruvalam, R.; Ab Rahim, M. H.; bin Saiman, M. I.;Enache, D. I.; Jenkins, R. L.; Dimitratos, N.; Lopez-Sanchez, J. A.;Taylor, S. H.; Knight, D. W.; Kiely, C. J.; Hutchings, G. *J.Science* **2011**, *331*, 195−199.

(13) Hinde, C. S.; Van Aswegen, S.; Collins, G.; Holmes, J. D.; Hor,T. S.; Raja, R. *Dalton Trans.***2013**, *42*, 12600−12605.

(14) Manzoli, M.; Shetti, V. N.; Blaine, J. A. L.; Zhu, L.; Isrow, D.;Yempally, V.; Captain, B.; Coluccia, S.; Raja, R.; Gianotti, E.*DaltonTrans.***2012**, *41*, 982−989.

(15) (a) Dumitriu, D.; Barjega, R.; Frunza, L.; Macovei, D.; Hu, T.;Xie, Y.; Parvulescu, V. I.; Kaliaguine, S.*J. Catal.***2003**, *219*, 337−351. (b) Zhao, J.; Qian, G.; Li, F.; Zhu, J.; Ji, S.; Li, L.Chin. *J. Catal.***2012**, *33*, 771− 776. (c) Qian, G.; Ji, D.; Lu, G.; Zhao, R.; Qi, Y.; Suo, J.*J.Catal.***2005**, *232*, 378−385.

(16) Hanna, T. A.*Coord. Chem. Rev.***2004**, *248*, 429−440.

(17) Rass, H. A.; Essayem, N.; Besson, M.*Green Chem.***2013**, *15*, 2240−2251.

(18) Wenkin, M.; Ruiz, P.; Delmon, B.; Devillers, M.J. *Mol. Catal. A:Chem.***2002**, *180*, 141−159.

(19) He, Y.; Wu, Y.; Yi, X.; Weng, W.; Wan, H.J. *Mol. Catal. A:Chem.***2010**, *331*, 1−6.

(20) Kruppa, W.; Blaeser, D.; Boese, R.; Schmid, G.*Org. Chem.***1982**, 37B(2), 209−213.

(21) SAINT+, version 6.2a, Bruker Analytical X-ray Systems, Inc., Madison, WI, **2001**.

55

(22) G. M. Sheldrick, SHELXTL, version 6.1, Bruker Analytical X-ray Systems, Inc., Madison, WI, **1997**

(23) Kirkland, J. B. *Niacin. In Handbook of Vitamins* 4th ed.; Rucker, R., Zempleni, J., Suttie, J. W., McCormick, D. B., Eds.; Taylor and Francis: New York, 2007; pp 191−232.

(24) (a) Ali, K. M.; Wonnerth, A.; Huber, K.; Wojta, J. Br. *J. Pharmacol.* **2012**, *167*, 1177− 1194. (b) Grundy, S. M. *Am. J. Cardiol.* **1992**, *70*, I27−I32.

(25) Chuck, R.*Appl. Catal. A* **2005**, *280*, 75−82

(26) Petzoldt, J.; Wilmer, H.; Rosowski F. WO Patent, WO**2005**/118, 2005.

(27) Shaw, N. M.; Robins, K. T.; Kiener, A. *Adv. Synth. Catal.* **2003**, *345*, 425−435.

(28) (a) Raja, R.; Thomas, J. M.; Greenhill-Hooper, M.; Doukova, V.*Chem. Commun.***2007**,1924−1926. (b) Vishnuvarthan, M.; Paterson, A. J.; Raja, R.; Piovani, A.;Bonino, F.; Gianotti, E.; Berlier, G. Microporous Mesoporous Mater. **2011**, *138*, 167−175. (c) Raja, R.;Thomas, J. M.; Xu, M.; Harris, K. D. M.; Greenhill-Hooper, M.; Quill,K.*Chem.Commun*.**2006**, 448−450.

(29) (a) Mallat, T.; Bodnar, Z.; Hug, P.; Baiker, A.*J. Catal*. **1995**, *153*, 131−143. (b) Brandner, A.; Lehnert, K.; Bienholz, L. M.; Claus, P.*Top. Catal*.**2009**, *52*, 278−287. (c) Jang, J. H.; Goddard, W. A., III*Top. Catal*.**2001**, *15*, 273−289. (d) Jang, J. H.; Goddard, W. A., III *J. Phys. Chem*. B**2002**, *106*, 5997−6013. (e) Pudar, S.; Oxgaard, J.;Chenoweth, K.; van Duin, A. C. T.; Goddard, W. A., III *J. Phys. Chem.C* **2007**, *111*, 16405−16415

CHAPTER 3

SYNTHESIS AND CHARACTERIZATIONS OF BISMUTH-BRIDGED TRIIRIDIUM CARBONYL
COMPLEXES CONTAINING GERMYL/GERMYLENE AND STANNYL/STANNYLENE LIGANDS[2]

57

Introduction

Germanium[1] and tin[2] are well known to be valuable modifiers for heterogeneous transition metal catalysts. Studies have shown that mixed metal cluster complexes can serve as precursors to valuable bi- and multi-metallic supported heterogeneous catalysts.[3] In recent studies we have synthesized a variety of transition metal carbonyl complexes containing germanium and tin ligands. Triphenylgermane, Ph_3GeH,[4] and triphenylstannane, Ph_3SnH,[5] react with polynuclear metal carbonyl complexes to yield cluster complexes containing bridging germylene/stannylene ligands **A** and/or bridging germylyne/stannylyne ligands **B** and **C**, E = Ge or Sn,(Figures 3.1-3.3); CO ligands are shown only as lines from the metal atoms, M = 2nd or 3rd row transition metal atom. These reactions invariably proceed through intermediates containing triphenylgermyl or triphenylstannyl ligands EPh_3, **D**, E = Ge or Sn. The bridging germylene/stannylene and bridging germylyne/stannylyne ligands are formed by the cleavage of phenyl group(s) from the triphenylgermyl and triphenylstannyl ligands. If hydride ligands are present in the complex, the phenyl groups are often eliminated from the complex in the form of benzene,(Figure 3.4) [4c,5b] and (Figure 3.5.) [6] It has recently been shown by a computational analysis that the α-cleavage of a phenyl group from a $GePh_3$ ligand in the transformation of the triiridium complex $Ir_3(CO)_6(\mu\text{-}CO)(\mu\text{-}GePh_2)_2(GePh_3)_3$ into the complex $Ir_3(CO)_6(\eta^1\text{-}Ph)(\mu\text{-}GePh_2)_3(GePh_3)_2$, (Figure 3.6), occurs at a single iridium atom.[7]

We have recently shown that rhenium-bismuth and rhenium-antimony carbonyl complexes can serve as precursors to excellent catalysts for the ammoxidation of 3-picoline.[8] In the present work, we have investigated the reactions of $Ir_3(CO)_9(\mu_3\text{-}Bi)$,

58

3.1(Figure 3.7) [9] the only previously known bismuth containing iridium carbonyl cluster complex, with Ph_3GeH and Ph_3SnH. The results of these studies are reported herein.

Experimental Details

General Data.

Reagent grade solvents were dried by the standard procedures and were freshly distilled prior to use. Infrared spectra were recorded on a Thermo Nicolet Avatar 360 FT-IR spectrophotometer. Room temperature ^1H NMR spectra were recorded on a Varian Mercury 300 spectrometer operating at 300.1 MHz. Variable temperature ^1H NMR spectra for compounds **3.2** and **3.3** were recorded on a Varian Mercury 400 spectrometer operating at 161.9 MHz. Positive/negative ion mass spectra were recorded on a Micromass Q-TOF instrument by using electrospray (ES) ionization. $Ir_4(CO)_{12}$ and $BiNO_3 \cdot 5H_2O$ were obtained from STREM and Ph_3GeH and Ph_3SnH were obtained from Gelest and Aldrich respectively and were used without further purification. $[PPN]Ir(CO)_4$[10] were prepared according to the previously reported procedures. $Ir_3(CO)_9(\mu_3\text{-Bi})$, **3.1** were prepared by a modification of the previously reported procedure,[9]. Product separations were performed by TLC in air on Analtech 0.25 silica gel 60 Å F254 glass plates. Dynamic NMR simulations for compounds **3.2** and **3.4** were performed by using the SpinWorks program.[11] The exchange rates were determined at seven different temperatures in the temperature range -20 to +60 ºC. The activation parameters were determined from a least squares Erying plot by using the program Microsoft Excel 2007.

Synthesis of $Ir_3(CO)_9(\mu_3\text{-Bi})$, 3.1

$Ir_3(CO)_9(\mu_3\text{-Bi})$ was prepared by a modified procedure of the method published by Schmid and co-workers.[9] In a typical experiment, 100.0 mg (0.1187 mmol) of $[PPN][Ir(CO)_4]$ was dissolved in 25 mL of THF in ice-bath for 5 min. Then 21.0 mg (0.0432 mmol) of $Bi(NO_3)_3\cdot5H_2O$ was added to the above solution and the mixture was stirred in ice-bath for 1 h. The solvent was removed *in vacuo*, and the product was then isolated by TLC using a 3/1 hexane/methylene chloride solvent mixture. 25.2 mg (61% yield) of yellow $Ir_3(CO)_9(\mu_3\text{-Bi})$, **3.1** was obtained.

Synthesis of $Ir_3(CO)_6(GePh_3)_3(\mu_3\text{-Bi})(\mu\text{-H})_3$, 3.2.

18.1 mg (0.05157 mmol) of Ph_3GeH was added to 13.9 mg (0.01340 mmol) of $Ir_3(CO)_9(\mu_3\text{-Bi})$ in 15 ml of methylene chloride. The reaction was heated to reflux for 7 h. The solvent was removed *in vacuo*, and the product was then isolated in a pure form by TLC by using a 4:1 hexane/methylene chloride solvent mixture. 8.0 mg (31% yield) of $Ir_3(CO)_6(GePh_3)_3(\mu_3\text{-Bi})(\mu\text{-H})_3$, **3.2**, was obtained. Spectral data for **3.2**: IR ν_{CO} (cm^{-1} in CH_2Cl_2): 2058(s), 2025(s), 2074(w). ^1H NMR (at -20 °C, in $CDCl_3$) δ = -17.63 (s, 3H, Ir - H), -17.14 (d, $J_{H\text{-}H}$ = 2.4 Hz, 1H, Ir-H, isomer B), -17.25 (d, $J_{H\text{-}H}$ = 2.4 Hz, 1H, Ir-H, isomer B), -17.55 (s, 1H, Ir-H, isomer B); at 25 °C, in CD_2Cl_2) δ = 7.25 − 7.49 (m, 45H, Ph), -17.24 (s, 1H, Ir-H, isomer B), -17.33 (s, 1H, Ir-H, isomer B), -17.57 (s, 1H, Ir-H, isomer B) , -17.68 (s, 3H, Ir – H, isomer A); at 60 °C, in $CDCl_3$, δ = -17.55 (s). The ratio of **A/B** was 7/3 at room temperature. Mass Spec: ES^- m/z = 1867 (M - H^-). UV-vis in CH_2Cl_2: λ_{max}= 559 nm, ε_{559} = 952 $L\cdot mol^{-1}\cdot cm^{-1}$; λ_{max} = 494 nm, ε_{494} = 2085 $L\cdot mol^{-1}\cdot cm^{-1}$; λ_{max} = 426 nm, ε_{426} = 9305 $L\cdot mol^{-1}\cdot cm^{-1}$.

60

Conversion of 3.2 to Ir$_3$(CO)$_6$(GePh$_2$)$_3$(μ$_3$-Bi), 3.3 .

10.20 mg (0.005274 mmol) of **3.2** was added to 10 ml of hexane. The reaction was heated to reflux for 4.5 h. The solvent was removed *in vacuo*, and the product was then isolated by TLC using a 4:1 hexane/methylene chloride solvent mixture. 7.60 mg (87% yield) of **2**. Spectral data for **2**: IR ν_{CO} (cm^{-1} in CH$_2$Cl$_2$): 2018(s), 1996(m), 2044(w). ^{1}H NMR (CDCl$_3$, in ppm) δ = 7.28-7.54 (m, 30H, Ph). Mass Spec: ES$^-$, m/z = 1679 (M + CO$_2$H$^-$).

Reaction of Ir$_3$(CO)$_9$(μ$_3$-Bi), 3.1 with Ph$_3$SnH

23.3 mg (0.0663 mmol) of Ph$_3$SnH was added to 17.2 mg (0.0166 mmol) of Ir$_3$(CO)$_9$(μ$_3$-Bi) in 15 ml of hexane. The reaction was heated to reflux for 4 h. The solvent was removed *in vacuo*, and the product was then isolated by TLC by using a 4:1 hexane/methylene chloride solvent mixture. 6.20 mg (21% yield) of Ir$_3$(CO)$_6$(μ-SnPh$_2$)$_3$(μ$_3$-Bi), **3.5** and 1.00 mg (3 % yield) of Ir$_3$(CO)$_6$(SnPh$_3$)$_3$(μ -H)$_3$(μ$_3$-Bi), **3.4** were obtained. Spectral data for **3.4**: IR ν_{CO} (cm^{-1} in CH$_2$Cl$_2$): 2053(s), 2020(s), 2068(w). ^{1}H NMR (at 25 ºC in CDCl$_3$): δ = 7.30 – 6.84 (m, 45H, Ph), -17.10 (s, 1H, Ir – H, isomer B), -17.50 (s, 1H, Ir – H, isomer B), -18.42 (s, 1H, Ir – H, isomer B), -17.99 (s, 3H, Ir – H, isomer A); (at -15 ºC in CDCl$_3$) δ = -17.10(s, 1H, Ir-H, isomer B) , δ = -17.52 (s, 1H, Ir-H, isomer B) , δ = -18.44 (s, 1H, Ir-H, isomer B) , δ= -18.01 (s, 3H, Ir-H, J $_{Sn-H1}$ = 25.2Hz , J$_{Sn-H2}$ = 92.9Hz, isomer A. The ratio of **A/B** was 7/3 at room temperature. Mass Spec: ES$^-$, m/z = 2005 (M - H$^-$). Spectral data for **4**: IR ν_{CO} (cm^{-1} in CH$_2$Cl$_2$): 2006 (s), 1984 (m), 2032(w), 1970(w). ^{1}H NMR (CDCl$_3$, in ppm) δ = 7.74 - 7.12 (m, 30H, Ph). Mass Spec: ES$^-$,m/z = 1817 (M + CO$_2$H$^-$).

Crystallographic Analyses:

Orange single crystals of **3.2** suitable for x-ray diffraction analyses were obtained by slow evaporation of solvent from a hexane/methylene chloride solvent mixture at -25 °C. Red single crystals of **3.3** suitable for x-ray diffraction analyses were obtained by slow evaporation of hexane at -25 °C. Yellow single crystals of **3.4** suitable for x-ray diffraction analyses were obtained by slow evaporation of heptane at -5 °C. Red single crystals of **3.5** suitable for x-ray diffraction analyses were obtained by slow evaporation of solvent from a hexane/methylene chloride solvent mixture at -25 °C. Each data crystal was glued onto the end of a thin glass fiber. X-ray intensity data were measured by using a Bruker SMART APEX CCD-based diffractometer using Mo Kα radiation (λ = 0.71073 Å). The raw data frames were integrated with the SAINT+ program by using a narrow-frame integration algorithm.[12] Correction for Lorentz and polarization effects were also applied with SAINT+. An empirical absorption correction based on the multiple measurement of equivalent reflections was applied using the program SADABS. All structures were solved by a combination of direct methods and difference Fourier syntheses, and refined by full-matrix least-squares on F^2, using the SHELXTL software package.[13] All non-hydrogen atoms were refined with anisotropic displacement parameters. The hydride ligands H1 and H3 in **1** were located and refined. The hydride ligand H2 was located and refined with the constraint Ir − H = 1.80 Å. All other hydrogen atoms were calculated and placed in geometrically idealized positions and included as standard riding atoms during the final cycles of least-squares refinement. Crystal data, data collection parameters, and results of the analyses are listed in Table 3.1.

Compounds **3.2** and **3.3** crystallized in the monoclinic crystal system. The space group *C*2/c was indicated by the systematic absences in the data and confirmed by the successful solutions and refinements for both structures. One molecule of hexane was co-crystallized with **3.2** in the asymmetric crystal unit. The carbon atoms of the hexane were refined with constraints, C – C = 1.44 Å, and hydrogen atoms on the hexane molecule were ignored. One quarter of a molecule of methylene chloride was cocrystallized with **3.3** in the asymmetric crystal unit. Compounds **3.4** and **3.5** both crystallized in the trigonal crystal system. The space group *P*31c was indicated based on the systematic absences in the data and confirmed by the successful solutions and refinements of both structures. For compound **3.4**, two phenyl rings on Sn2 (C5-C10 and C17-C22) were disordered over two sites with 50% populations each. The disorder is a rotation about the Sn-C(ipso) bond. Each of the four half-occupied rings was refined as a regular hexagon with C - C bonds constrained to 1.39 Å and the carbon atoms were refined with a single isotropic thermal parameter for both of the two disordered rings. For compound **3.4**, the unit cell contains several solvent molecules (total potential solvent accessible void vol = 128.2 $Å^3$ and electron count/cell = 11) which have been treated as a diffuse contribution to the overall scattering without specific atom positions by SQUEEZE/PLATON. The crystal of **4.5** was also refined as an inversion twin based on the absolute structure (Flack) parameter near the end of the refinement. The fraction of the minor twin domain refined to 0.11(1). The unit cell of **4.5** contains solvent molecules (Total Potential Solvent Accessible Void volume is 1020.0 $Å^3$ and Electron Count/Cell is 373) which was treated as a diffuse contribution to the overall scattering without specific atom positions by SQUEEZE/PLATON.

Computational Details.

All density functional theory (DFT) calculations were performed with the Amsterdam Density Functional (ADF) suite of programs[14a] by using the PBEsol functional[14b] with Slater-type triple-zeta polarized TZP basis sets with small frozen cores, and scalar relativistic correction. The geometric structure of **3 .4** was optimized as gas-phase. The time-dependent DFT (TDDFT) calculation was performed at the same theory level. The transitions to triplet and higher order multiplet excited states from the ground state are forbidden because the ground states of the species in this study are singlets. Even if some of these forbidden transitions gain intensity by spin-orbit splitting, their intensities in absorption spectrum should still be very weak relative to the transitions to the singlet excited states.

Results and Discussion

The new compound $Ir_3(CO)_6(GePh_3)_3(\mu_3-Bi)(\mu-H)_3$, **3.2** was obtained in 31% yield from the reaction of $Ir_3(CO)_9(\mu_3-Bi)$, **3.1** with Ph_3GeH in a solution in methylene chloride solvent at reflux for 7 h. Compound **3.2** was characterized by a combination of IR and ^1H NMR spectroscopy, mass spectrometry and a single-crystal X-ray diffraction analysis. An ORTEP diagram of the molecular structure of **3.2** is shown in Figure 3.8. Like its parent $Ir_3(CO)_9(\mu_3-Bi)$, compound **3.2** consists of a triangle of three iridium atoms with a triply-bridging bismuth atom. Each Ir atom contains one $GePh_3$ ligand that lies approximately in the plane of the Ir_3 triangle. Each Ir atom also contains two terminal CO ligands; one lies in the plane of the Ir_3 triangle; the other lies approximately

64

perpendicular to the plane of the Ir_3 triangle. Overall the Ir_3BiGe_3 portion of the molecule has approximate C_3 symmetry. There are three bridging hydride ligands; one on each Ir – Ir bond. They lie approximately on the plane of the Ir_3 triangle. The Ir – Ir bond distances in **3.2**, Ir(1) – Ir(2) = 3.0094(8) Å, Ir(1) – Ir(3) = 3.0071(8) Å, Ir(2) – Ir(3) = 3.0073(9) Å, are significantly longer than those found in $Ir_3(CO)_9(\mu_3$-Bi), 2.759(2) Å.[9] This is probably due to the presence of three bridging hydride ligands,[15] but may also be due in part by steric effects produced by the bulky $GePh_3$ ligands. The Ir – Bi distances in **3.2**, Ir(1) – Bi(1) = 2.7610(9) Å, Ir(2) – Bi(1) = 2.7597(9) Å, Ir(3) – Bi(1) = 2.7668(9) Å are quite similar to the Ir – Bi distances in $Ir_3(CO)_9(\mu_3$-Bi), 2.734(2) Å. The Ir – Ge distances in **3.2**, Ir(1) – Ge(1) = 2.5032(18) Å, Ir(2) – Ge(2) = 2.5054(16) Å, Ir(3) – Ge(3) = 2.5046(18) Å, are significantly shorter than the Ir – $GePh_3$ distances found in the triiridium complexes: $Ir_3(CO)_6(\mu$-CO)$(\mu$-$GePh_2)_2(GePh_3)_3$,[7] 2.5098(14), 2.5155(16) and 2.5401(15), $Ir_3(CO)_6(\eta^1$-Ph)$(\mu$-$GePh_2)_3(GePh_3)_2$,[7] 2.551(2), 2.5519(19), and $Ir_3(CO)_6(\mu$-$GePh_2)_3(GePh_3)_3$, 2.5754(7), 2.5959(7), and 2.5534(8) Å.[16] This may be due to steric crowding caused by the presence of three hydride ligands that lie in the Ir_3 plane of **1** but are not present in the other molecules. The metal atoms in compound **3.2** contain total of 48 electrons, thus each metal atom formally has an 18 electron configuration.

The ^1H NMR spectrum of **3.2** can be interpreted only by the presence of two isomers in solution. The major isomer **A** shows as single resonance at δ = -17.67. This resonance can be attributed to the structure of **3.2** as found in the solid state. Three additional hydride resonances observed at δ = -17.24, -17.33 and -17.57 each of intensity one can be attributed to a less symmetric isomer **B**. The ratio of **A/B** was 7/3 at room temperature. The structure proposed for isomer **B** is shown in Figure 3.9. This isomer is

preferred over other possibilities because the GePh$_3$ ligands all lie in the Ir$_3$ plane as found in isomer **A**. Isomer **B** has C$_1$ symmetry and thus the three hydride ligands are inequivalent. The resonances of both isomers are broad at room temperature which is indicative of a dynamical exchange process that is rapid on the ^{1}H NMR timescale. This process was confirmed by variable temperature NMR measurements. The resonances sharpen at lower temperature and broaden and merge into a broad average resonance at δ = -17.55 when the temperature is raised to 60 $^\circ$C. A stacked plot of the hydride spectra at various temperatures is shown in Figure 3.10. A polytopal trigonal-twist mechanism, as has been observed for M(CO)$_3$ groups and phosphine-substituted M(CO)$_3$ groups in metal carbonyl cluster complexes,[17] is proposed to explain the isomerization of isomers **A** and **B**, (Scheme 3.1). Line shape analyses provided rates which provided the following activation parameters for the process: $\Delta H^{\ddagger}$ = 49.5 KJ/mol, $\Delta S^{\ddagger}$ = 29.7 J/K·mol.

When a solution of **3.2** was heated to reflux in hexane solvent for 4.5 h, it was converted into compound **3.3** in 87% yield. Compound **3.3** was also characterized by a single-crystal X-ray diffraction analysis and an ORTEP diagram of the molecular structure of **3.3** is shown in Figure 3.11. Compound **3.3** consists of an Ir$_3$ triangular cluster with a triply bridging bismuth atom. There are three bridging GePh$_2$ ligands, one across each Ir – Ir bond and two terminal CO ligands on each Ir atom. One CO ligand lies approximately in the plane of the Ir$_3$ triangle; the other is approximately perpendicular to it. The Ir – Ir bond distances in **3.3**, Ir(1) – Ir(2) = 2.8356(14) Å, Ir(2) – Ir(3) = 2.8383(15) Å, Ir(1) – Ir(3) = 2.8568(15) Å, are significantly shorter than those in **3.1** but longer than those in Ir$_3$(CO)$_9$(μ_3-Bi).[9] The Ir – Bi distances in **3.3**, Ir(1) – Bi(1) = 2.7651(12) Å, Ir(2) – Bi(1) = 2.7678(13) Å, Ir(3) – Bi(1) = 2.7751(12) Å, are virtually

66

www.manaraa.com

the same as those in **3.2**. The Ir – Ge distances to the bridging GePh$_2$ ligands, Ir(1) – Ge(1) = 2.516(2) Å, Ir(2) – Ge(1) = 2.477(2) Å, Ir(2) – Ge(2) = 2.509(2) Å, Ir(3) – Ge(2) = 2.487(2) Å, Ir(3) – Ge(3) = 2.506(2) Å, Ir(1) – Ge(3) = 2.498(2) Å, are very similar to the Ir – Ge distances to the terminal GePh$_3$ ligands in **3.2**. The transformation of **3.2** to **3.3** involves the cleavage of a phenyl ring from each of the GePh$_3$ ligands in **3.2** and their elimination from the molecule together with the hydride ligands, presumably in the form of benzene, (Scheme 3.2.) Like **3.2**, the metal atoms in compound **3.3** contain at total of 48 electrons, and each metal atom formally has an 18 electron configuration.

The reaction of Ir$_3$(CO)$_9$(μ$_3$-Bi) with Ph$_3$SnH is similar to the reaction of Ir$_3$(CO)$_9$(μ$_3$-Bi) with Ph$_3$GeH except that both products Ir$_3$(CO)$_6$(SnPh$_3$)$_3$(μ-H)$_3$(μ$_3$-Bi), **3.4** (3% yield) and **3.5** (21% yield) are obtained together. The yield of **3.4** is very low and could not be improved by doing the reaction at lower temperature. Compounds **3.4** and **3.5** were both characterized crystallographically. ORTEP diagrams of the molecular structures of **3.4** and **3.5** are shown in Figures 3.12 and 3.13, respectively. The structures of **3.4** and **3.5** are analogous to those of **3.2** and **3.3** with the replacement of the GePh$_3$ ligands with SnPh$_3$ ligands and GePh$_2$ ligands with SnPh$_2$ ligands. Compounds **3.4** and **3.5** both crystallized in the space group *P*31c and have crystallographically imposed C$_3$ symmetry. Due to the large number of heavy atoms, it was not possible to locate the hydride ligands in the structural analysis of **3.4**. The Ir – Ir and Ir – Bi distances are similar to those in **3.2** and **3.3**, respectively. The Ir – Sn distances, Ir – SnPh$_3$ = 2.660(1) Å and Ir – SnPh$_2$ = 2.6347(16) Å and 2.6437(16) Å are similar to those found in Ir$_3$(CO)$_6$(SnPh$_3$)$_3$(μ-SnPh$_2$)$_3$.[5c]

The ^{1}H NMR spectrum of **3.4** shows that it also exists in solution as a mixture of two isomers **A** and **B** in a 7/3 ratio at room temperature, δ = 7.30 – 6.84 (m, 45H, Ph), -17.10 (s, 1H, Ir – H, isomer B), -17.50 (s, 1H, Ir – H, isomer B), -18.42 (s, 1H, Ir – H, isomer B) and -17.99 (s, 3H, Ir – H, isomer A). Like **3.2**, these isomers are also in a dynamic equilibrium. Line shape analyses of the spectra at different temperatures provided the following activation parameters: $\Delta H^{\ddagger}$= 69.8 KJ/mol, $\Delta S^{\ddagger}$ = 26.1 J/K·mol.

Compounds **3.3** and **3.4** are a dark red in color indicating that they have significant absorptions in the visible region of the spectrum. Since they are both electronically saturated, we decided to investigate the spectrum of **3.3** in detail. A UV-vis absorption spectrum of **3.3** is shown in Figure 3.14. There are three absorptions: λ_{max}= 559 nm, ε_{559} = 952 L•mol^{-1}•cm^{-1}; λ_{max} = 494 nm, ε_{494} = 2085 L•mol^{-1}•cm^{-1}; λ_{max} = 426 nm, ε_{426} = 9305 L•mol^{-1}•cm^{-1}. The broad absorption at 494 nm is responsible for the observed red color of the compound. In order to understand the bonding and electronic transitions in **3.3**, geometry-optimized DFT and TD-DFT molecular orbital calculations were performed by using the PBEsol functional of the Amsterdam Density Functional program library. Important selected molecular orbitals for **3.3** are shown in Figure 3.15. The MOs HOMO through HOMO-4 are dominated by bonding between the bismuth atom and the iridium atoms. The LUMO is Ir - Ir antibonding across the Ir$_3$ triangle. The UV – vis absorption spectrum for **3.3** was calculated from our geometry-optimized structure by using a time-dependent PBEsol calculation is shown in Figure 3.16. The calculated absorptions appear are (1) at 556 nm, which is a combination of two transitions: the HOMO-1 to LUMO, f = 0.043 and HOMO-2 to LUMO, f = 0.051; (2) at 486 nm, which is a combination of two transitions: the HOMO-3 to LUMO, f = 0.040 and HOMO-4 to

68

LUMO, f = 0.022; and (3) at 404 nm, which involves transitions from the phenyl rings to the LUMO and LUMO+1. Calculated transition (1) corresponds to the observed transition at 559 nm. Calculated transition (2) corresponds to the observed transition at 496 nm. Calculated transition (3) corresponds to the observed transition at 426 nm. The excitations for the absorptions in the visible region, 559 nm and 496 nm, are due electronic transitions from the Ir - Bi bonding orbitals to the antibonding Ir − Ir LUMO, (Figure 3.15).

Summary

The tris-EPh$_3$ complexes **3.2.** and **3.3**, E = Ge and Sn, were obtained from the reactions of Ir$_3$(CO)$_9$(μ_3-Bi) with the compounds Ph$_3$EH. They can be converted into the tris-EPh$_2$, complexes **3.3** and **3.5**, E = Ge and Sn, thermally by cleavage and elimination of a phenyl ring from each EPh$_3$ ligand together with the elimination of the three hydride ligands. These transformations are similar to the transformations of the compounds Ru$_3$(CO)$_9$(EPh$_3$)$_3$(μ-H)$_3$, E = Ge and Sn, into the compounds Ru$_3$(CO)$_9$(μ-EPh$_2$)$_3$, Figure 3.3,[4c,5b] further demonstrating the scope and viability of these phenyl cleavage reactions for the synthesis of new transition metal complexes containing bridging germylene and bridging stannylene ligands. It is anticipated that these complexes will be able to serve as precursors to new stoichiometrically-precise supported Ge and Sn containing multimetallic heterogeneous catalysts by thermal removal of the CO ligands and phenyl rings.[3]

69

www.manaraa.com
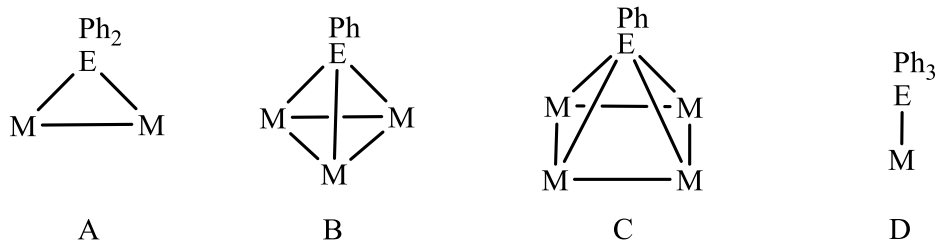
Figure 3.1 Bridging modes of germylyne/stannylyne ligands in polynuclear
metal carbonyl complexes

$Ru_5(CO)_{15}(\mu_5\text{-}C)$ $Ru_5(CO)_{11}(\mu\text{-}EPh_2)_4(\mu_5\text{-}C)$
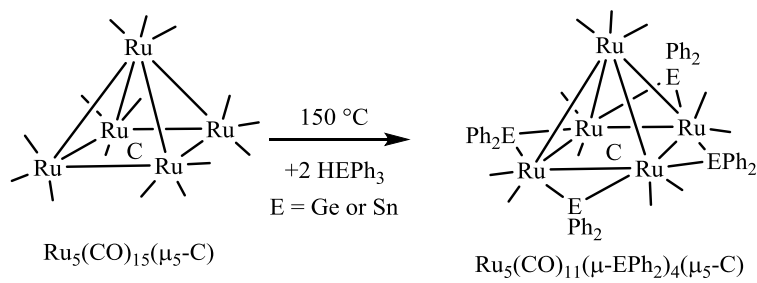
Figure 3.2 Bridging germylene/stannylene ligands in Ruthenium carbonyl complexes
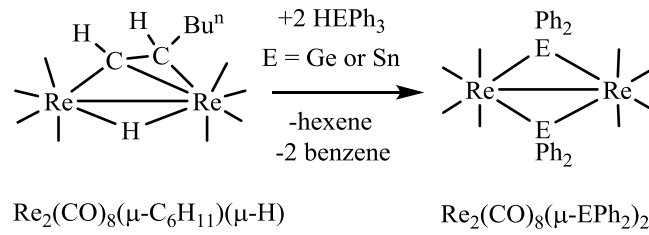
Figure 3.3 Bridging germylene/stannylene ligands in Rhenium carbonyl complexes

IrRu₃(CO)₁₁(GePh₃)₃(μ-H)₄   IrRu₃(CO)₁₀(μ-C₆H₅)(μ₄-GePh)₂   IrRu₃(CO)₉(μ-C₆H₅)(μ₄-GePh)₂(μ-GePh₂)
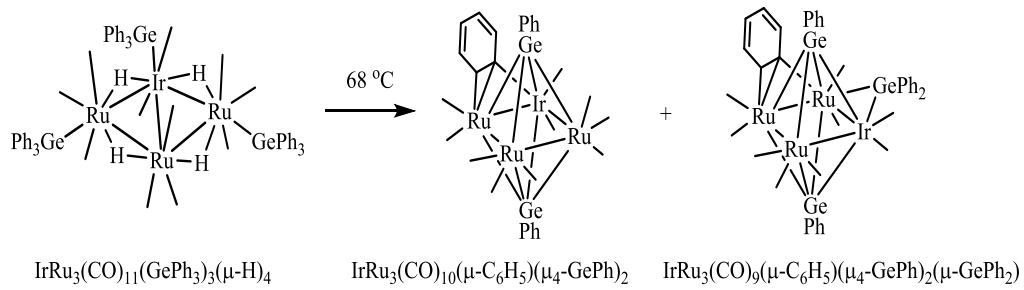
Figure 3.4 Phenyl cleavage and benzene elimination from germyl/stannyl ligands in polynuclear metal carbonyl complexes giving rise to bridging germylyne/stannylyne ligands.
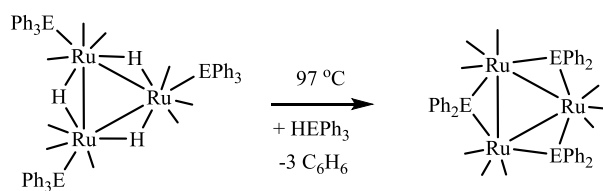
Figure 3.5 α-cleavage of three phenyl groups eliminating three benzenes and giving rise to bridging germylene/stannylene ligands in ruthenium carbonyl complexes .
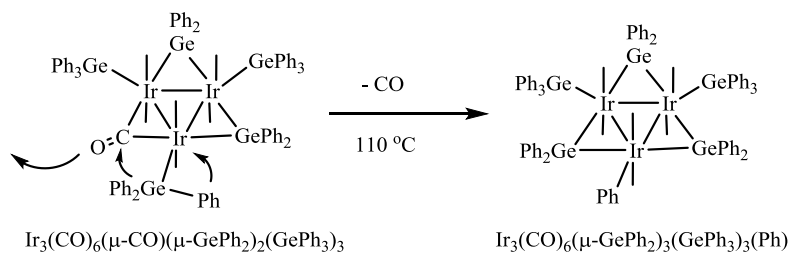
Figure 3.6 Phenyl cleavage occuring at a single Ir atom
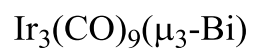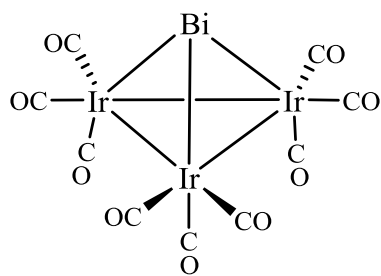
$$Ir_3(CO)_9(\mu_3\text{-Bi})$$

Figure 3.7 $Ir_3(CO)_9(\mu_3\text{-Bi})$, **3.1** the only previously known bismuth containing iridium carbonyl cluster complex.
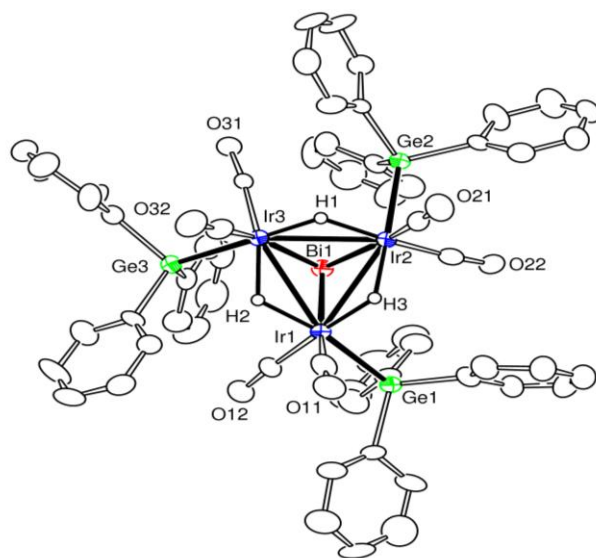
Figure 3.8 An ORTEP diagram of the molecular structure of $Ir_3(CO)_6(GePh_3)_3(\mu_3\text{-Bi})(\mu\text{-H})_3$, **3.2** showing 30% thermal ellipsoid probability.
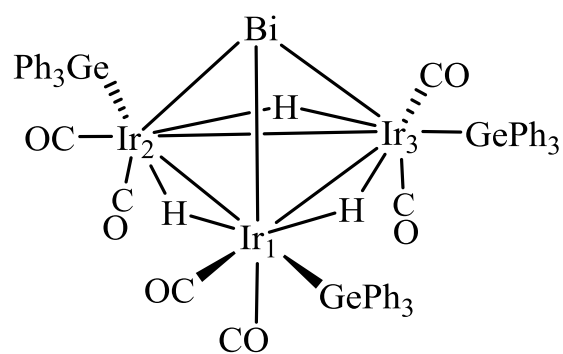
Figure 3.9 The structure proposed for isomer
B of $Ir_3(CO)_6(GePh_3)_3(\mu_3\text{-Bi})(\mu\text{-H})_3$, **3.2.**
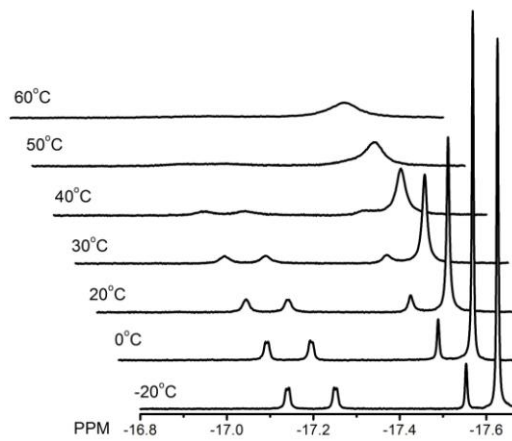
Figure 3.10 A stacked plot of ^{1}H NMR spectra for compound **3.2** at various temperatures in a CDCl$_3$ solution.

www.manaraa.com
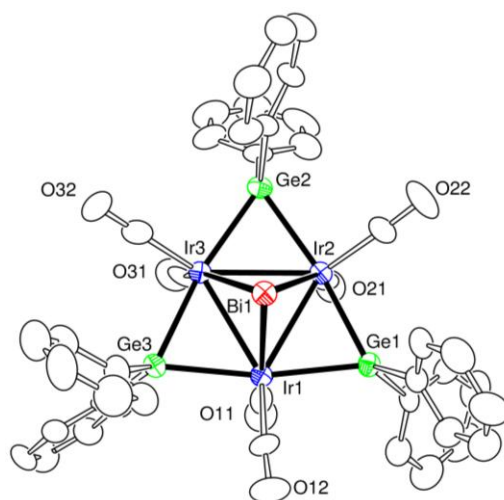
Figure 3.11 An ORTEP diagram of the molecular structure of $Ir_3(CO)_6(\mu\text{-}GePh_2)_3(\mu_3\text{-}Bi)$, **3.3** showing 30% thermal ellipsoid probability.
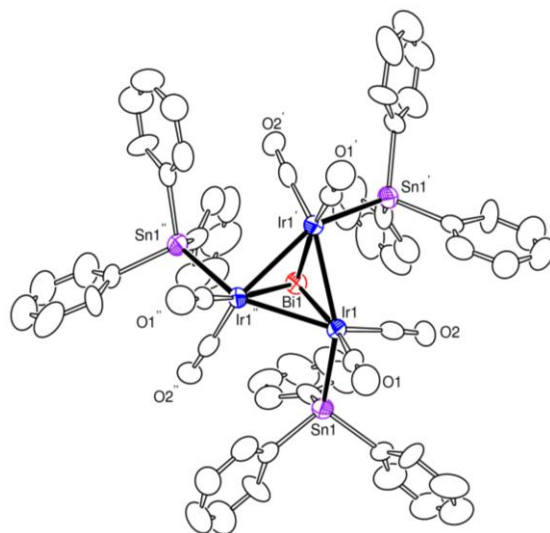
Figure 3.12 An ORTEP diagram of the molecular structure of $Ir_3(CO)_6(SnPh_3)_3(\mu\text{-}H)_3(\mu_3\text{-Bi})$, **3.4** showing 30% thermal ellipsoid probability.
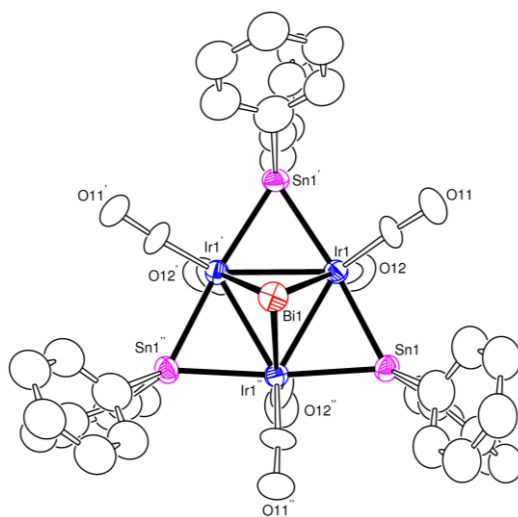
Figure 3.13 An ORTEP diagram of the molecular structure of $Ir_3(CO)_6(\mu\text{-}SnPh_2)_3(\mu_3\text{-}Bi)$, **3.5** showing 30% thermal ellipsoid probability.
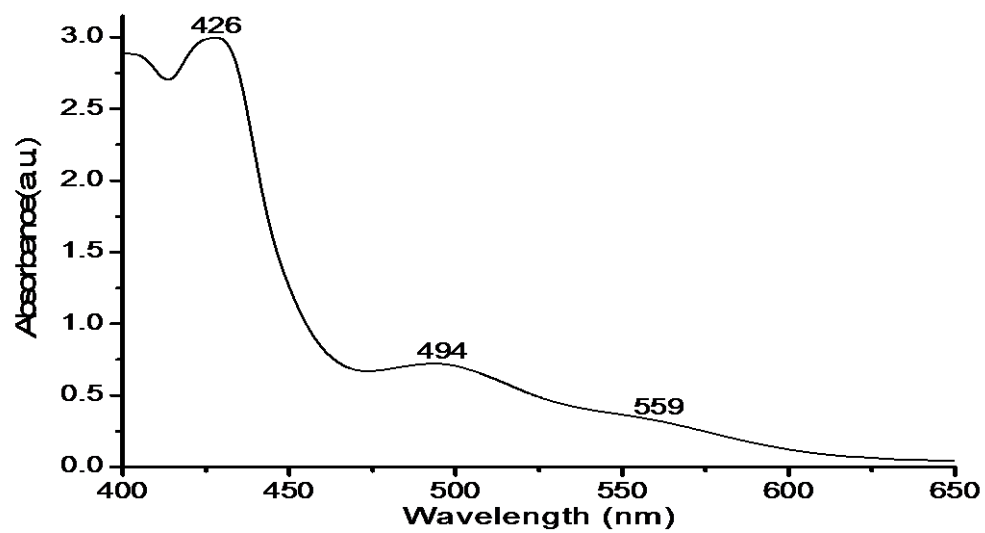
Figure 3.14 The UV-vis absorption spectrum of **3.3** in a CH$_2$Cl$_2$ solution.
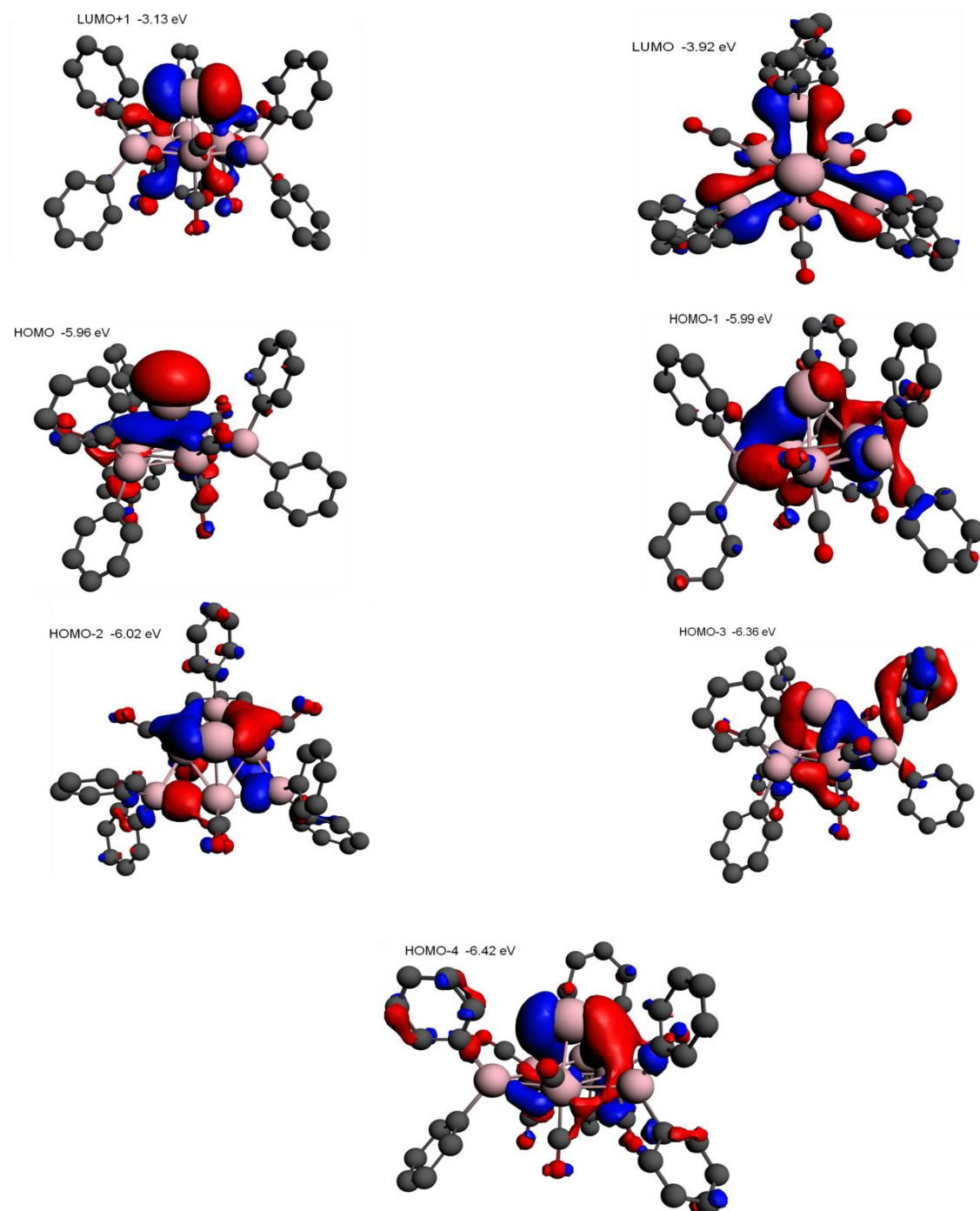
Figure 3.15 Selected molecular orbitals for compound **3.3.**

84
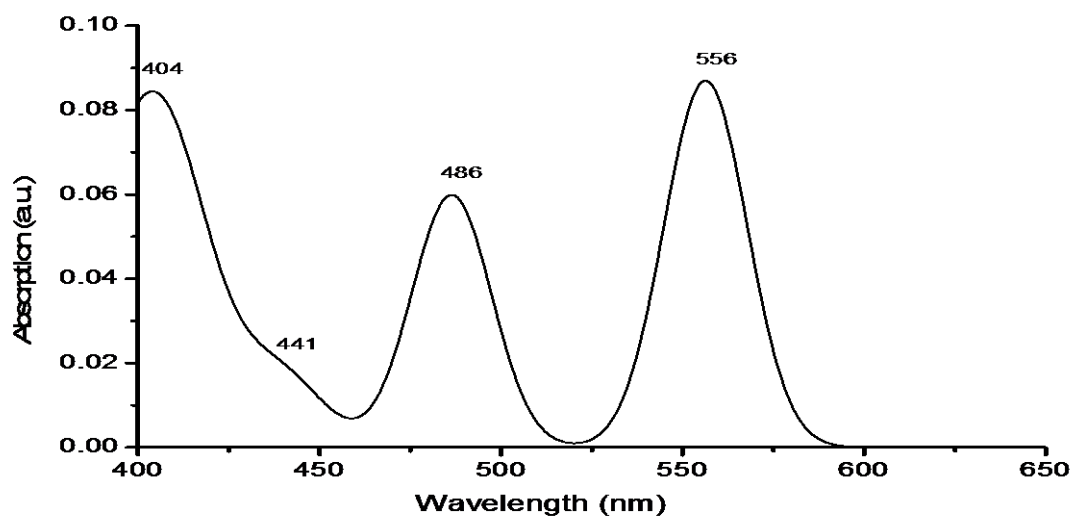
Figure 3.16 The TD-PBEsol calculated UV–vis spectrum of compound **3.3.**

3.2A, C3   3.2B, C1
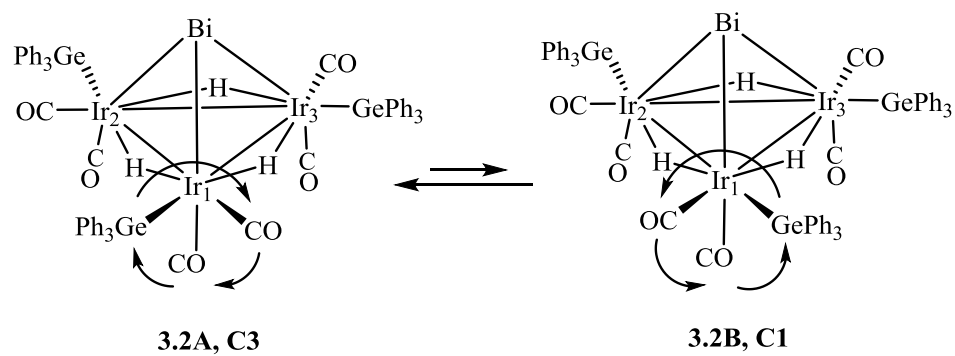
Scheme 3.1 Polytopal trigonal - twist mechanism showing the isomerization
between isomers A and B.
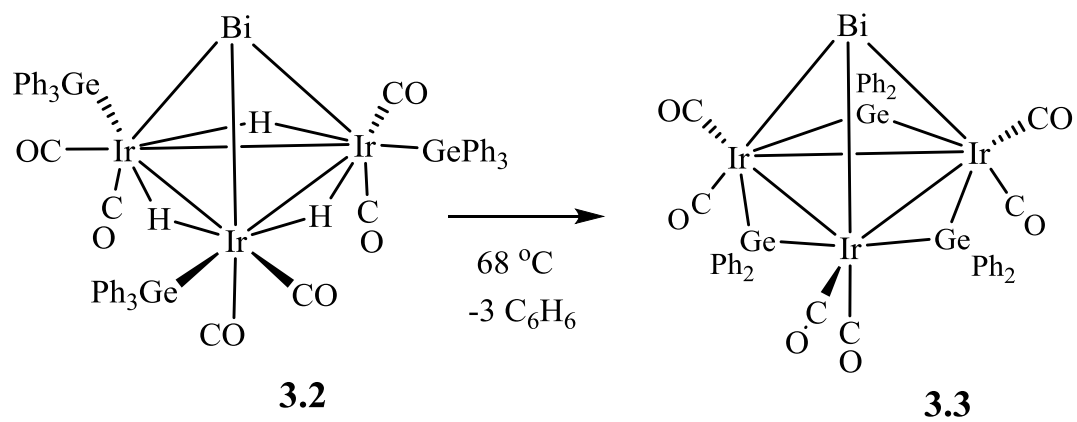
Scheme 3.2 Transformation of compound **3.2** to **3.3** through a α-phenyl cleavage of three phenyl groups eliminating three molecules of benzene.

Table 3.1 Crystallographic Data for Compounds **3.2** and **3.3**[a]

Compound	**3.2**	**3.3**
Empirical formula	$Ir_3BiGe_3O_6C_{60}H_{48} \cdot C_6$	$Ir_3BiGe_3O_6C_{42}H_{30} \cdot {}^{1}\!/_4 CH_2Cl_2$
Formula weight	1934.39	1655.24
Crystal system	Monoclinic	Monoclinic
Lattice parameters		
a (Å)	25.6331(17)	33.584(17)
b (Å)	15.4787(11)	14.609(6)
c (Å)	30.772(2)	37.282(16)
α (deg)	90.00	90.00
β (deg)	97.328(2)	98.623(14)
γ (deg)	90.00	90.00
V (Å^3)	12109.7(14)	18084(14)
Space group	$C2/c$	$C2/c$
Z value	8	16
ρ_{calc} (g / cm^3)	2.122	2.432
μ (Mo Kα) (mm^{-1})	10.981	14.712
Temperature (K)	293(2)	294(2)
$2\Theta_{max}$ (°)	50.40	52.80
No. Obs. (I > 2σ(I))	6818	9287
No. Parameters	684	967
Goodness of fit (GOF)*	1.068	1.037
Max. shift final cycle	0.006	0.001
Residuals*: R1; wR2	0.0586 ; 0.1351	0.0637; 0.1345
Abs. Correction, Max/min	Multi-scan 1.000 / 00.485	Multi-scan 1.000 / 0.375
Largest peak in Final Diff. Map (e$^-$ / Å^3)	1.58	2.07

* $R1 = \Sigma_{hkl}(||F_{obs}| - |F_{calc}||)/\Sigma_{hkl}|F_{obs}|$; $wR2 = [\Sigma_{hkl}w(|F_{obs}| - |F_{calc}|)^2/\Sigma_{hkl}wF^2_{obs}]^{1/2}$; $w = 1/\sigma^2(F_{obs})$; $GOF = [\Sigma_{hkl}w(|F_{obs}| - |F_{calc}|)^2/(n_{data} - n_{vari})]^{1/2}$.

Table 3.2 Crystallographic Data for Compounds **3.4** and **3.5**[a]

Compound	**3.4**	**3.5**
Empirical formula	$^1/_3[Ir_3BiSn_3O_6C_{60}H_{48}]$	$^1/_3[Ir_3BiSn_3O_6C_{42}H_{30}]$
Formula weight	668.88	590.77
Crystal system	Trigonal	Trigonal
Lattice parameters		
a (Å)	15.4057(2)	12.4372(3)
b (Å)	15.4057(2)	12.4372(3)
c (Å)	30.9537(7)	38.7624(19)
α (deg)	90.00	90.00
β (deg)	90.00	90.00
γ (deg)	120.00	120.00
V (Å^3)	6362.18(19)	5192.6(3)
Space group	$P31c$	$P31c$
Z value	12	12
ρ_{calc} (g / cm^3)	2.095	2.267
μ (Mo Kα) (mm^{-1})	10.207	12.489
Temperature (K)	293(2)	294(2)
$2\Theta_{max}$ (°)	43.66	50.04
No. Obs. (I > 2σ(I))	6986	6166
No. Parameters	368	238
Goodness of fi (GOF)*	1.075	1.090
Max. shift final cycle	0.000	0.001
Residuals*: R1; wR2	0.0363; 0.0877	0.0450; 0.1055
Abs. Correction, Max/min	Multi-scan 1.000 / 0.479	Multi-scan 1.000 / 0.570
Largest peak in Final Diff. Map (e$^-$ / Å^3)	1.52	0.82

* $R1 = \Sigma_{hkl}(\,|\,|F_{obs}|\,-\,|F_{calc}|\,|\,)/\Sigma_{hkl}|F_{obs}|$; $wR2 = [\Sigma_{hkl}w(\,|F_{obs}|\,-\,|F_{calc}|\,)^2/\Sigma_{hkl}wF^2{}_{obs}]^{1/2}$; $w = 1/\sigma^2(F_{obs})$; $GOF = [\Sigma_{hkl}w(\,|F_{obs}|\,-\,|F_{calc}|\,)^2/(n_{data} - n_{vari})]^{1/2}$.

89

Table 3.3 Selected intermolecular angles and bond distances for **3.2** [a]

Atom	Atom	Distance	Atom	Atom	Atom	Angle
Ir1	Ir2	3.0094(8)	Ge1	Ir1	Bi1	93.79(5)
Ir2	Ir3	3.0073(9)	Ge1	Ir1	Ir3	150.33(5)
Ir3	Ir1	3.0071(8)	Bi1	Ir1	Ir3	57.13(2),
Ir1	Bi1	2.7610(9)	Ge1	Ir1	Ir2	100.91(4)
Ir2	Bi1	2.7597(9)	Ir3	Ir1	Ir2	59.97(2)
Ir3	Bi1	2.7668(9)				
Ir1	Ge1	2.5032(18)				
Ir2	Ge2	2.5054(16)				
Ir3	Ge3	2.5046(18)				
Ir1	H2	1.75(2)				
Ir1	H3	1.8(2)				
Ir2	H1	1.7(2)				
Ir2	H3	1.8(2)				
Ir3	H2	1.76(2)				
Ir3	H1	1.6(2)				
Ir3	H2	1.76(2)				

[a] Estimated standard deviations in the least significant figure are given in parenthesis.

Table 3.4 Selected intermolecular angles and bond distances for **3.3** [a]

Atom	Atom	Distance	Atom	Atom	Atom	Angle
Ir1	Ir2	2.8356(14)	Ir1	Ir1	Ge1	165.95(7)
Ir2	Ir3	2.8383(15)	Ge3	Ir1	Bi1	82.38(5)
Ir1	Ir3	2.8568(15)	Bi2	Ir1	Ir3	57.814(18)
Ir1	Bi1	2.7651(12)	Ge3	Ir1	Ir2	114.81(6)
Ir2	Bi1	2.7678(13)	Ge1	Ir1	Ir2	54.74(6)
Ir3	Bi1	2.7751(12)	Bi1	Ir1	Ir2	59.22(3)
Ir1	Ge1	2.516(2)	Ir2	Ir1	Ir3	59.82(3)
Ir2	Ge1	2.477(2)				
Ir2	Ge2	2.509(2)				
Ir3	Ge2	2.487(2)				
Ir3	Ge3	2.506(2)				
Ir1	Ge3	2.498(2)				

[a] Estimated standard deviations in the least significant figure are given in parenthesis.

Table 3.5 Selected intermolecular angles and bond distances for **3.4** [a]

Atom	Atom	Distance	Atom	Atom	Atom	Angle
Ir1	Ir1	2.9969(8)	Ir1	Bi1	Ir1	65.49(3)
Ir1	Bi1	2.7702(9)	Sn1	Ir1	Bi1	88.47(3)
Ir1	Sn1	2.660(1)	Sn1	Ir1	Ir1	96.71(3)
			Bi1	Ir1	Ir1	57.254(13)
			Sn1	Ir1	Ir1	144.88(3)

[a] Estimated standard deviations in the least significant figure are given in parenthesis.

92

Table 3.6 Selected intermolecular angles and bond distances for **3.5** [a]

Atom	Atom	Distance	Atom	Atom	Atom	Angle
Ir1	Ir1	2.8697(13)	Sn1	Ir1	Sn1	171.16(6)
Ir1	Bi1	2.7505(12)	Sn1	Ir1	Bi1	85.69(4)
Ir1	Sn1	2.6347(16)	Bi2	Ir1	Ir3	57.814(18)
Ir1'	Sn1	2.6437(16)	Sn1	Ir1	Ir1	57.22(4)
			Sn1	Ir1	Ir1	116.81(4)
			Bi1	Ir1	Ir1	58.556(18)
			Bi2	Ir1	Bi3	173.43(3)
			Ir1	Bi1	Ir1	62.89(4)

[a] Estimated standard deviations in the least significant figure are given in parenthesis.

93

REFERENCES

1. (a) Ekou, T. A.; Lafaye,V. G.; Especel, C.; Marecot, P. *Appl Catal. A Gen..* **2006**, *314*, 73-80. (b) Lafaye, V.G.; Micheaud-Especel, C.; Montassier, C.; Marecot. *Appl. Catal. A Gen.* **2002**, *230*, 19-30. (c) Lafaye, G.; Micheaud-Especel, C.; Montassier, C.; Marecot *Appl. Catal. A Gen.* **2004**, *257*, 107-117. (d) Macleod, N.; Fryer, J. R.; Stirling, D.; Webb, G. *Catal. Today* **1998**, *46*, 37-54.

2. (a) Burch, R. *J. Catal.* **1981**, *71*, 348-359. (b) Burch, R.; Garla, L. C. *J. Catal.* **1981**, *71*, 360-372. (c) Srinivasan R.; Davis, B. H. *Platinum Metals Rev.* **1992**, *36*, 151-163. (d) Fujikawa, T.; Ribeiro, F. H.; Somorjai, G. A. *J. Catal.* **1998**, *178*, 58. (e) Park, Y.K.; Ribeiro F. H.; Somorjai, G. A.*J. Catal.* **1998**, *178*, 66-75. (f) Epron, F.; Carnevillier, C.; Marecot, P. *Appl. Catal.* **2005**, *295*, 157. (g) Cortright, R. D.; Dumesic, J. *J. Catal.* **1997**, *148*, 771-778. (h) Dautzenberg, F. M.;.Helle, J. N;. Biolen, P.; Sachtler, W. M. H.; *J. Catal.* **1980**, *63*, 119-128. (i) Huber, G. W.; Shabaker, J. W.; Dumesic, J. A. *Science* **2003**, *300*, 2075-2077. (j) Shabaker, J. W.; Simonetti, D. A.; Cortright, R. D.; Dumesic, J. A. *J. Catal.* **2005**, *231*, 67. (k) Guidotti, M.; Aanto, V. Dal.; Gallo, A.; Gianotti, E.; Peli, G.; Psaro, R.; Sordelli, L. *Catal. Lett.* **2006**, *112*, 89. (l) Cortright, R. D.; Hill, J. M.; Dumesic, J. *Catal. Today* **2000**, *55*, 213. (m) Hermans, S.; Raja, R.; Thomas, J. M.; Johnson, B. F. G.; Sankar, G.; Gleeson, D. *Angew. Chem., Int. Ed.* **2001**, *40*, 1211-1215. (n) Johnson, B. F. G.; Raynor, S. A.; Brown, D. B.; Shephard, D. S.; Mashmeyer, T.; Thomas, J. M.;. Hermans, S Raja, R.; Sankar, G.; *J. Mol. Catal. A: Chem* **2002**, *182-183*, 89. (o) Hermans, S.; Johnson, F. G. *Chem. Commun.* (2000) 1955. (p) Adams, R. D.; Blom,

D. A.; Captain, B.; Raja, R.; Thomas, J. M.; Trufan, E. *Langmuir,* **2008**, *24*, 9223-9226.

3. (a) Thomas, J. M.; Johnson, B. F. G.; Raja, R.; Sankar, G.; Midgley, P. A. *Acc. Chem. Res*. **2003**, *36*, 20-30. (b) Braunstein, P.; Rose, J.; *Catalysis by Di- and Polynuclear Metal Cluster Complexes*, Adams R. D.; Cotton, F. A.; Eds, Wiley-VCH, New York, 1998, Ch. 13. (c) Braunstein, P. ; Rose, J. *Metal Clusters in Chemistry*, Braunstein, P.; Oro, L.A.; Raithby, P.R.; Wiley-VCH, Weinheim, Vol. 2, 1999, Ch. 2.2, pp 616-677.

4. (a) Adams, R. D.; Boswell, E. M.; Captain, B.; Patel, M. A. *Inorg. Chem.* **2007**, *46*, 533 - 540. (b) Adams, R. D.; Captain, B.; Smith, Jr., J. L. *Inorg. Chem.* **2005**, *44*, 1413-1420. (c) R Adams, R. D.; Captain, B.; Trufan, E. *J. Cluster Sci.* **2007**, *18*, 642-659. (d) Adams, R. D.; Captain, B.; Fu, W. *Inorg. Chem.*, **2003**, *42*, 1328-1333. (e) Adams, R. D.; Captain, B.; Herber, R. H.; Johansson, M.; Nowik, I.; Smith, Jr., J. L.; Smith, M. D. *Inorg. Chem.* **2005**, *44*, 6346-6358. (f) Adams, R. D.; Captain, B.; Fu, W. *J. Organomet. Chem.* **2003**, *671*, 158 – 165. (g) Adams, R. D.; Captain, B.; Zhu, L. *J. Organomet. Chem.* **2005**, *46*, 6623 - 6631.

5. (a) Adams, R. D.; Trufan, E. *Phil. Trans. R. Soc. A* **2010**, *368*, 1473-1479. (b) Adams, R. D.; Captain, B.; Trufan, E. *J. Organomet. Chem*. **2008**, *693*, 3593-3602. (c) Adams, R. D.; Captain, B.; Smith, Jr., J. L.; Hall, M. B.; Beddie, C. L.; Webster, C. E. *Inorg. Chem.* **2004**, *43*, 7576 - 7578. (d) Adams, R. D.; Captain, B.; Fu, W.; Smith, M. D. *Inorg. Chem.* **2002**, *41*, 5593 - 5601. (e) Adams, R. D.; Captain, B.; Fu, W.; Smith, M. D. *Inorg. Chem.* **2002**, *41*, 2302 - 2303. (f) Adams, R. D.; Boswell, E. M.;

Captain, B.; Hungria, A. B.; Midgley, P. A.; Raja, R.; Thomas, J. M. *Angew. Chem.. int. Ed.,* **2007**, *46*, 8182 - 8185.

6. Adams, R. D.; Kan, Y.; Zhang, Q. *Organometallics*, **2011**, *30*, 328-333.

7. Adams, R. D.; F. Fang, Q. Zhang, M. B. Hall, E. Trufan, *Organometallics*, **2012**, *31*, 2621-2630.

8. Raja, R.; Adams, R. D.; Blom, D. A.; Pearl Jr., W. C.; Gianotti, E.; Thomas, J. M. *Langmuir,* **2009**, *25*, 7200-7204.

9. Kruppa, W.; Blaeser, D.; Boese, R.; Schmid, G. *Organische Chemie*, **1982**, *37B(2)*, 209-213.

10. Garlaschelli, L.; Della Pergola, R.; Martinengo, S. *Inorg. Synth*., **1990**, *28*, 211-215.

11. (a) SpinWorks 3.1.7, Copyright ©, Kirk Marat, University of Manitoba, 2010. (b) A. R. Quirt, J. S. Martin, *J. Magn. Reson.* 5 (1971) 318-327.

12. SAINT+, version 6.2a, Bruker Analytical X-ray Systems, Inc., Madison, WI, 2001.

13. Sheldrick, G. M. SHELXTL, version 6.1, Bruker Analytical X-ray Systems, Inc., Madison, WI, 1997.

14. (a) Spek, A.L.J. Appl. Crystallogr. 2003,36,7−13. (b) van der Sluis, P.; Spek, A. L. Acta Crystallogr.1990,A46, 194−201., 136406.

15. (a) ADF2012, SCM, Theoretical Chemistry, Vrije Universiteit, Amsterdam, The Netherlands, http://www.scm.com. (b) J.P. Perdew, A. Ruzsinszky, G.I. Csonka, O.A. Vydrov, G.E. Scuseria, PRL 100 (2008) 136406.

16. Bau, R.; Drabnis, M. H. *Inorg. Chim. Acta* **1997**, *259*, 27 - 50. (b) Teller, R. G.; Bau, R., *Struc. Bonding* **1981**, *41*, 1 - 82.

17. Adams, R. D.; Captain, B.; Smith, J. L., Jr. *Inorg. Chem.* **2005**, *44*, 1413–1420.

18. (a) Colin, E. R.; Jackson, W. G.; Johnson, B. F.; Lewis, J.; Matheson, T. W. *J. Chem. Soc., Chem. Commun.* **1975**, 1958 – 1960. (b) Bryan, E. G.; Forster, A.; Johnson, B. F.; Lewis, J.; Matheson, T. W. *J. Chem. Soc., Dalton* **1978**, 196 – 198. (c) Gavens, P. D.; Mays, M. J. *J. Organomet. Chem.* **1978**, *162*, 389 - 401. (d) Rosenber, E.; Thorsen, C. B.; Milone, L.; Aime, S. *Inorg. Chem.* **1985**, *24*, 231 – 233. (e) Alex, R. F.; Pomeroy, R. K. *Organometallics* **1987**, *6*, 2437 – 2446. (f) Beringhelli, T.; D'Alfonso, G.; Molinari, H.; Mann, B. E.; Pickup, B. T.; Spencer, C. M. *J. Chem. Soc., Chem. Commun.* **1986**, 796 – 798. (g) Farrar, D. H.; Lunniss, J. A. *J. Chem. Soc., Dalton* **1987**, 1249 – 1252.

CHAPTER 4

THE ADDITION OF GOLD AND TIN TO BISMUTH -TRIIRIDIUM CARBONYL COMPLEXES[3]

---

[3] Adams, R. D. and Elpitiya, G. Submitted to *Inorg. Chem*, 06/05/2015

Introduction

Bismuth has been found to exhibit valuable properties as a catalyst and cocatalyst for the selective oxidation and ammoxidation of hydrocarbons.[1] We have recently shown that iridium-bismuth nanoparticles derived from bimetallic iridium-bismuth carbonyl complexes exhibit good activity for the direct conversion of 3-picoline to Niacin at 65 $^{\circ}$C by using acetylperoxyborate as the oxidant (Figure 4.1).[2] Gold clusters and nanoparticles have recently been shown to exhibit remarkable activity for the selective oxidation of hydrocarbons.[3] Tin is also well known to be a modifier of heterogeneous transition metal catalysts.[4] We have already shown that $HSnPh_3$ and $HGePh_3$ can be added to $Ir_3(CO)_9(\mu_3$-Bi) to yield products containing terminal EPh_3 ligands, $Ir_3(CO)_6(EPh_3)_3(\mu_3$-Bi)$(\mu$-H)$_3$, E = Sn and Ge, and bridging EPh_2 ligands, $Ir_3(CO)_6(\mu$-$EPh_2)_3(\mu_3$-Bi), E = Sn and Ge (Figure 4.2)We have recently shown the molecule $PhAu(PPh_3)$ can be oxidatively added to substitutionally active metal carbonyl cluster complexes under mild conditions to yield transition metal – gold complexes containing phenyl ligand(s) (Figure 4.3).[6-8] With this in mind we have now embarked on a study to synthesize new iridium-bismuth complexes derived from $Ir_3(CO)_9(\mu_3$-Bi) that contain gold and gold plus tin ligands that could potentially be converted into new multimetallic nanoparticles for applications in selective oxidation catalysis. The results of these studies are reported herein.

Experimental Details

General Data.

Reagent grade solvents were dried by the standard procedures and were freshly distilled prior to use. All reactions were performed under an atmosphere of nitrogen unless indicated otherwise. Infrared spectra were recorded on a Thermo Nicolet Avatar

99

360 FT-IR spectrophotometer. Room temperature ^{1}H NMR spectra were recorded on a Varian Mercury 300 spectrometer operating at 300.1 MHz. Variable temperature ^{1}H NMR spectra were recorded on a Varian Mercury 400 spectrometer operating at 161.9 MHz. Positive/negative ion mass spectra were recorded on a Micromass Q-TOF instrument by using electrospray (ES) ionization. $Ir_4(CO)_{12}$, ClAu(NHC), NHC = 1,3-[Bis(2,6-diisopropylphenyl-imidazol-2-ylidene)] and $BiNO_3 \cdot 5H_2O$ were obtained from STREM and were used without further purification. Ph_3SnH was obtained from Aldrich and were used without further purification. PhAu(NHC), **4.1** was prepared from ClAu(NHC) by a slightly modified version of the reported procedure for $PhAu(PPh_3)$, see below.[9] $[PPN]Ir(CO)_4$ was prepared according to the previously reported procedure.[10] $Ir_3(CO)_9(\mu_3\text{-Bi})$ was prepared by a modified procedure according to the previous reports.[5,11] Product separations were performed by TLC in air on Analtech 0.25 mm silica gel 60 Å F254 and 0.25 mm aluminum oxide 60 Å F254 glass plates.

Synthesis of 1,3-Bis(2,6-di-isopropylphenyl)imidazol-2-ylidenegold(I)phenyl, 4.1.

In dry isopropanol (10 mL) the phenyl boronic acid (56.94 mg, 0.467 mmol) was dissolved and Cs_2CO_3 (146.89 mg, 0.451 mmol) was added. To this suspension was added ClAu(NHC) (150.0 mg, 0.241 mmol) under N_2 and the resultant mixture was stirred at 50 °C for 24 h . The solvent was then removed in vacuo, and the solid was extracted with benzene, filtered through Celite, concentrated in vacuo to dryness. This gave 155.0 mg of the colorless product **4.1** (97% yield). ^{1}H NMR spectrum of **4.1** was identical to that reported in the original work.[12]

100

Synthesis of Ir$_3$(CO)$_8$(Ph)(μ$_3$-Bi)[μ-Au(NHC)], 4.2.

A 39.3mg (0.063 mmol) portion of **4.1** was added to 24.6 mg (0.021 mmol) of Ir$_3$(CO)$_9$(μ$_3$-Bi) that was dissolved in 30 mL of hexane. The reaction was heated to reflux for 45 min. The solvent was then removed *in vacuo*, and the product was isolated by TLC with a 6/1 hexane/methylene chloride solvent ratio as the eluent. This gave 14.6 mg (0.009 mmol) of red Ir$_3$(CO)$_8$(Ph)(μ$_3$-Bi)[μ-Au(NHC)], **4.2**, 42% yield). Spectral data for **4.2**: IR υ(CO) (cm^{-1} in CH$_2$Cl$_2$): 2065(m) , 2037(vs), 2010 (s), 2003 (s). ^{1}H NMR (CD$_2$Cl$_2$, δ in ppm): 7.55 (t, ^{3}J$_{H-H}$ = 6 Hz, 2H, para-C**H**), 7.37 (d, ^{3}J$_{H-H}$ = 9 Hz, 4H, meta-C**H**), 7.31 (s, 2H,NC**H$_2$**), 2.63 (sept, ^{3}J$_{H-H}$ = 6Hz, 4H, C**H**(CH$_3$)$_2$), 1.33 (d, ^{3}J = 9Hz, 12H, CHC(C**H$_3$**)$_2$)**,** 1.22 (d, ^{3}J$_{H-H}$ = 6Hz ,12H, CHC(C**H$_3$**)$_2$)**,** 6.68-7.22 (m, 5H, σ-Ph). MS ES (negative ion) for **4.2** : m/z 1785 ((M+triflate)-); MS ES (positive ion) for **4.2**: m/z : 1672 (M+) The isotope distribution pattern is consistent with the presence of three iridium atoms, one bismuth atom and a gold atom.

Synthesis of Ir$_3$(CO)$_7$(SnPh$_3$)$_2$(μ$_3$-Bi)[μ-Au(NHC)](μ-H), 4.3.

A 42.3 mg (0.025 mmol) portion of **4.2** dissolved in 20 mL of CH$_2$Cl$_2$ was stirred with 68.0 mg (0.192 mmol) of HSnPh$_3$ for 1 h at room temperature. The solvent was then removed in vacuo, and the product was isolated by TLC on alumina by using a 6/1 hexane/methylene chloride solvent mixture. This gave 13.1 mg (0.0060 mmol) of orange Ir$_3$(CO)$_7$(SnPh$_3$)$_2$(μ$_3$-Bi)[μ-Au(NHC)[(μ-H)**, 4.3,** 24% yield). Spectral data for **4.3**: IR υ(CO) (cm^{-1} in CH$_2$Cl$_2$) 2058(s)**,** 2035(vs), 2018 (m), 2005 (s); ^{1}H NMR (CD$_2$Cl$_2$, δ in ppm at 25 ^{o}C): 7.8-6.92 (m, 36H, Ph), 2.57 (sept, J^3$_{H-H}$ = 6Hz,4H,C**H**(CH$_3$)$_2$), -19.57 (s,br, 1H, Ir-H). At -80 ^{o}C the hydride signal appears as two resonances at δ = -18.00 (s,

101

1H, Ir-H, $^2J_{Sn-H}$ = 20 Hz) and δ = -21.69 (s, 1H, Ir-H, $^2J_{Sn-H}$ = 20 Hz). MS ES (positive ion) for **4.3**: m/z: 2307 (M+K$^+$). The isotope distribution pattern is consistent with the presence of three iridium atoms, one bismuth atom, a gold atom and two tin atoms.

Synthesis of Ir$_3$(μ$_3$-Bi)(CO)$_7$[μ-Ph$_2$Sn(OH)SnPh$_2$][μ-Au(NHC], 4.4.

A 7.8 mg (0.003 mmol) portion of **4.3** dissolved in 4 mL of CD$_2$Cl$_2$ in a NMR tube. 0.1 mL of water was added and the sample was heated to 40 °C for 3h. The product was isolated by TLC on alumina by using a 6/1 hexane/methylene chloride solvent mixture as the eluent. This gave 1.8 mg (0.0008 mmol) of orange Ir$_3$(μ$_3$-Bi)(CO)$_7$[μ-Ph$_2$Sn(OH)SnPh$_2$][μ-Au(NHC)], **4.4**, 24 % yield). Spectral data for **4.4**: IR υ(CO) (cm^{-1} in CH$_2$Cl$_2$) 2043(s), 1993.99 (vs), 1948.54 (w). ^{1}H NMR (CD$_2$Cl$_2$, δ in ppm): 7.8-6.88 (m, 26H, Ph), 2.62 (sept, $^3J_{H-H}$ = 6Hz, 4H, C**H**(CH$_3$)$_2$), 3.15 (s, OH, Sn-OH, $^2J_{Sn-OH}$ = 15 Hz). MS ES (positive ion) for **4.4**: m/z: 2169 (M+K$^+$). The isotope distribution pattern is consistent with the presence of three iridium atoms, one bismuth atom, a gold atom, two tin atoms and an OH.

Reaction of 4.2 with Ph$_3$SnH and H$_2$O.

A 27.4 mg (0.016 mmol) portion of **4.2** dissolved in 4 mL of CD$_2$Cl$_2$ in an NMR tube was mixed to react with 0.1 mL of H$_2$O and 17.4 mg (0.049 mmol) of HSnPh$_3$ for 24 h at 25 °C. The products were isolated by TLC on alumina by using a 6/1 hexane/methylene chloride solvent mixture for elution. This gave 4.5 mg (0.002 mmol) of compound **4.3** (24 % yield) and 2.2 mg (0.001 mmol) of compound **4.4** (13 % yield).

Crystallographic Analyses:

Red single crystals of **4.2** and orange single crystals of **4.3** and **4.4** suitable for x-ray diffraction analyses were obtained by slow evaporation of solvent from a solution of the compound in hexane at room temperature. Each data crystal was glued onto the end of a thin glass fiber. X-ray intensity data were measured by using a Bruker SMART APEX CCD-based diffractometer by using Mo Kα radiation (λ = 0.71073 Å). The raw data frames were integrated with the SAINT+ program by using a narrow-frame integration algorithm.[13] Corrections for Lorentz and polarization effects were also applied with SAINT+. All structures were solved by a combination of direct methods and difference Fourier syntheses, and refined by full-matrix least-squares on F^2 by using the SHELXTL software package.[14] All non-hydrogen atoms were refined with anisotropic displacement parameters. Crystal data, data collection parameters, and results of the analyses are listed in Table 4.1.

Computational Details.

All density functional theory (DFT) calculations were performed with the Amsterdam Density Functional (ADF) suite of programs[15] by using the PBEsol functional[16] with valence quadruple-ζ + 4 polarization function, relativistically optimized (QZ4P) basis sets for iridium, bismuth, and gold atoms, and double-ζ (DZ) basis sets for carbon, oxygen, nitrogen and hydrogen atoms with no frozen cores. The molecular orbitals and their energies were determined by a geometry optimized calculation with scalar relativistic corrections that were initiated by using the atom positional parameters as determined from the crystal structure analyses. Electron densities at the bond critical

103

points were calculated by using the Bader Quantum Theory of Atoms in Molecules (QTAIM) model, see Supporting Information.[17, 18]

Results and Discussion

The reaction of PhAu(NHC), **4.1** with $Ir_3(CO)_9(\mu_3\text{-Bi})$ in hexane solvent at reflux for 45 min yielded the new compound $Ir_3(CO)_8(Ph)(\mu_3\text{-Bi})[\mu\text{-Au(NHC)}]$, **4.2** in 42% yield. Compound **4.2** was characterized by a combination of IR and ^{1}H NMR spectroscopies, mass spectrometry and a single-crystal X-ray diffraction analysis. An ORTEP diagram of the molecular structure of **4.2** is shown in Figure 4.4. Like its parent $Ir_3(CO)_9(\mu_3\text{-Bi})$, compound **4.2** consists of a triangular cluster of three iridium atoms with a triply-bridging bismuth atom. The Ir − Ir bond lengths in **4.2**, Ir(1) - Ir(2) = 2.8115 (3), Ir(1) − Ir (3) = 2.8150 (3), Ir (2) − Ir(3) = 2.7647 (3) are slightly longer than those in $Ir_3(CO)_9(\mu_3\text{-Bi})$, ave 2.734 (2) Å.[11] Compound **4.2** contains an Au(NHC) group that bridges one of the Ir - Bi bonds. The Ir − Au distance, Ir(1) − Au(1) = 2.7165 (3) Å, is similar to that found in the compound, $Ir_4(CO)_{11}(Ph)[\mu\text{-AuPPh}_3]$, Ir(1)−Au(1) = 2.7332(4) Å and Ir(2) − Au(1) = 2.8056(4) Å.[19] The Au − Bi bond distance in **4.2**, Au(1) − Bi(1) = 2.8189(3) Å, is only slightly longer than the Ir − Au distance. There are very few structural characterizations of complexes containing gold − bismuth bonds with which to compare. We have been able to find only one example in the form of the pincer complex $[o\text{-}(Ph_2P)C_6H_4]_2BiClAuCl$ and the Au − Bi distance in **4.2** is much shorter than the Au − Bi distance in this compound, 2.9738(17) Å[20] and 2.9979(3) Å[21]. The Ir − Bi distances in **4.2**, Ir(1) − Bi(1) = 2.9461(3) Å, Ir(2) − Bi (1) = 2.6738 (3) Å, Ir(3) −Bi(1) =

104

2.7166(4) Å are similar to those in $Ir_3(CO)_9(\mu_3-Bi)$ (average 2.734(2) Å), except for the gold – bridged Ir – Bi bond Ir(1) – Bi(1) which is considerably longer. There is a terminally-coordinated phenyl ligand bonded to Ir(2), Ir(2) – C(58) = 2.090(7) Å which has a similar Ir – C distance to the phenyl ligand found in the tetrairidium compounds $Ir_4(CO)_{11}(Ph)[\mu-Au(PPh_3)]$, Ir – C = 2.100(7) Å[19] and $[Ir_4(CO)_{11}Ph]^-$, Ir - C = 2.125(13) Å.[22]

In order to understand the bonding of the gold atom to the bismuth atom in **4.2**, a DFT molecular orbital analysis was performed by using the PBEsol functional of the ADF program library. Selected molecular orbitals for **4.2** are shown in Figure 4.5. The bonding of the Bi atom to the Ir_3 cluster is represented in the HOMO, HOMO-1 and HOMO-2. These molecular orbitals are principally Bi – Ir cluster bonding. Au – Ir bonding is shown in the HOMO-7 and Au – Bi bonding is shown in the HOMO-10. The Au – Bi bond is composed principally of the 6s orbital on Au and the $6p_z$ orbital on Bi in the coordinate system shown in Figure 4.5. In order to analyze the Au – Bi bonding further, we have calculated the electron densities at the bond critical points (bcps) for a number of heavy atom pairs by using the Bader QTAIM model.[17, 18] A plot of **4.2** that shows the locations of the various bcps is shown Figure 4.6 and a listing of the geometry-optimized (GO) bond distances with their electron densities ($e^-/Bohr^3$) at the bcps is given in Table 4.2. The GO DFT Au – Bi bond distance is slightly longer 2.8674 Å than the experimental value, Au(1) – Bi(1) = 2.8189(3) Å. The DFT calculation maybe slightly under estimating the strength of the Au – Bi bond. Nevertheless, the QTAIM electron density at the Au – Bi bcp, 0.04756 $e^-/Bohr^3$, is only slightly smaller than that of the Ir – Au bond, 0.05902 $e^-/Bohr^3$, the electron density at Ir – Bi bond bcps, range 0.05382 -

0.06665 e$^-$/Bohr^3 and those of the Ir – Ir bonds, range 0.05463 - 0.05621 e$^-$/Bohr^3. The Ir atoms in compound **4.2** contain a total of 48 cluster valence electrons and with three Ir – Ir bonds, the complex is formally electron precise, i.e. all of the iridium atoms have 18 electron configurations.

Next the reaction of **4.2** with HSnPh$_3$ was investigated. The reaction of **4.2** with HSnPh$_3$ at room temperature for 1 h yielded the new Ir$_3$(CO)$_7$(SnPh$_3$)$_2$(μ_3-Bi)[μ-Au(NHC)](μ-H) compound **4.3** in 24% yield. Compound **4.3** was characterized by a combination of IR and ^{1}H NMR spectroscopies, mass spectrometry and a single-crystal X-ray diffraction analysis. An ORTEP diagram of the molecular structure of **4.3** is shown in Figure 4.7 Compound **4.3** contains a Bi-bridged Ir$_3$ triangle with an Au(NHC) grouping that bridges one of the Ir – Bi bonds which is similar to that observed in **4.2**. In addition, compound **4.3** contains two SnPh$_3$ ligands which occupy equatorial coordination sites, one on each of two Ir(CO)$_2$ groups. The Ir – Sn bond distances are similar in length, Ir(3) - Sn(1) = 2.6415(18) Å, Ir(2) - Sn(2) = 2.6413(19) Å, and are similar to those found in the compounds Ir$_3$(CO)$_6$(SnPh$_3$)$_3$(μ-H)$_3$(μ_3-Bi)[5] and Ir$_3$(CO)$_6$(SnPh$_3$)$_3$(μ-SnPh$_2$)$_3$.[24] There is a hydride ligand bridging the Ir – Ir bond between the two Sn substituted Ir atoms. At room temperature, the ^{1}H NMR resonance of the hydrido ligand was observed at δ = -19.57, but the signal was very broad. Suspecting dynamical activity, variable temperature H NMR spectra of **4.2** were obtained. At -80 ^{o}C, the hydride signal for **4.2** appears as two sharp resonances at δ = -18.00 (s, ^{2}J$_{Sn-H}$ = 20 Hz) and δ = -21.69 (s, ^{2}J$_{Sn-H}$ = 20 Hz) with relative intensities of 0.4/0.6. These resonances broaden and coalesce at -19.57 ppm as the temperature is raised to 25 ^{o}C. This observation can be explained by the presence of two coordination isomers of **4.2** in

106

solution that interconvert rapidly on the NMR timescale at 25 ^{o}C. Similar dynamical activity was observed for the very similar compound Ir$_3$(CO)$_6$(GePh$_3$)$_3$(μ-H)$_3$(μ$_3$-Bi).[5] The Ir – Ir bond distances in **4.3** are similar to those found in **4.2**, Ir(1) - Ir(3) = 2.8211(14) Å, Ir(1) - Ir(2) = 2.8221(13) Å, except for the hydride-bridged Ir – Ir bond Ir(2) - Ir(3) = 2.9098(14) Å, which is elongated due to the presence of the hydride ligand.[23] The Ir – Bi distances are similar to those found in **4.2**, Ir(1)-Bi(1) = 2.9919(13) Å, Ir(3)-Bi(1) = 2.7125(12) Å, Ir(2)-Bi(1) = 2.6937(14) Å and the gold-bridged Ir - Bi bond, Ir(1)-Bi(1), is significantly longer than the unbridged Ir – Bi bonds. Compound **4.3** contains also an Au – Bi bond that is similar in length to that found on **4.2**, Au(1) - Bi(1) = 2.8295(13) Å. The iridium atoms in compound **4.3** contain a total of 48 cluster valence electrons and with three Ir – Ir bonds, the complex is formally electron precise.

When compound **4.2** was allowed to react with HSnPh$_3$ in the presence of H$_2$O for 24 h at 25 ^{o}C, compound **4.3** was obtained in 24 % yield together with the new compound **4.4** in 13 % yield. It was subsequently shown that compound **4.4** can be obtained in an even better yield (24 %) directly by the reaction of **4.3** with H$_2$O. Compound **4.4** was characterized by a combination of IR and ^{1}H NMR spectroscopies, mass spectrometry and a single-crystal X-ray diffraction analysis. An ORTEP diagram of the molecular structure of **4.4** is shown in Figure 4.8. Compound **4.4** contains an AuBiIr$_3$ cluster of metal atoms that is similar to that in compounds **4.2** and **4.3**. The Bi atom is bonded to all three Ir atoms and an Au(NHC) group bridges one of the Ir – Bi bonds. As in **4.2** and **4.3**, the Au(NHC) bridged Ir – Bi bond, Bi(1)-Ir(1), is substantially longer than the unbridged Ir – Bi bonds, Bi(1)-Ir(1) = 2.9406(6) Å, Bi(1)-Ir(3) = 2.6979(6) Å, Bi(1)-Ir(2) = 2.7036(6) Å. The Ir – Ir bond distances, Ir(1)-Ir(2) = 2.8082(7) Å, Ir(1)-Ir(3) =

2.8087(7) Å and Ir(2)-Ir(3) = 2.7736(7) Å, are similar to those in **4.2**. The most

interesting ligand in **4.4** is a $Ph_2Sn(OH)SnPh_2$ group that bridges the Ir(2) – Ir(3) bond of

the cluster as a chelating ligand; one tin atom is bonded to each of the two Ir atoms. The

Ir – Sn distances, Ir(2) - Sn(1) = 2.5505(9) Å and Ir(3) - Sn(2) = 2.5565(10) Å, are

significantly shorter (approx. 0.09 Å) than the Ir – Sn distances in **4.3**. An OH group

bridges the two Sn atoms, O(1) – Sn(1) = 2.118(8) Å and O(1) – Sn(2) = 2.143(8) Å. The

hydrogen atom on the oxygen atom O(1) was not located in this structural analysis, but

was detected in the ^1H NMR spectrum of **4.4** at δ = 3.15 ($^2J_{Sn-OH}$ = 15 Hz). Bridging

$Ph_2Sn(OH)SnPh_2$ ligands are rare, but one was observed and structurally characterized

previously   in   the   compound $[Mn_2(CO)_6(μ-H)\{μ-Ph_2SnO(H)SnPh_2\}[μ-$

$(EtO)_2POP(OEt)_2)]$, Sn – O = 2.12(1) Å which was obtained from the reaction of

$[Mn_2(CO)_6(μ-H)_2(μ-(EtO)_2POP(OEt)_2)]$ with $HSnPh_3$; the oxygen atom between the tin

atoms was suspected as being derived from traces of water in the reaction mixture.[25] The

reaction of $Re_2(CO)_8[μ-C(H)C(H)Bu^n](μ-H)$ with $HGePh_3$ in the presence of H_2O yielded

the   compound $Re_2(CO)_8[μ-Ph_2GeO(H)GePh_2](μ-H)$ containing   a   bridging

$Ph_2Ge(OH)GePh_2$ ligand and the addition of OMe^- to $Re_2(CO)_8(μ-SnPh_2)_2$ yielded the

anionic   compound $Re_2(CO)_8[μ-Ph_2Sn(OMe)SnPh_2]^-$ containing   a   bridging

$Ph_2Sn(OMe)SnPh_2$ ligand.[26] Viewing the bridging $Ph_2Sn(OH)SnPh_2$ ligand without a

charge, it would serve as a 3-electron donor to the cluster; thus the three Ir atoms would

have a total of 48 cluster valence electrons and with three Ir – Ir bonds each of the

iridium atoms would formally have an 18 electron configuration.

108

Summary

A summary of the reactions studied in this work are shown in Scheme 4.1. $Ir_3(CO)_9(\mu_3\text{-}Bi)$ was found to react with PhAu(NHC) by losing one CO ligand and then oxidatively adding the Au − C bond to the phenyl ligand of the PhAu(NHC) to one of the iridium atoms to yield the compound **4.2** that contains a σ-phenyl coordinated ligand and an Au(NHC) group bridging one of the Ir − Bi bonds of the cluster. Based on the structural analysis and the MO and QTAIM calculations, the Au − Bi interaction is substantial and is comparable in character to the Ir − Bi and Ir − Ir bonds in this cluster. We have shown previously that $Ir_3(CO)_9(\mu_3\text{-}Bi)$ reacts with $HSnPh_3$ by adding three equivalents of $HSnPh_3$ to yield the compound $Ir_3(CO)_6(SnPh_3)_3(\mu_3\text{-}Bi)(\mu\text{-}H)_3$, (Figure 4.2).[5] Compound **4.2** will add only two equivalents of $HSnPh_3$ to yield **4.3**. It is possible that the bridging Au(NHC) group with the bulky NHC ligand inhibits a third addition of $HSnPh_3$ by producing a blocking effect proximate to the third Ir atom. Finally, we observed that water can facilitate the cleavage of phenyl groups from the $SnPh_3$ ligands in **4.3** presumably with the formation of some benzene and the formation of an OH grouping bridging the two tin atoms to yield the compound **4.4**. The O-bridged linking of tin and germanium ligands could lead to design and synthesis of interesting new chelating ligands in polynuclear metal complexes in the future.

3-picoline   +   APB   →   catalysts Ir$_3$Bi and Ir$_5$Bi$_3$ nanoclusters   →   Niacin

APB = acetylperoxyborate

Figure 4.1 The direct conversion of 3-picoline to Niacin at 65 ^{o}C by using acetylperoxyborate as the oxidant

Figure 4.2 Terminal EPh$_3$ ligands and bridging EPh$_2$ ligands on Ir$_3$(CO)$_9$(μ_3-Bi) cluster
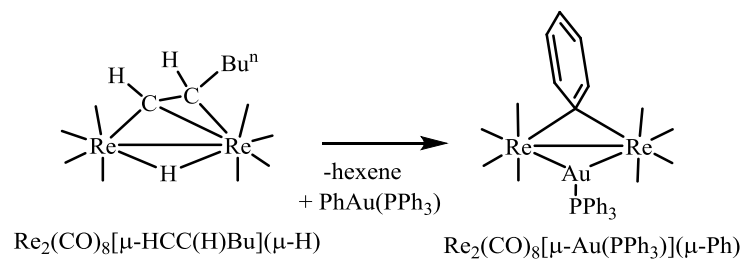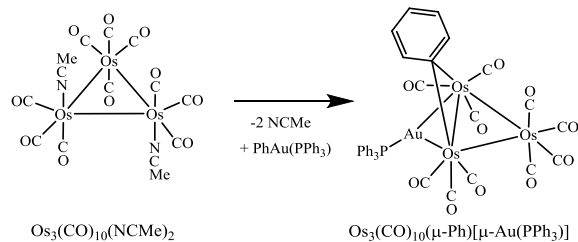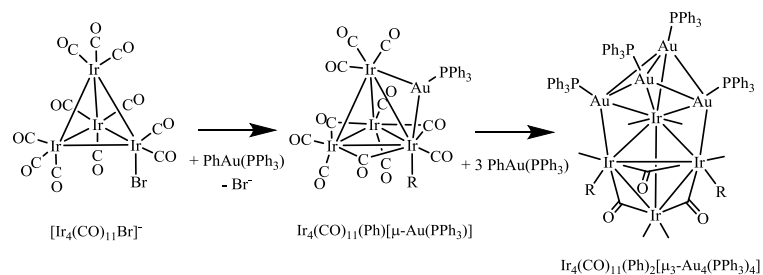
Figure 4.3 Addition of PhAu(PPh$_3$) to substitutionally active metal carbonyl cluster complexes.
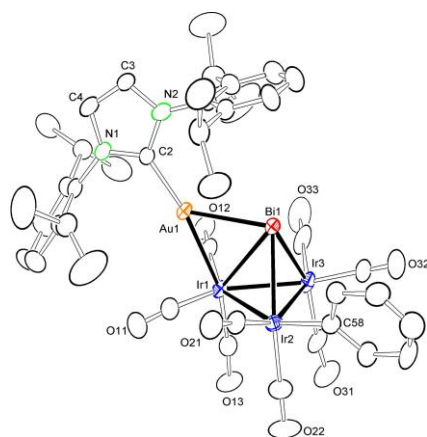
Figure 4.4 An ORTEP diagram of the molecular structure of $Ir_3(CO)_8(Ph)(\mu_3\text{-}Bi)[\mu\text{-}Au(NHC)]$, **4.2** showing 20% thermal ellipsoid probability.

113
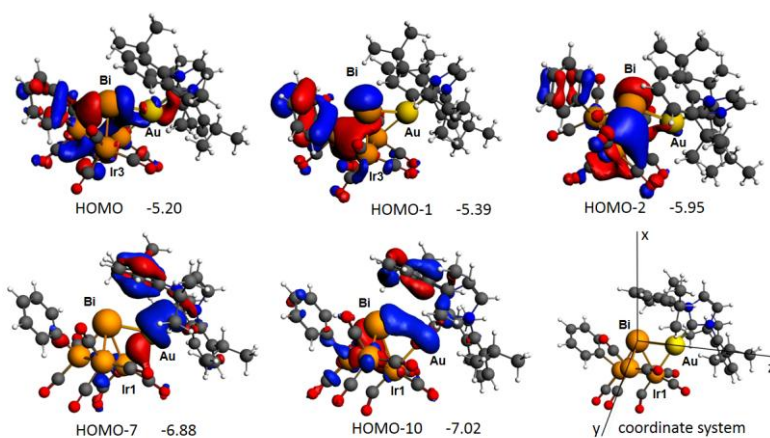
Figure 4.5 Selected GO DFT molecular orbitals for compound **4.2** with corresponding energies in electron volts (eV) and a view showing the orientation of the applied coordinate system. (Iso values are 0.03. Bi – Au bond is the z-axis in the coordinate system that was used.)
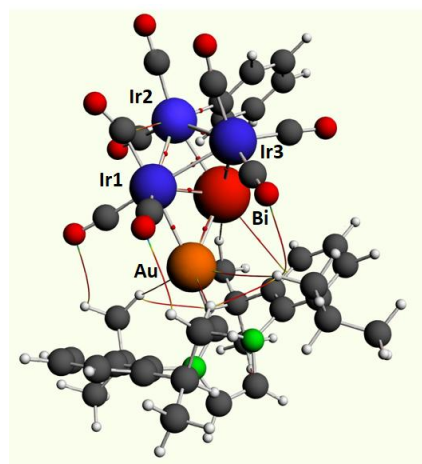
Figure 4.6 A plot of the geometry - optimized DFT structure of **4.2** showing the locations of selected bond critical points in red.
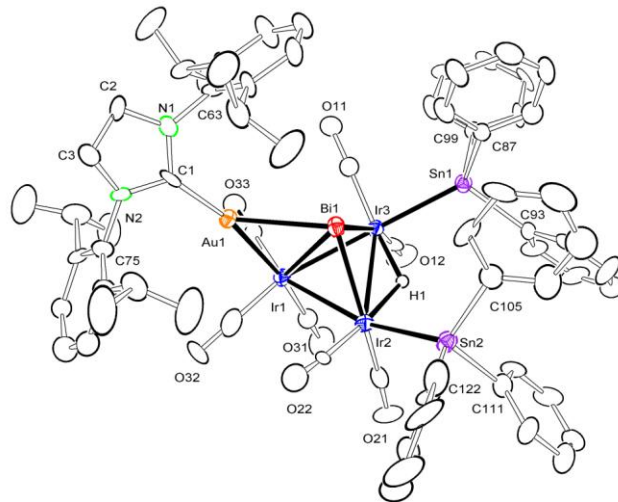
Figure 4.7 An ORTEP diagram of the molecular structure of $Ir_3(CO)_7(SnPh_3)_2(\mu_3\text{-Bi})[\mu\text{-Au(NHC)}](\mu\text{-H})$, **4.3** showing 20% thermal ellipsoid probability.
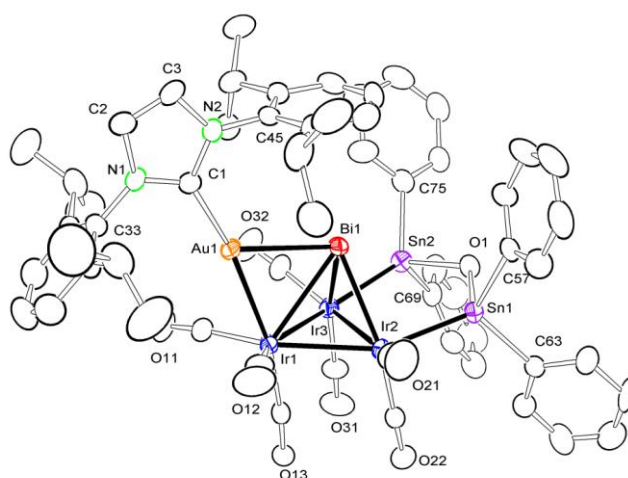
Figure 4.8 An ORTEP diagram of the molecular
structure of $Ir_3(CO)_7(\mu_3\text{-Bi})[\mu\text{-}Ph_2Sn(OH)SnPh_2][\mu\text{-}Au(NHC)]$, **4.4** showing 20% thermal ellipsoid
probability.
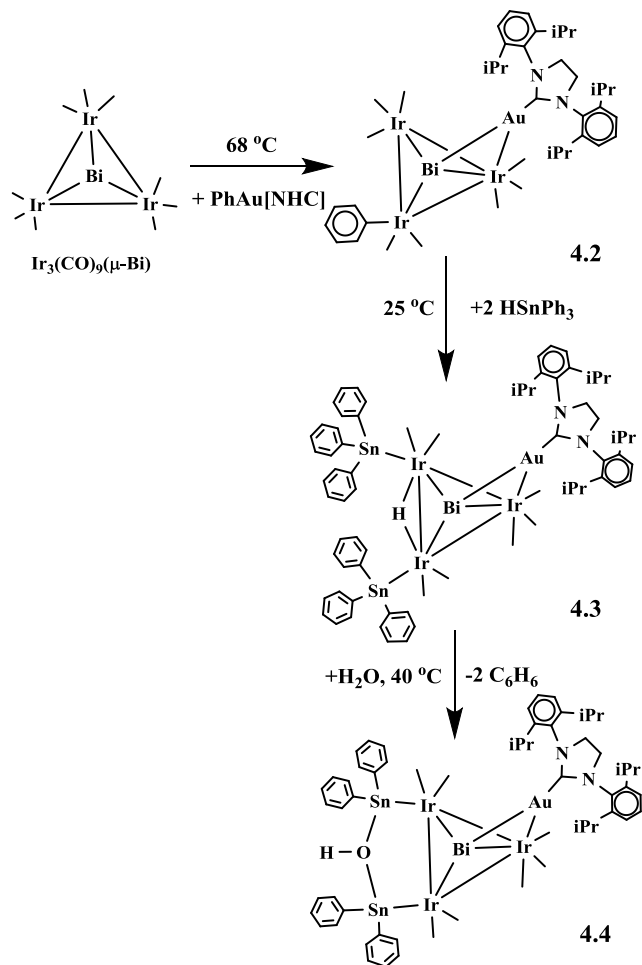
Scheme 4.1.Summary of the synthesis of compounds **4.2**-**4.4.**

118

Table 4.1 Crystallographic data for **4.2**-**4.4**[a]

Compound	**4.2**	**4.3**	**4.4**
Empirical formula	$Ir_3BiAuO_8N_2C_{41}H_{41}$	$Ir_3BiAuSn_2O_7N_2C_{70}H_6$	$Ir_3BiAuSn_2O_8N_2C_{61}H_{54}$
Formula weight	1672.30	2268.29	2162.99
Crystal system	Monoclinic	Orthorhombic	Monoclinic
Lattice parameters			
a (Å)	20.0583(6)	31.348(3)	26.3349(7)
b (Å)	11.5659(3)	10.5109(11)	13.0557(3)
c (Å)	20.6645(6)	42.587(5)	21.6626(6)
α (deg)	90	90	90
β (deg)	101.8800(10)	90	111.5200(10)
γ (deg)	90	90	90
V ($Å^3$)	4691.3(2)	14032(3)	6928.8(3)
Space group	$P2(1)/c$	$Pca2(1)$	$P2(1)/c$
Z value	4	8	4
ρ_{calc} (g / cm^3)	2.368	2.147	2.073
μ (Mo Kα) (mm^{-1})	15.381	11.000	11.133
Temperature (K)	294(2)	296(2)	294(2)
$2\Theta_{max}$ (°)	56.44	47.74	46.40
No. Obs. (I > 2σ(I))	9373	4469	7240
No. Parameters	513	1480	703

119

Goodness of fit (GOF)	1.058	0.992	1.037
Max. shift in cycle	0.001	0.002	0.001
Residuals*: R1; wR2	0.0301:0.0698	0.0538:0.0807	0.0410:0.0990
Absorption Correction, Max/min	Multi-scan 1.000/0.336	Multi-scan 1.000/0.060	Multi-scan 1.000/0.480
Largest peak in Final Diff. Map (e⁻ / Å³)	0.73	1.730	1.246

* R1 = $\Sigma_{hkl}(||F_{obs}|-|F_{calc}||)/\Sigma_{hkl}|F_{obs}|$; wR2 = $[\Sigma_{hkl}w(|F_{obs}|-|F_{calc}|)^2/\Sigma_{hkl}wF^2_{obs}]^{1/2}$; w = $1/\sigma^2(F_{obs})$; GOF = $[\Sigma_{hkl}w(|F_{obs}|-|F_{calc}|)^2/(n_{data} - n_{vari})]^{1/2}$.

Table 4.2. Geometry Optimized-DFT calculated bond distances (Å) with corresponding QTAIM electron densities (e$^-$/Bohr^3) at the bond critical points (bcps) for compound **4.2**.

Atom1	Atom2	Bond distance	electron density at bcp
Au	Bi	2.8674	0.04756
Au	Bi	2.8674	0.04756
Au	Ir1	2.6862	0.05902
Bi	Ir1	2.8681	0.05382
Bi	Ir2	2.7348	0.06665
Bi	Ir3	2.7589	0.06181
Ir1	Ir2	2.7750	0.05463
Ir1	Ir3	2.7610	0.05621
Ir2	Ir3	2.7825	0.05498

Table 4.3 Selected intermolecular angles and bond distances for **4.2** [a]

Atom	Atom	Distance	Atom	Atom	Atom	Angle
Ir1	Au1	2.7165 (3)	Ir1	Au1	Bi1	64.281 (8)
Au1	Bi1	2.8189(3)	Ir2	Bi1	Au1	101.342(10)
Ir1	Bi1	2.9461(3)	Ir3	Bi1	Au1	111.587(11)
Ir2	Bi1	2.6738 (3)	Ir2	Bi1	Ir3	61.709 (9)
Ir3	Bi1	2.7166(4)	Ir2	Bi1	Ir1	59.804 (8)
Ir1	Ir2	2.8115 (3)	Ir2	Ir1	Ir3	59.704(17)
Ir1	Ir3	2.8150(3)	Ir3	Bi1	Ir1	56.173 (7)
Ir2	Ir3	2.7647(3)	Ir1	Ir3	Ir2	60.507 (8)

[a] Estimated standard deviations in the least significant figure are given in parenthesis

Table 4.4 Selected intermolecular angles and bond distances for **4.3** [a]

Atom	Atom	Distance	Atom	Atom	Atom	Angle
Ir1	Ir3	2.8211(14)	Ir1	Au1	Bi1	65.39(3)
Ir1	Ir2	2.8221(13)	Ir3	Bi1	Ir1	59.04(3)
Ir2	Ir3	2.9098(14)	Ir2	Bi1	Ir1	59.24(3)
Ir2	H1	1.699(10)	Ir2	Bi1	Ir3	65.13(3)
Ir3	H1	1.696(10)	Ir1	Ir3	Ir2	58.98(3)
Ir1	Bi1	2.9919(13)	Ir1	Ir2	Ir3	58.94(3)
Ir3	Bi1	2.7125(12)	Ir3	Ir1	Ir2	62.08(3)
Ir2	Bi1	2.6937(14)	Ir2	Bi1	Au1	106.41(4)
Au1	Bi1	2.8295(13)	Ir3	Bi1	Au1	103.42(4)
Ir3	Sn1	2.6415(18)				
Ir2	Sn2	2.6413(19)				

[a] Estimated standard deviations in the least significant figure are given in parenthesis

Table 4.5 Selected intermolecular angles and bond distances for **4.4** [a]

Atom	Atom	Distance	Atom	Atom	Atom	Angle
Au1	Ir1	2.7080(6)	Ir1	Au1	Bi1	63.547(16)
Au1	Bi1	2.8703(6)	Ir2	Ir3	Ir1	60.401(18)
Bi1	Ir3	2.6979(6)	Ir3	Ir2	Ir1	60.418(18)
Bi1	Ir2	2.7036(6)	Ir2	Ir1	Ir3	59.181(17)
Bi1	Ir1	2.9406(6)	Ir2	Bi1	Ir1	59.498(16)
Ir2	Sn1	2.5505(9)	Ir1	Ir2	Ir3	58.94(3)
Ir2	Ir3	2.7736(7)	Ir3	Bi1	Ir1	59.567(17)
Ir2	Ir1	2.8082(7)	Ir3	Bi1	Ir2	61.792(18)
Ir3	Sn2	2.5565(10)	Sn1	O1	Sn2	121.2(4)
Ir3	Ir1	2.8087(7)				

[a] Estimated standard deviations in the least significant figure are given in parenthesis

124

Table 4.6. Cartesian coordinates for geometry optimization of compound **4.2**

Atom	X	Y	Z
Au	2.4328	4.6715	9.0840
Bi	4.6271	5.3410	7.3639
Ir	1.9586	6.3385	7.0318
Ir	3.9347	6.7572	5.1291
Ir	4.0644	8.0316	7.5991
C	6.0047	6.6312	4.8590
C	6.8018	7.7854	4.9885
H	6.3400	8.7562	5.1904
C	8.1954	7.7213	4.8679
H	8.7856	8.6364	4.9764
C	8.8303	6.5024	4.6077
H	9.9191	6.4539	4.5144
C	8.0521	5.3537	4.4417
H	8.5267	4.3972	4.2027
C	6.6587	5.4187	4.5658
H	6.0812	4.5036	4.4077
C	2.5988	3.3958	10.6286
C	3.4310	2.0182	12.2506
H	4.1969	1.5830	12.8852
C	2.0729	1.8433	12.2220
H	1.4164	1.2067	12.8070
C	0.2358	2.8055	10.7469
C	0.9436	4.8772	6.4560
C	0.7921	6.9898	8.3384
C	1.6063	7.4227	5.4826
C	-1.4108	2.2043	9.1115
H	-1.7367	1.6026	8.2590
C	-0.1411	1.9943	9.6635
C	5.0464	3.4376	10.9018
C	5.7042	2.8697	9.7935
C	6.9308	3.4334	9.4176
H	7.4734	3.0219	8.5647
C	5.8919	8.1425	8.0067
C	7.4679	4.5198	10.1151
H	8.4193	4.9514	9.7991
C	6.7934	5.0554	11.2129
H	7.2195	5.9089	11.7469
C	5.5628	4.5214	11.6260
C	3.6300	5.2395	4.1329
C	3.7826	8.1227	3.8446
C	0.3072	5.9885	12.0568
H	1.1611	5.9108	11.3642

H	0.6201	6.5917	12.9281
H	-0.4966	6.5275	11.5278
C	-0.1688	4.6001	12.5082
H	0.6852	4.0813	12.9801
C	-1.2753	4.7154	13.5638
H	-2.0980	5.3630	13.2145
H	-0.8715	5.1685	14.4861
H	-1.6942	3.7243	13.8110
C	4.7876	5.1402	12.7703
H	3.9906	4.4331	13.0617
C	4.1211	6.4407	12.3050
H	3.5081	6.8799	13.1119
H	3.4700	6.2608	11.4330
H	4.8841	7.1831	12.0107
C	5.6640	5.3767	14.0052
H	6.1884	4.4522	14.3040
H	5.0400	5.7179	14.8495
H	6.4226	6.1563	13.8197
C	5.1136	1.6933	9.0425
H	4.0209	1.8492	8.9768
C	5.3708	0.3825	9.8066
H	6.4560	0.2500	9.9680
H	4.9937	-0.4782	9.2254
H	4.8713	0.3739	10.7889
C	5.6487	1.5599	7.6155
H	5.5820	2.5086	7.0564
H	5.0599	0.8048	7.0677
H	6.6996	1.2203	7.6110
C	0.7757	0.9262	9.1035
H	1.6216	0.8004	9.8025
C	3.6471	9.5193	6.5314
C	1.3427	1.3350	7.7392
H	1.9993	0.5392	7.3431
H	1.9285	2.2684	7.8172
H	0.5303	1.5119	7.0137
C	3.4115	8.4583	9.3020
C	0.0518	-0.4258	9.0147
H	-0.7221	-0.4129	8.2273
H	-0.4372	-0.6766	9.9718
H	0.7689	-1.2273	8.7627
C	-0.6112	3.7662	11.3229
C	-1.8761	3.9347	10.7458
H	-2.5655	4.6731	11.1621
C	-2.2643	3.1761	9.6382
H	-3.2487	3.3336	9.1903

N	1.5859	2.6934	11.2270
N	3.7356	2.9574	11.2590
O	7.0053	8.2784	8.3798
O	3.4782	10.5257	5.9299
O	3.0133	8.8028	10.3612
O	0.2269	4.0317	6.0496
O	-0.0232	7.4072	9.0855
O	0.9237	8.1092	4.7817
O	3.4156	4.2576	3.5061
O	3.7155	8.9153	2.9726

1. (a) Grasselli, R. K. *Catal. Today* **2014**, *238*, 10–27. (b) Grasselli, R. K., *Topics in Catal.* **2002**, *21*, 79 – 88. (c) Grasselli, R.K. *Handbook of Heterogeneous Catalysis*, Ertl, G., Knozinger, H., Weitkamp, J., VCH Publishers, Weinheim, vol. 5, **1997**, pp 2302-2326. (d) Grasselli, R.K., *Catal. Today*, **2005**, *99*, 23-31. (e) Goddard III, W. A.; Chenoweth, K.; Pudar, S.; van Duin, A. C. T.; Cheng, M.-J. *Top Catal*. **2008**, *50*, 2–18. (f) Jang, Y. H.; Goddard III, W. A. *J. Phys. Chem. B* **2002**, *106,* 5997-6013.

2. Adams, R. D.; Chen, M.; Elpitiya, G.; Potter, M. E.; Raja, R., *ACS Catal.*, **2013**, *3*, 3106−3110.

3. (a) Yamazoe, S.; Koyasu, K.; Tsukuda, T., *Acc. Chem. Res.*, 2014, *47*, 816 - 824 (b) Miyamura, H.; Matsubara, R.; Kobayashi, S. *Chem. Commun*., **2008**, 2031 - 2033. (c) Hutchings, G. J.; Kiely, C. J., *Acc. Chem. Res.* **2013**, *46*, 1759 – 1772. (d) Hutchings, G. J., *Catalysis Today* **2014**, *238*, 69–73. (e) Zhang, Y.; Cui, X.; Shi, F.; Deng, Y., *Chem. Rev*. **2012**, *112*, 2467 – 2505. (f) Hutchings, G. J., *Chem. Commun.* **2008**, 1148 – 1164. (g) Lopez-Sanchez, J. A.; Dimitratos, N.; Glanvilla, N,; Kesavan, L.; Hammond, C.; Edwards, J. K.; Carley, A. F.; Kiely, C. J.; Hutchings, G. J., *Applied Catalysis A: General* **2011**, *391,* 400 – 406. (h) Enache, D. I.; Edwards, J. K.; Landon, P.; Solsona-Espriu, B.; Carley, A. F.; Herzing, A. A.; Watanabe, M.; Kiely, C. J.; Knight, D. W.; Hutchings, G. J., *Science* **2006**, *311*, 362 – 365. (i) Miedziak, P.; Sankar, M.; Dimitratos, M.; Lopez Sanchez, J. A.; Carley, A. F.; Knight, D. W.; Taylor, S. H.; Kiely, C. J.; Hutchings, G. J., *Catal. Today* **2011**, *164,* 315–319. (j) Wang, R.; Zhiwei Wu, Z.; Chen, C. Zhangfeng

Qin, Z.; Zhu, H.; Wang, G.; Wang, H.; Wu, C.; Dong, W.; Fan, W.; Wang, J. *Chem. Commun.,* **2013**, *49*, 8250-8252.

4. (a) Holt, M. S.; Wilson, W. L.; Nelson, J. H. *Chem. Rev*. **1989**, *89*, 11–49. (b) Burch, R.; Garla, L. C. *J. Catal*. **1981**, *71*, 360–372. (c) Park, Y.-K.; Ribeiro, F. H.; Somorjai, G. A. *J. Catal.* **1998**, *178*, 66–75. (d) Jerdev, D. I.; Olivas, A.; Koel, B. E. *J. Catal.* **2002**, *205*, 278–288. (e) Adams, R. D.; Trufan, E. *Phil. Trans. R. Soc*. **2010**, *368*, 1473–1493. (f) Thomas, J. M.; Adams, R. D.; Boswell, E. M.; Captain, B.; Gronbeck, H.; Raja, R. *Faraday Discuss*. **2008**, *138*, 301–315. (g) Hungria, A. B.; Raja, R.; Adams, R. D.; Captain, B.; Thomas, J. M.; Midgley, P. A.; Golvenko, V.; Johnson, B. F. G. *Angew. Chem., Int. Ed*. **2006**, *45*, 4782–4785. (h) Adams, R. D.; Boswell, E. M.; Captain, B.; Hungria, A. B.; Midgley, P. A.; Raja, R.; Thomas, J. M. *Angew. Chem., Int. Ed*. **2007**, *46*, 8182–8185. (i) Adams, R. D.; Blom, D. A.; Captain, B.; Raja, R.; Thomas, J. M.; Trufan, E. *Langmuir* **2008**, *24*, 9223–9226. (j) D. Das, S. S. Mohapatra, S. Roy, *Chem. Soc. Rev.,* **2015**, *44*, 3666-3690.

5. Adams, R. D.; Chen, M., Elpitiya, G.; Zhang, Q., *Organometallics*, **2012**, *31*, 7264 - 7271.

6. Adams, R. D.; Chen, M., *Organometallics* **2012**, *31*, 6457−6465.

7. (a) Adams, R. D.; Rassolov, V.; Zhang, Q. *Organometallics* **2013**, *32*, 6368−6378. (b) Adams, R. D.; Rassolov, V.; Zhang, Q., *Organometallics* 32 (2013) 1587 - 1590.

8. Adams, R. D.; Rassolov, V.; Wong, Y. O. *Angew. Chem.* **2014**, *53*, 11006 -11009.

9. Hashmi, A.S.K.; Ramamurthi, T.D.; Rominger, F.; *J. Organomet. Chem*, **2009**, *694*, 592–597.

10. Garlaschelli, L.; Della Pergola, R.; Martinengo, S., *Inorg. Synth*. **1990**, 28, 211-215.

11. Kruppa, W.; Blaeser, D.; Boese, R.; Schmid, G., *Organisch. Chem.*, **1982**, *37B*, 209-213.

12. Gaillard, S.; Slawin, A. M. Z.; Nolan, S. P., *Chem. Commun*, **2010**, *46*, 2742-2744.

13. SAINT+, version 6.2a, Bruker Analytical X-ray Systems, Inc., Madison, WI, 2001.

14. Sheldrick, G. M. SHELXTL, version 6.1, Bruker Analytical X-ray Systems, Inc., Madison, WI, 1997.

15. ADF2013; SCM Theoretical Chemistry,Vrije Universiteit: Amsterdam, The Netherlands. http://www.scm.com.

16. Perdew, J. P.; Ruzsinszky, A.; Csonka, G. I.; Vydrov, O. A.; Scuseria, G. E. *Phys. Rev. Lett*. **2008**, *100*, 136406.

17. (a) Bader, R. F. W. Atoms in Molecules: A Quantum Theory; Clarendon: Oxford, U.K., 1990. (b) Cortés-Guzmán, F.; Bader, R. F. W. *Coord. Chem. Rev*. **2005**, *249*, 633−662.

18. Keith, T. A. AIMAll, Version 12.11.09; TK Gristmill Software: Overland Park, KS, 2012. aim.tkgristmill.com.

19. Adams, R. D.; Chen, M., Yang, X. *Organometallics* **2012**, *31*, 3588−3598.

20. Lin, T.-P.; Ke, I.-S.; Gabbai, F. P. *Angew. Chem. Int. Ed*. **2012**, *51*, 4985 – 4988.

21. Tschersich, C.; Limberg, C.; Roggan, S.; Herwig, C.; Ernsting, N.; Kovalenko, S.; Mebs, S. *Angew. Chem. Int. Ed*. **2012**, *51*, 4989 – 4992.

22. Adams, R. D.; Chen, M., *Organometallics* **2011**, *30*, 5867–5872.

23. (a) Bau, R.; Drabnis, M. H. *Inorg. Chim. Acta* **1997**, *259*, 27 - 50. (b) Teller, R. G.; Bau, R., *Struc. Bonding* **1981**, *41*, 1 - 82.

24. Adams, R. D.; Captain, B.; Smith, Jr., J. L.; Hall, M. B.; Beddie, C. L.; Webster, C. E. *Inorg. Chem.* 43 (2004) 7576 – 7578.

25. Alvarez, M. A.; Alvarez, M. P.; Carreño, R.; Ruiz, M. A.; Bois, C. *J. Organomet. Chem.* 696 (2011) 1736 – 1748.

26. Adams, R. D.; Captain, B.; Hollandsworth, C. B.; Johansson, M.; Smith, J. L., Jr, *Organometallics* **2006**, *25*, 3848 – 3855.

CHAPTER 5

IRIDIUM-BISMUTH CARBONYL CLUSTER COMPLEXES[4]

---

[4] Adams, R.D. and Elpitiya, G. Submitted to *J. Organomet. Chem.*, 06/19/2015

Introduction

Interest in transition metal - bismuth compounds stems from ability of these materials to serve as catalysts for the selective oxidation and ammoxidation of hydrocarbons[1]. In recent studies we have synthesized new ReBi carbonyl cluster compounds that have been found to be precursors to effective catalysts for the ammoxidation of 3-picoline to nicotinonitrile (Figure 5.1)[2]. There are very few examples of iridium-bismuth carbonyl cluster complexes[3-5]. We have previously shown that the compound $Ir_3(CO)_9(\mu_3$-Bi), **5.1** can be converted into the higher nuclearity complex $Ir_5(CO)_{10}(\mu_3$-Bi)$_2(\mu_4$-Bi) by reaction with $BiPh_3$ (Figure 5.2)[4], and have shown that **5.1** and $Ir_5(CO)_{10}(\mu_3$-Bi)$_2(\mu_4$-Bi) are precursors to effective catalysts for the direct oxidation of 3-picoline to nicotinic acid, also known as Niacin, by using the oxidant acetylperoxyborate (Figure 5.3)[4]. We have also prepared a number of iridium-bismuth complexes containing germanium and tin ligands from complex **5.1** by reactions with $HGePh_3$ and $HSnPh_3$, (Figure 5.4)[5]. In the continuation of our studies of the chemistry of iridium-bismuth carbonyl cluster complexes, we have now investigated the self-condensation of **5.1** and its reactions with PPh_3 and with $Ru_3(CO)_{10}(NCMe)_2$. The results of these studies are reported in this chapter.

Experimental Details

General Data.

Reagent grade solvents were dried by the standard procedures and were freshly distilled prior to use. Infrared spectra were recorded on a Thermo Nicolet Avatar 360 FT-IR spectrophotometer. Room temperature ^{1}H NMR spectra were recorded on a Varian

Mercury 300 spectrometer operating at 300.1 MHz. $^{31}P\{^1H\}$ NMR were recorded on a Bruker Avance/DRX 400 NMR spectrometer operating at 162.0 MHz. Mass spectrometric (MS) measurements performed by a direct-exposure probe using either electron impact ionization (EI) or electrospray ionization (ESI) using a Micromass Q-TOF instrument. $Ir_4(CO)_{12}$, $Ru_3(CO)_{12}$ and PPh_3 were obtained from STREM and Sigma-Aldrich, respectively and were used without further purification. $[PPN]Ir(CO)_4$ [6] and $Ru_3(CO)_{10}(NCMe)_2$ [7] were prepared according to the previously reported procedures. $Ir_3(CO)_9(\mu_3\text{-Bi})$, **5.1** [3] was prepared by a modified procedure reported previously[4]. All product separations were performed by TLC in air on Analtech 0.25mm silica gel 60 Å F254 and 0.25mm aluminum oxide 60 Å F254 glass plates.

Synthesis of $Ir_6(CO)_{13}(\mu_3\text{-Bi})(\mu_4\text{-Bi})$, 5.2.

A 13.2 mg (0.013 mmol) portion of **5.1** were dissolved in 15 mL of hexane. The reaction was heated to reflux for 18 h. The solvent was then removed *in vacuo*, and the product was isolated by TLC with a 4/1 hexane/methylene chloride solvent ratio as the eluent. This gave 10.31 mg (0.005 mmol) of dark green $Ir_6(CO)_{13}(\mu_3\text{-Bi})(\mu_4\text{-Bi})$, **5.2** (84% yield). Spectral data for **5.2**: IR υ_{CO} (cm^{-1} in CH_2Cl_2) 2095(w), 2067(w), 2042 (vs), 2021 (w), 2007 (w)ˑ 1992 (w). ES (negative) /MS for **5.2**: m/z = 2015 (M + Br$^-$). The isotope distribution pattern is consistent with the presence of six iridium atoms and two bismuth atoms.

Synthesis of $Ir_3(CO)_8(PPh_3)(\mu_3\text{-Bi})$, 5.3.

24.00 mg (0.023 mmol) of **5.1** was dissolved in 10 mL of CH_2Cl_2. 6.00 mg (0.023 mmol) of PPh_3 was added and the reaction mixture was heated to reflux for 15.5 h. The

134

solvent was then removed *in vacuo*, and the product was isolated by TLC with a 6/1 hexane/methylene chloride solvent ratio as the eluent. This gave 16.50 mg of the product yellow $Ir_3(CO)_8(PPh_3)(\mu_3\text{-Bi})$, **5.3**, (56 % yield). Spectral data for **5.3**: IR υ_{CO} (cm-1 in CH_2Cl_2) 2073(m), 2041 (vs), 2018 (s), 2007 (m); ^{31}P {^1H} NMR (CDCl_3) δ = -8.54 ppm (s,1PPh_3) Mass Spec. ES (positive) /MS for 1: m/z = 1272 (M^+). The isotope distribution pattern is consistent with the presence of three iridium atoms and one bismuth atom.

Synthesis of $Ir_3(CO)_7(PPh_3)_2(\mu_3\text{-Bi})$, 5.4.

A 13.0 mg (0.050 mmol) portion of PPh_3 was added to 25.0 mg (0.024 mmol) of **5.1** that was dissolved in 15 mL of methylene chloride. The reaction was heated to reflux for 3.5h. The solvent was then removed *in vacuo*, and the product was isolated by TLC with a 6/1 hexane/methylene chloride solvent ratio as the eluent. This gave 30.0 mg (0.02 mmol) of orange $Ir_3(CO)_7(PPh_3)_2(\mu_3\text{-Bi})$, (**5.4**, 83% yield). Spectral data for **5.4**: IR υ_{CO} (cm^{-1} in CH_2Cl_2) 2046(m), 2014(s), 1984 (s), 1952 (vw); ^{31}P {^1H} NMR (CDCl_3) δ = -11.13 ppm (s, 2 PPh_3). ES (positive)/MS for **5.4**: m/z = 1506 (M^+). The isotope distribution pattern is consistent with the presence of three iridium atoms, one bismuth atom and a phosphorus atom.

Synthesis of $Ir_3(CO)_6(PPh_3)_3(\mu_3\text{-Bi})$, 5.5.

A 17.0 mg (0.065 mmol) portion of PPh_3 was added to 33.0 mg (0.022 mmol) of **5.1** that was dissolved in 15 mL of methylene chloride. The reaction was heated to reflux for 3 h. The solvent was then removed *in vacuo*, and the product was isolated by TLC with a 6/1 hexane/methylene chloride solvent ratio as the eluent. This gave 27.8 mg (0.016 mmol) of dark orange $Ir_3(CO)_6(PPh_3)_3(\mu_3\text{-Bi})$, **5.1** (73% yield). Spectral data for

5.1: IR v_{CO} (cm^{-1} in CH$_2$Cl$_2$) 2006(m), 1973(vs), 1951 (s); ^{31}P {^{1}H} NMR (CDCl$_3$) δ = -4.96 ppm (s, 3 PPh$_3$) ES (positive) /MS for **5.1**: m/z = 1740 (M^{+}). The isotope distribution pattern is consistent with the presence of three iridium atoms and one bismuth atom.

Synthesis of Ir$_6$(CO)$_{12}$(PPh$_3$)(μ$_3$-Bi)(μ$_4$-Bi), 5.6.

A 12.0 mg (0.046 mmol) portion of PPh$_3$ were added to 10.0 mg (0.005 mmol) of **5.2** that had been previously dissolved in 10 mL of benzene. The reaction was heated to reflux for 0.5 h. The solvent was then removed *in vacuo*, and the product was isolated by TLC with a 4/1 hexane/methylene chloride solvent ratio as the eluent. This gave 8.00 mg (0.0040 mmol) of brown Ir$_6$(CO)$_{12}$(PPh$_3$)(μ$_3$-Bi)(μ$_4$-Bi), **5.6** (69 % yield). Spectral data for **5.6**: IR v_{CO} (cm^{-1} in CH$_2$Cl$_2$) 2062 (w), 2027(s), 2008 (m), 1983 (w). ^{31}P {^{1}H} NMR (CD$_2$Cl$_2$) δ = -27.35 ppm (s, 1 PPh$_3$). ES (negative) /MS for **5.6**: m/z = 2205 (M + Cl$^-$). The isotope distribution pattern is consistent with the presence of six iridium atoms and two bismuth atoms.

Synthesis of Ir$_3$(CO)$_6$ (PPh$_3$)(μ-C$_6$H$_4$PPh$_2$)(μ-H)(μ$_3$-Bi), 5.7.

A 17.0 mg (0.011 mmol) portion of **5.4** was dissolved in 15 mL of benzene. The reaction mixture was heated to reflux for 5.5 h. The solvent was then removed *in vacuo*, and the product was isolated by TLC with a 6/1 hexane/methylene chloride solvent ratio as the eluent. This gave 14.6 mg (0.010 mmol) of orange Ir$_3$(CO)$_6$(PPh$_3$)(μ-C$_6$H$_4$PPh$_2$)(μ-H)(μ$_3$-Bi), **5.7** (87 % yield). Spectral data for **5.7**: IR vCO (cm^{-1} in CH$_2$Cl$_2$) 2039 (m), 2016(vs), 1988 (s), 1948 (w). ^{1}H NMR (CD$_2$Cl$_2$): δ = -19.78 (d, 1 H, J_{P-H} = 9Hz), 7.54-7.10 ppm (m, 25 H, phenyls on PPh$_3$ and PPh$_2$), 5.90 (t of d, 1 H, H$_{52}$, $^3J_{P-H}$ = 9Hz, $^3J_{H-H}$

= 7Hz), 6.69 (d of t, 1 H, H_{53}, $^3J_{H-H}$ = 7Hz), 6.93 (d of t, 1 H, H_{54}, $^3J_{H-H}$ = 7Hz), 7.70 (d of d, 1 H, H_{55}, $^3J_{H-H}$ = 6.4 Hz). $^{31}P \{^1H\}$ NMR (CD$_2$Cl$_2$) δ = -11.23 ppm (d, 1 PPh$_3$, J_{P-P} = 62 Hz), -47.53 ppm (d, 1 PPh$_2$, J_{P-P} = 62 Hz). EI /MS for **7**: m/z = 1478. The isotope distribution pattern is consistent with the presence of three iridium atoms and one bismuth atom.

Pyrolysis of 5.3.

A 33.0 mg (0.026 mmol) portion of **5.3** was dissolved in 20 mL of benzene. The reaction mixture was heated to reflux for 6 h. The solvent was then removed *in vacuo*, and the products were isolated by TLC with a 6/1 hexane/methylene chloride solvent ratio as the eluent. This yielded three bands in order of elution: band 1 (orange) 6.0 mg of **5.7** (16 % yield); band 2 (brown) 1.0 mg, Ir$_5$(CO)$_9$(μ-PPh$_2$)$_2$(μ-C$_6$H$_4$)(μ$_4$-Bi), **5.8** (3.4% yield) and band 3 (green) 12.0 mg of **5.6** (43% yield). Spectral data for **5.8**: IR v_{CO} (cm^{-1} in CH$_2$Cl$_2$) 2053 (w), 2029(s), 1997 (m). EI /MS for **5.8**: m/z = 1868. The isotope distribution pattern is consistent with the presence of five iridium atoms and one bismuth atom.

Synthesis of Ir$_3$Ru$_4$(CO)$_{18}$(μ$_3$-Bi), 5.9 and Ir$_3$Ru$_3$(CO)$_{15}$)(μ$_4$-Bi), 5.10.

A 11.6 mg (0.011 mmol) amount of **5.1** was dissolved in 15 mL of CH$_2$Cl$_2$ and the reaction flask was placed in a dry ice/acetone bath and a 30.0 mg (0.045 mmol) amount of Ru$_3$(CO)$_{10}$(NCMe)$_2$ was added. The reaction mixture was allowed to warm to 25 ^{o}C and was then allowed to stir for 18 h. The solvent was then removed *in vacuo*, and the products were isolated by TLC by using a 4/1 hexane/methylene chloride solvent mixture as the eluent. Band 4 yielded 5.8 mg (0.003 mmol) of brown Ir$_3$Ru$_4$(CO)$_{18}$(μ$_3$-

137

Bi), **5.9** (band 4, 30% yield) and band 2 yielded 1.0 mg (0.0006 mmol) of red Ir$_3$Ru$_3$(CO)$_{15}$(μ_4-Bi), **5.10** (band 2, 6% yield). Spectral data for **5.9**: IR vCO (cm^{-1} in CH$_2$Cl$_2$) 2097 (w), 2069 (s), 2045 (vs), 2031 (m), 2027 (m), 1996 (vw). EI/MS for **5.9**: m/z = 1695. The isotope distribution pattern is consistent with the presence of three iridium atoms and one bismuth atom and four ruthenium atoms. Spectral data for **5.10**: IR vCO (cm^{-1} in CH$_2$Cl$_2$) 2097 (w), 2057 (m), 2043 (s), 1991 (vw). EI/MS for **5.10**: m/z = 1510. The isotope distribution pattern is consistent with the presence of three iridium atoms and one bismuth atom and three ruthenium atoms.

Crystallographic Analyses:

Green crystals of **5.2** and orange crystals of **5.3** and **5.4** suitable for x-ray diffraction analyses were obtained by slow evaporation of solvent from a solution of the compound in hexane at room temperature. Yellow crystals of **5.5** suitable for x-ray diffraction analyses were obtained by slow evaporation of solvent from a solution of the compound in benzene at room temperature. Brown crystals of **5.6**, black crystals of **5.9** and red crystals of **5.10** suitable for x-ray diffraction were obtained by slow evaporation of solvent from a solution of the pure compound in methylene chloride and a hexane mixture at room temperature. Orange crystals of **5.7** and brown crystals of **5.8** suitable for x-ray diffraction analyses were obtained from solutions in methylene chloride/benzene solvent mixtures by slow evaporation of the solvent at room temperature. All data crystals were glued onto the end of a thin glass fibers. X-ray intensity data were measured by using a Bruker SMART APEX CCD-based diffractometer using Mo Kα radiation (λ = 0.71073 Å). The raw data frames were integrated with the SAINT+ program by using a narrow-frame integration algorithm[8]. Correction for Lorentz and

polarization effects was also applied with SAINT+. An empirical absorption correction based on the multiple measurement of equivalent reflections was applied using the program SADABS. All structures were solved by a combination of direct methods and difference Fourier syntheses, and refined by full-matrix least-squares on F^2 by using the SHELXTL software package[9]. All non-hydrogen atoms were refined with anisotropic displacement parameters. Hydrogen atoms were placed in geometrically idealized positions and included as standard riding atoms during the final cycles of least-squares refinements. Crystal data, data collection parameters, and results of the analyses are listed in Tables 5.1 – 5.3.

Compounds **5.2**, **5.3**, **5.6**, **5.7**, **5.8** and **5.10** crystallized in the monoclinic crystal system. The space group $P2_1/n$ was indicated by the systematic absences in the data for all of these crystals except for compounds **5.8** and **5.10** for which the alternative setting $P2_1/c$ was used. All analyses were confirmed by the successful solution and refinement of each structure. Compound **5.4** crystallized in the triclinic crystal system. The space group P-1 was chosen and confirmed by the successful solution and refinement of the structure. One molecule of hexane (disordered) from the crystallization solvent was co-crystallized with compound **5.4**. Compound **5.5** crystallized in the orthorhombic crystal system. The space group Pbca was identified on the basis on the systematic absences in the data and confirmed by the successful solution and refinement of the structure. One molecule of benzene co-crystallized with the asymmetric crystal unit of compound **5.5** from the crystallization solvent. It was disordered and was refined as a rigid group. The hydrido ligand in **5.7** was located in a difference Fourier map as a bridge across the Ir(1) – Ir(2) bond, and was refined with a isotropic thermal parameter. Compound **5.9** crystallized in

139

the orthorhombic crystal system. The space group *P*nma was indicated on the basis of the systematic absences in the data and confirmed by the successful solution and refinement of the structure.

Results and Discussion

The new compound $Ir_6(CO)_{13}(\mu_3\text{-Bi})(\mu_4\text{-Bi})$, **5.2** was obtained in 84% yield by the thermal decarbonylation and self-condensation of **5.1** by heating a solution in hexane solvent to reflux for 18 h. Compound **5.2** was characterized by IR and mass spectral analysis and by a single crystal X-ray diffraction analysis. An ORTEP drawing of the molecular structure of **5.2** as it is found in the solid state is shown in Figure 5.5. The cluster of compound **5.2** can be described as a capped square-pyramidal cluster of six iridium atoms which contains one quadruply bridging bismuth ligand Bi(1) across the base of the square pyramid and triply bridging bismuth ligand Bi(2) across the Ir(2), Ir(5), Ir(6) triangular face. The Ir − Ir bond distances in the square pyramid range from 2.7286(7) Å to 2.7996(7) Å and are similar in length to the Ir − Ir distances observed in the square pyramid of the pentairidiuim cluster in the compound $Ir_5(CO)_{10}(\mu_3\text{-Bi})_2(\mu_4\text{-Bi})$, **5.11**, 2.7796(9) Å - 2.8255(9) Å [4]. Two of the Ir − Ir distances to the capping $Ir(CO)_3$ group in **5.2** are relatively short, Ir(1) − Ir(3) = 2.6533(7) Å, Ir(1) - Ir(4) = 2.6632(7) Å while the distance to the apical atom of the square pyramid Ir(2) is much longer, Ir(1) - Ir(2) = 2.7317(7) Å. The longer Ir(1) - Ir(2) distance could be a steric effect because Ir(2) has eight atoms bonded to it while atoms Ir(2) and Ir(3) have only seven atoms bonded to them. The Ir − Bi distances to the quadruply bridging bismuth ligand Bi(1), 2.7800(7) Å – 2.8153(7) Å are similar in length to those observed in **5.10**, 2.8004(7) Å – 2.8185(7) Å. The Ir – Bi distances to the triply bridging Bi atom Bi(2) are

140

www.manaraa.com

significantly different; two are short, Ir(5) − Bi(2) = 2.7031(7) Å, Ir(6) − Bi(2) = 2.7066(8) Å and one Ir(2) - Bi(2) = 2.7803(7) Å is long. As described above for the bonding to Ir(1), this could also be explained by a steric effect. Assuming that each Bi ligand serves as a three electron donor, then cluster of **5.2** contains a total of 86 cluster valence electrons and its structure obeys the predictions of the Wade-Mingos Skeletal Electron Pair Theory[10].

Three PPh$_3$ derivatives of **5.1**, Ir$_3$(CO)$_{9-n}$(PPh$_3$)$_n$(μ_3-Bi), (**5.3 – 5.5**, n = 1 - 3) were obtained by the reactions of **5.1** with PPh$_3$ in the stochiometrically appropriate quantities. Each of these new compounds was characterized by IR, ^{1}H NMR, ^{31}P NMR, mass spec and single crystal X-ray diffraction analyses. ORTEP diagrams of these three new compounds are shown in Figures 5.6 − 5.8, respectively. Each compound contains a triangular cluster of three iridium atoms with three Ir − Ir bonds with a triply bridging bismuth atom. The Ir − Ir distances in each product: **5.2**, 2.7668(6) Å – 2.7916(6) Å; **5.3**, 2.7725(4)Å – 2.7930(4) Å and **5.4**, 2.7907(6) Å - 2.8029(6) Å, are slightly longer than those in **5.1**, 2.759(2) Å. The increased Ir − Ir bond lengths may be due in part to steric effects produced by the bulky PPh$_3$ ligands. All PPh$_3$ ligands occupy "equatorial" coordination sites in the Ir$_3$ plane, *cis* to the bridging Bi ligand. These sites should have lower steric effects than the "axial" sites. The Ir − Bi distances are not significantly different from those in **5.1**.

When compound **5.2** was treated with PPh$_3$ in benzene solution at reflux the new compound Ir$_6$(CO)$_{12}$(PPh$_3$)(μ_3-Bi)(μ_4-Bi)$_3$, **5.6** was formed in 69 % yield. Compound **5.6** was formed by the replacement of one of the CO ligands in **5.2** with a PPh$_3$ ligand. The location of the substitution was established by a single crystal X-ray diffraction analysis

141

of **5.6**, (Figure 5.9) . The cluster of **5.6** contains a capped square-pyramidal cluster of six Ir atoms with a quadruply bridging bismuth ligand and a triply bridging bismuth ligand arranged similar to that of **5.2**. The PPh$_3$ ligand is located on the Ir capping group *trans* to the Ir(1) – Ir(2) bond. As in **5.2**, the Ir – Ir bond distance to the apical Ir atom, Ir(1) – Ir(2) = 2.7550(8) Å, is significantly longer than the other two Ir – Ir bonds to the capping atom Ir(1), Ir(1) – Ir(3) = 2.6644(7) Å and Ir(1) – Ir(4) = 2.6854(7) Å. The Ir(1) – Ir(2) bond in **5.6** is also slightly longer than that in **5.2**, 2.7317(7) Å. This could be due to a slight *trans*-structural effect caused by the PPh$_3$ ligand. The other Ir – Ir and Ir - Bi bonds in **5.6** are similar to those in **5.2**.

Efforts were made to try to obtain self-condensation products from **5.3** and **5.4** by thermal treatments. Pyrolysis of **5.3** in benzene solution a reflux for 6 h (80 ^{o}C) yielded **5.6** (43% yield), a new compound Ir$_3$(CO)$_6$(PPh$_3$)(μ-C$_6$H$_4$PPh$_2$)(μ-H)(μ_3-Bi), **5.7** (16% yield) and a trace of a Ir$_5$Bi complex **5.8** (3.4% yield). Compound **5.7** was obtained in a much better yield (87%) by the pyrolysis of **5.4** in benzene solvent at reflux.

An ORTEP diagram of the molecular structure of **5.7** is shown in Figure 5.10. Compound **5.7** contains a bismuth-bridged Ir$_3$ triangular cluster similar to those of **5.1** and **5.3** – **5.5**. There is a PPh$_3$ ligand on atom Ir(1) and an *o*-metallated PPh$_3$ ligand bridging the Ir(2) – Ir(3) bond. The Ir(2) – Ir(3) bond distance, Ir(2) – Ir(3) = 2.7278(6) Å, is slightly shorter than the the Ir – Ir bonds in **5.1** and **5.3** – **5.5**, perhaps due to the presence of the bridging C$_6$H$_4$PPh$_2$ ligand. The Ir(1) – Ir(3) bond is normal, 2.7775(6) Å. The Ir(1) – Ir(2) bond is significantly longer, 2.9255(6) Å, which is almost certainly a consequence of the presence of a hydrido ligand that bridges this bond[11], δ = -19.78 (d, *J*

$_{P-H}$ = 9Hz). The cluster of **5.7** contains 48 valence electrons which is consist with the observation of a closed cluster having three Ir – Ir bonds.

An ORTEP diagram of the molecular structure of $Ir_5(CO)_9(\mu-PPh_2)_2(\mu-C_6H_4)(\mu_4-Bi)$, **5.8** is shown in Figure 5.11. Compound **5.8** contains a square pyramidal cluster of five iridium atoms with a quadruply bridging bismuth atom across the base of the square pyramid. Compound **5.8** contains nine carbonyl ligands, two bridging phosphido (PPh_2) ligands and one edge bridging $\mu-\eta^2$-benzyne (C_6H_4) ligand; the latter was almost certainly derived from a phenyl ring cleaved from a PPh_3 ligand which then also yielded one of the bridging PPh_2 ligands. The eight Ir – Ir bond distances in cluster range from 2.7309(7) Å to 2.8510(8) Å. The shortest distance, Ir(2) – Ir(3) = 2.7309(7) Å, is bridged by one of the phosphide ligands. The Ir - Bi distances 2.8294(8) Å - 2.8817(7) Å are similar to the Ir – Bi distances to the quadruply bridging Bi ligands found in **5.2** and **5.6**. $\mu-\eta^2$-C_6H_4 ligands are rare. Previous examples include the compounds: $Os_5(CO)_{18}$ $\mu-\eta^2$-$C_6H_4)(\mu_4-Bi)(\mu-H)$ [12] and $Os_6(CO)_{20}(\mu-\eta^2-C_6H_4)$ $(\mu_4-Bi)(\mu-H)$ [13]. The Ir – C σ-bonding distances to the benzyne ligand in **5.8** are Ir(1) – C(53) = 2.077(14) Å and Ir(3) - C(58) = 2.091(14) Å. Assuming the phosphido ligands serve as 3-electron donors and the benzyne ligand is a 2-electron donor, then the metal atoms of the cluster of **5.8** contains a total of 74 valence electrons which is consistent with the observation of a square pyramidal cluster of five metal atoms [10].

Years ago, Lewis and Johnson reported the synthesis and structures of a number of bismuth-ruthenium carbonyl cluster complexes by reactions of the ruthenium carbonyl cluster complexes with $Bi(NO_3)_3$ and $NaBiO_3$ [14 - 15]. To complete the current study, it was decided to try to synthesize the first bismuth-containing iridium-ruthenium complexes by

143

condensation of **5.1** with $Ru_3(CO)_{10}(NCMe)_2$. The reaction of **5.1** with $Ru_3(CO)_{10}(NCMe)_2$ at 25 ^{o}C for 18 h yielded the two new iridium-ruthenium compounds $Ir_3Ru_4(CO)_{18}(\mu_3\text{-Bi})$, **5.9** (30% yield) and $Ir_3Ru_3(CO)_{15}(\mu_4\text{-Bi})$, **5.10** (6% yield). Both products were characterized by IR, mass spec and single crystal X-ray diffraction analyses. An ORTEP diagram of the molecular structure of **5.9** is shown in Figure 5.12. Compound **5.9** contains a total of seven metal atoms, three of iridium and four of ruthenium. The molecule contains reflection symmetry in the solid state. The cluster can be described as a $Ru(CO)_3$ capped Ir_3Ru_3 octahedron. The $Ru(CO)_3$ group caps an Ir_3 triangle. There is a triply bridging bismuth ligand on one of the $IrRu_2$ triangles. Compound **5.9** contains eighteen CO ligands distributed as shown in Figure 5.12. The cluster of **5.9** contains a total of 98 electrons which is consistent with the observed structure of a monocapped octahedral arrangement for the seven metal atoms[10]. Compound **5.10** is an obvious condensation product that contains three Ir atoms and three Ru atoms in the cluster of metal atoms. The structure of **5.10** which is shown in Figure 5.13 consists of a capped square pyramidal cluster of six metal atoms with a quadruply bridging bismuth ligands across the base of the square pyramid. Somehow the Ru atoms have become separated; two of them, Ru(1) and Ru(2), lie in the base of the square pyramid while the third one Ru(3) serves as the $Ru(CO)_3$ capping group on the Ir_3 triangle in the square pyramid. The Ru – Bi distances, 2.8220(7)Å and 2.8337(7) Å are slightly longer than the Ir – Bi distances, 2.7898(4) Å and 2.7918(5) Å. Compound **5.10** contains a total of 84 cluster valence electrons which violates the Wade-Mingos formulation of 86 for a monocapped octahedron [10].

144

Summary and Conclusions

A summary of the results of this work are presented in Schemes 5.1 and 5.2. Compound **5.1** readily loses CO upon heating and condenses to from the hexairidium product **5.2**. Years ago, Adams et al. showed that bridging sulfido ligands could facilitate condensation and self-condensation reactions of osmium and ruthenium carbonyl cluster complexes to produce higher nuclearity complexes [16 – 19]. The lone pair of electrons on the sulfido ligands clearly played a key role in the formation of new bonds between the condensing species [17-19]. The bridging bismuth ligand in **5.1** formally contains a lone pair of electrons and these electrons may also serve to facilitate the self-condensation of **5.1** to form the hexairidium complex **5.2** even though no intermediates were isolated that would confirm that such interactions did in fact occur in the course of the formation of **5.2**. Because of its facile elimination of CO, it was easy to prepare the PPh_3 derivatives **5.3** - **5.5** of **5.1** by reactions between **5.1** and PPh_3. Compound **5.3** eliminated CO and PPh_3 to yield **5.6**, the PPh_3 derivative of **5.2** by a condensation reaction, but **5.6** could be obtained in an even better yield by treatment of **5.2** with PPh_3. Pyrolysis of **5.3** also yielded a pentairidum complex **5.8** having a square pyramidal cluster of metal atoms in a very low yield by a combination of cluster and ligand degradation and reassembly. Compound **5.8** has an interesting structure and ligands. Unfortunately, we have not yet been able to synthesize compound **5.8** in a systematic way. Pyrolysis of **5.4** did not yield any higher nuclearity metal compounds, but did yield the complex **5.7**, an o-metallated PPh_3 derivative of **5.4** in a high yield. Complex **5.7** was also obtained in a low yield from the pyrolysis of **5.3**. The condensation of **5.1** with $Ru_3(CO)_{10}(NCMe)_2$ yielded compounds **5.9** and **5.10**, (Scheme 5.2) , the first examples of iridium-ruthenium carbonyl complexes

containing bismuth ligands. We have not been able to establish the mechanisms of the formation of **5.9** and **5.10** in this work, but we suspect that the Bi ligand in **5.1** probably played a role in the condensation processes leading to these products.
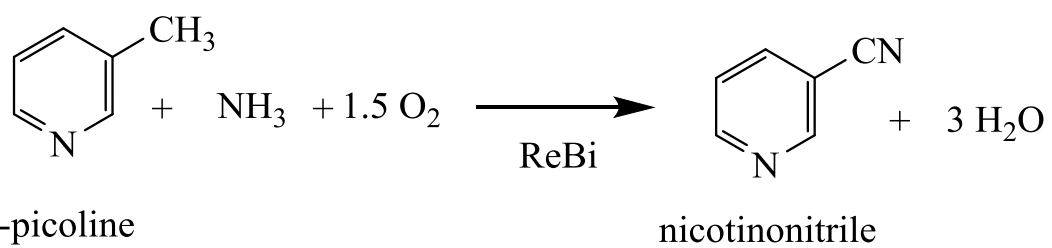
146

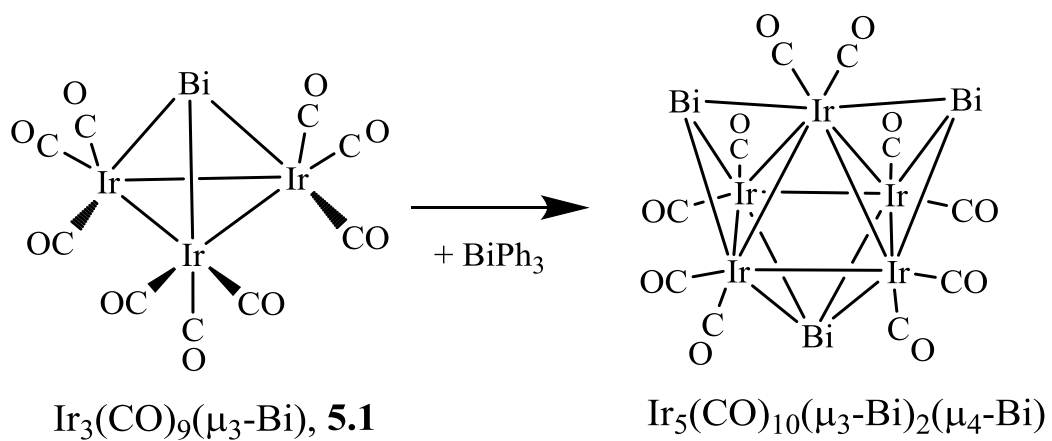Figure 5.1 Ammoxidation of 3-picoline to nicotinonitrile using ReBi catalysts.

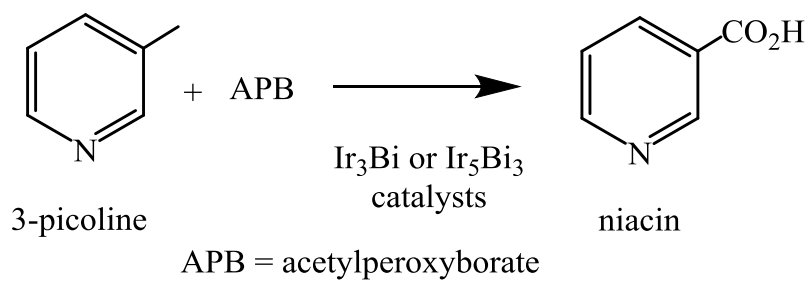Figure 5.2 Conversion of compound **5.1** to $Ir_5(CO)_{10}(\mu_3\text{-Bi})_2(\mu_3\text{-Bi})$.

Ir$_3$(CO)$_9$(μ_3-Bi), **5.1**

Ir$_5$(CO)$_{10}$(μ_3-Bi)$_2$(μ_4-Bi)

+ BiPh$_3$

148

Figure 5.3 Conversion of 3-picoline to niacin using IrBi nano partilcles.
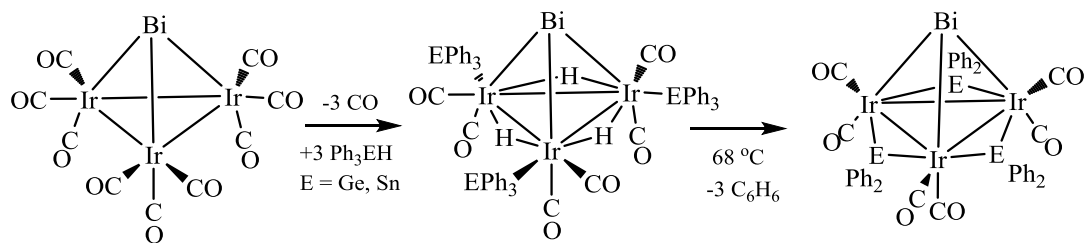
Figure 5.4 Iridium-bismuth complexes containing germanium and tin ligands.
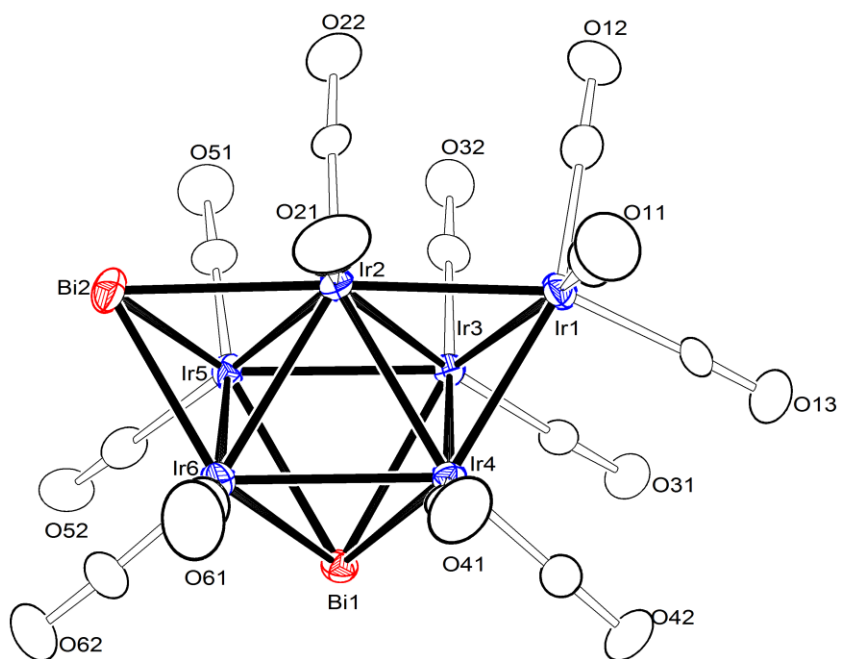
Figure 5.5 An ORTEP diagram of the molecular structure of $Ir_6(CO)_{13}(\mu_3\text{-Bi})(\mu_4\text{-Bi})$, **5.2** showing 30% thermal ellipsoid probability.

151
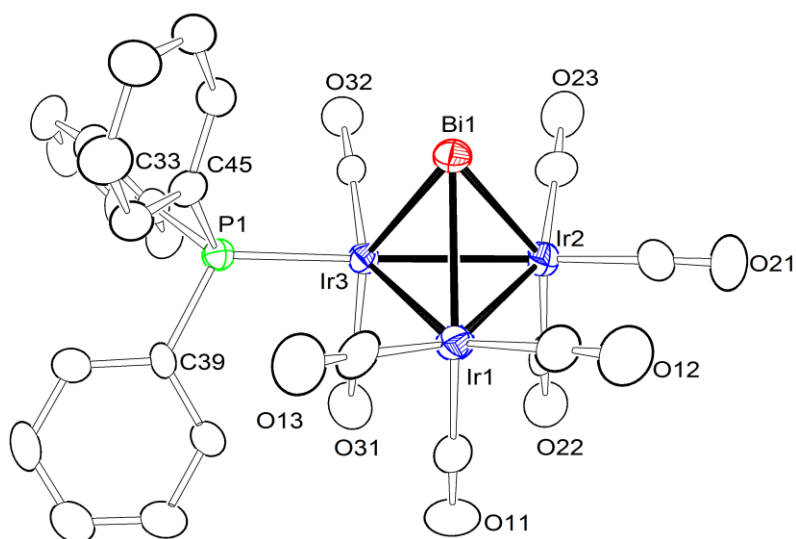
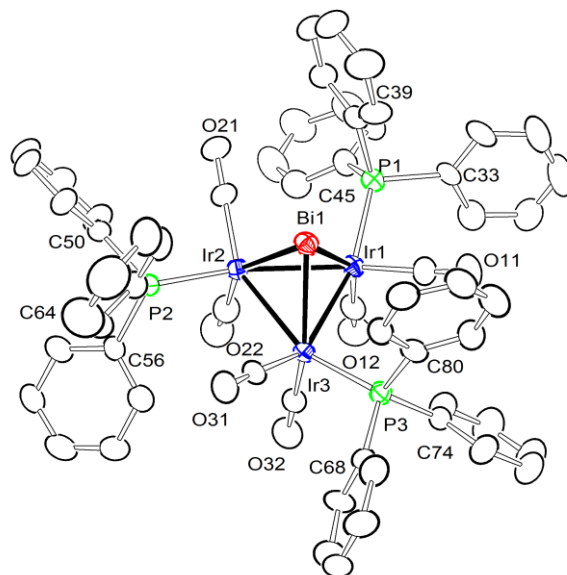Figure 5.6 An ORTEP diagram of the molecular structure of Ir$_3$(CO)$_8$(PPh$_3$)(μ$_3$-Bi), **5.3** showing 30% thermal ellipsoid probability.
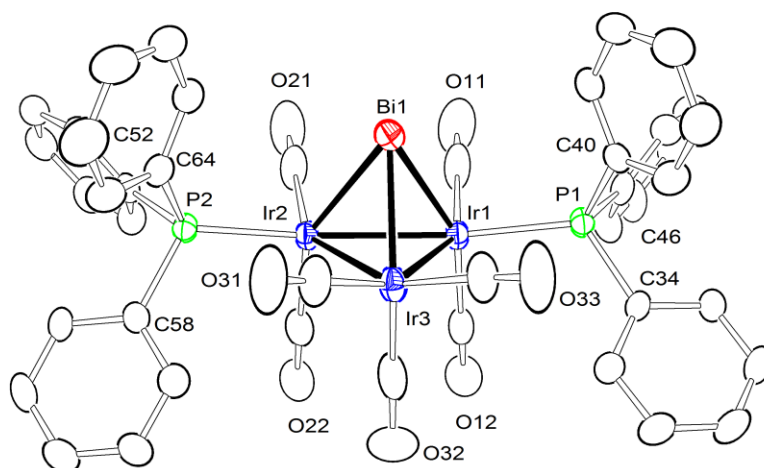
Figure 5.7 An ORTEP diagram of the molecular structure of
$Ir_3(CO)_7$ $(PPh_3)_2(\mu_3$-Bi), **5.4** showing 30% thermal ellipsoid
Probability.

Figure 5.8 An ORTEP diagram of the molecular structure of $Ir_3(CO)_6(PPh_3)_3(\mu_3\text{-Bi})$, **5.5** showing 30% thermal ellipsoid probability.
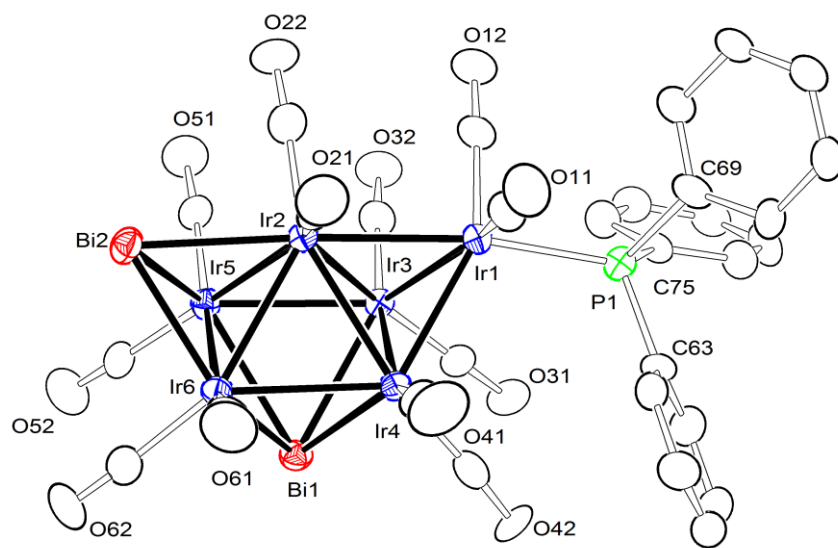
.

Figure 5.9 An ORTEP diagram of the molecular structure of $Ir_6(CO)_{12}(PPh_3)(\mu_3\text{-Bi})(\mu_4\text{-Bi})$, **5.6** showing 30% thermal ellipsoid probability.
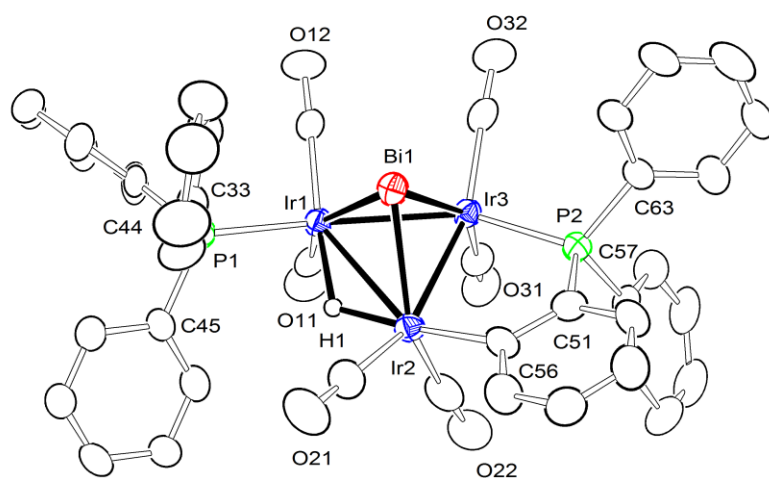
Figure 5.10 An ORTEP of the moleculecular structure
$Ir_3(CO)_6(PPh_3)(\mu_2\text{-}C_6H_4PPh_2)(\mu\text{-}H)(\mu_3\text{-}Bi)$, **5.7** showing
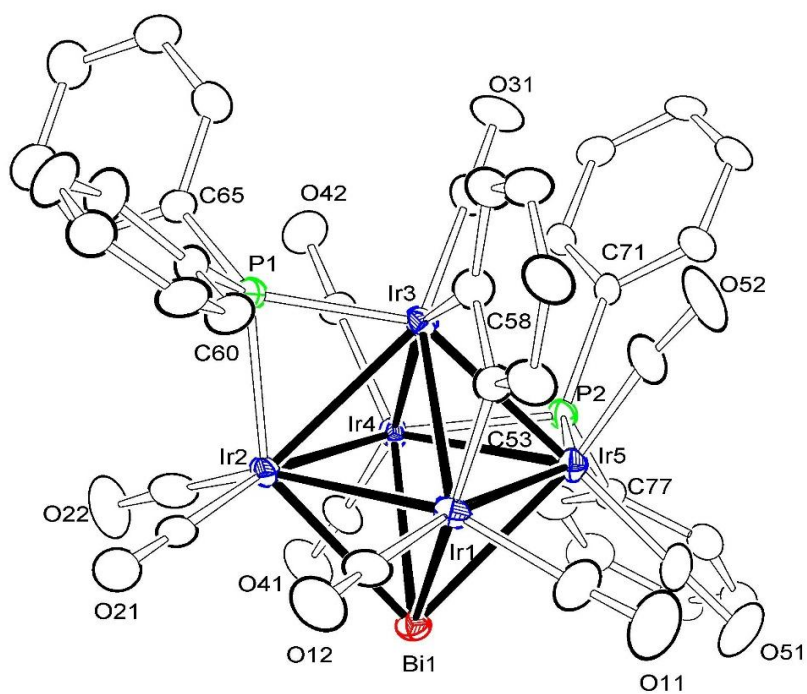20% thermal ellipsoid probability.

Figure 5.11 An ORTEP diagram of the molecular structure of $Ir_5(CO)_9(\mu\text{-}PPh_2)_2(\mu_4\text{-}C_6H_4)(\mu_4\text{-}Bi)$, **5.8** showing 15% thermal ellipsoid probability.
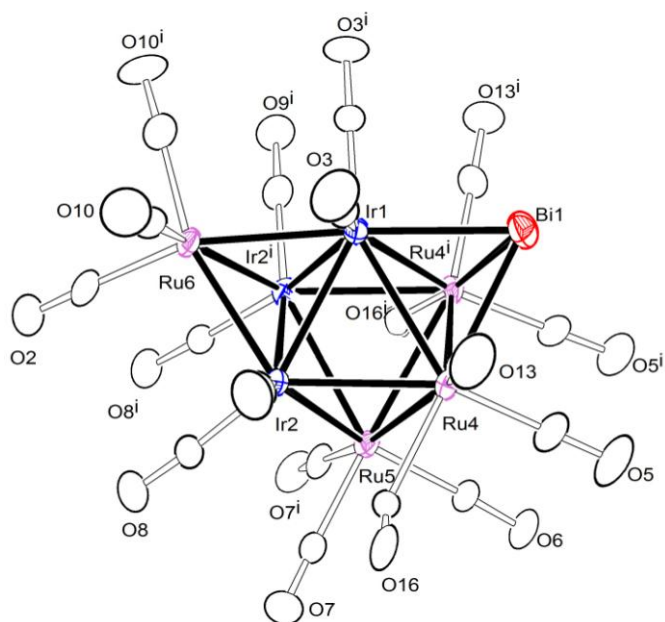
Figure 5.12. An ORTEP diagram of the molecular structure of
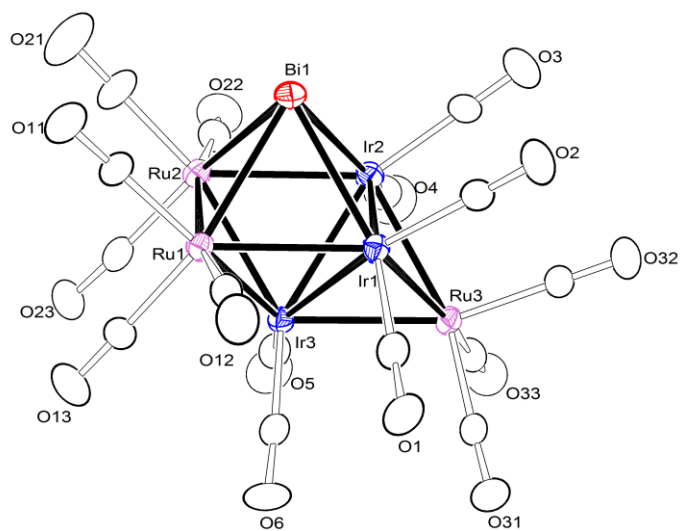$Ir_3Ru_4(CO)_{18}(\mu_3\text{-Bi})$, **5.9** showing 40% thermal ellipsoid
probability.

158

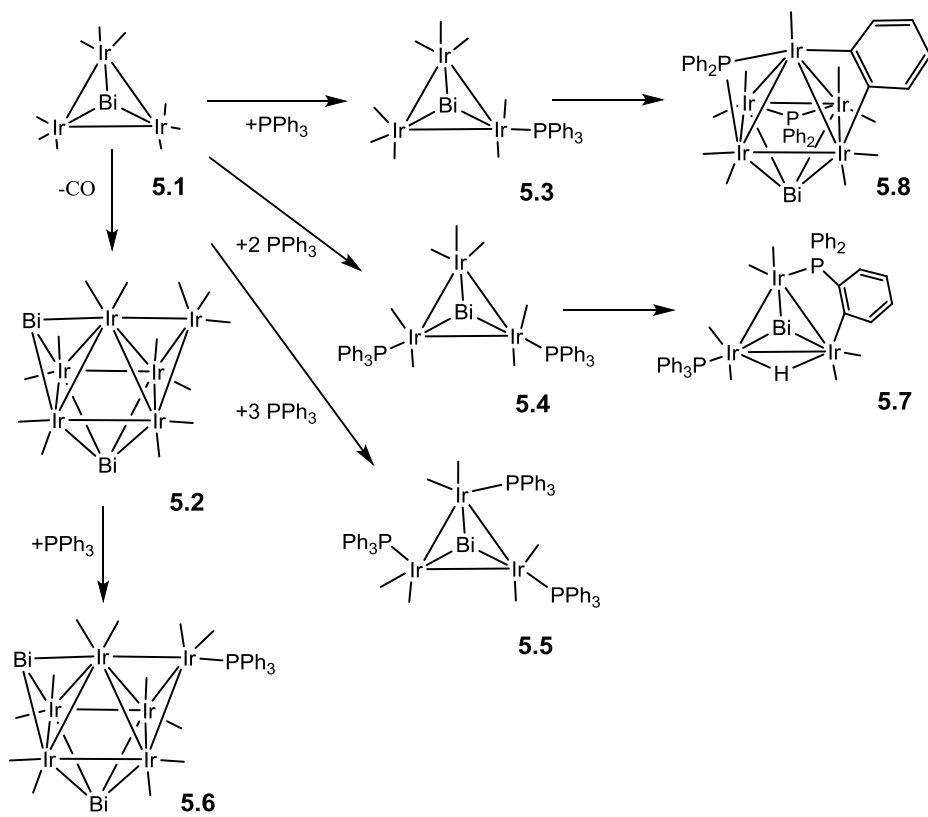Figure 5.13 An ORTEP diagram of the molecular structure of Ir$_3$Ru$_3$(CO)$_{15}$)(μ_4-Bi), **5.10** showing 30% thermal ellipsoid probability.

Scheme 5.1 Summary of the reactions showing the synthesis of
Compounds **5.2-5.8** from **5.1**.

Ir$_3$Ru$_4$(CO)$_{18}$(μ_3-Bi), **5.9**

Ir$_3$Ru$_3$Bi(CO)$_{15}$(μ_4Bi),**5.10**
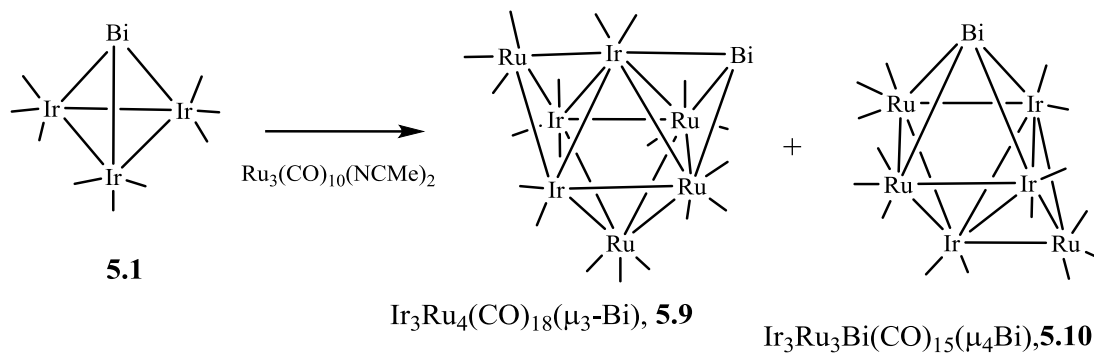
Scheme 5.2 Summary of the reactions showing the synthesis of compound **5.9 - 5.10** from **5.1**.

Table 5.1. Crystallographic Data for Compounds **5.2 - 5.4**[a].

Compound	**5.2**	**5.3**	**5.4**
Empirical formula	$Ir_6Bi_2O_{13}C_{13}$	$Ir_3BiPO_8C_{26}H_{15}$	$Ir_3BiP_2O_7C_{49}H_{44}$
Formula weight	1935.29	1271.93	1592.42
Crystal system	Monoclinic	Monoclinic	Triclinic
Lattice parameters			
a (Å)	9.9809 (5)	12.1768(5)	12.3518(11)
b (Å)	20.9530 (11)	16.4651(7)	15.2697(14)
c (Å)	11.7111 (6)	15.3158(7)	15.6403(14)
α (deg)	90	90	65.838(2)
β (deg)	92.295 (10)	105.836(1)	75.427(2)
γ (deg)	90	90	66.874(2)
V (Å^3)	2447.2 (2)	2954.2 (2)	2460.6 (4)
Space group	$P2_1$/n	$P2_1$/n	P-1
Z value	4	4	2
ρ_{calc} (g / cm^3)	5.253	2.860	2.149
μ (Mo Kα) (mm^{-1})	46.874	19.509	11.764
Temperature (K)	294(2)	294(2)	294(2)
$2\Theta_{max}$ (°)	50.04	50.06	50.06
No. Obs. (I > 2σ(I))	4316	5218	8702
No. Parameters	307	352	505
Goodness of fit (GOF)	1.039	1.045	1.057
Max. shift in cycle	0.001	0.001	0.001
Residuals*: R1; wR2	0.0326; 0.0928	0.0434; 0.0515	0.0308; 0.0837
Absorption Corr.Max/min	Multi-scan 1.000/0.264	Multi-scan 1.000/0.838	Multi-scan 1.000/0.696
Largest peak in Final Diff. Map (e$^-$ / Å^3)	1.456	0.884	2.788

* R1 $= \Sigma_{hkl}(||F_{obs}| - |F_{calc}||)/\Sigma_{hkl}|F_{obs}|$; wR2 $= [\Sigma_{hkl}w(|F_{obs}| - |F_{calc}|)^2/\Sigma_{hkl}wF^2_{obs}]^{1/2}$; w $= 1/\sigma^2(F_{obs})$; GOF $= [\Sigma_{hkl}w(|F_{obs}| - |F_{calc}|)^2/(n_{data} - n_{vari})]^{1/2}$.

Table 5.2. Crystallographic Data for Compounds **5.5 - 5.7**[a].

Compound	**5.5**	**5.6**	**5.7**
Empirical formula	$Ir_3BiP_3O_6C_{66}H_{51}$	$Ir_6Bi_2PO_{12}C_{30}H_{15}$	$Ir_3BiP_2O_6C_{42}H_{30}$
Formula weight	1818.56	2169.55	1478.18
Crystal system	Orthorhombic	Monoclinic	Monoclinic
Lattice parameters			
a (Å)	23.6355(13)	9.7831 (7)	13.7951 (5)
b (Å)	18.0823(10)	15.1472 (11)	16.6035 (6)
c (Å)	29.6151(17)	25.0740 (18)	19.0814 (7)
α (deg)	90	90	90
β (deg)	90	94.881(2)	109.376 (10)
γ (deg)	90	90	90
V ($\mathring{A}^3$)	12657.0 (12)	3702.2 (5)	4123.0 (3)
Space group	Pbca	$P2_1$/n	$P2_1$/n
Z value	8	4	4
ρ_{calc} (g / cm^3)	1.909	3.892	2.381
μ (Mo Kα) (mm^{-1})	9.185	31.047	14.030
Temperature (K)	294(2)	294(2)	294(2)
$2\Theta_{max}$ (°)	50.06	50.06	50.06
No. Obs. (I > 2σ(I))	11183	6543	7290
No. Parameters	670	460	490
Goodness of fit (GOF)	1.096	1.005	1.017
Max. shift in cycle	0.004	0.006	0.001
Residuals*: R1; wR2	0.0508; 0.1108	0.0368; 0.0745	0.0394; 0.0914

164

Absorption Corr.Max/min	Multi-scan 1.000/0.402	Multi-scan 1.000/0.303	Multi-scan 1.000/0.513
Largest peak in Final Diff. Map (e⁻ / Å³)	1.320	1.739	2.633

* $R1 = \Sigma_{hkl}(||F_{obs}| - |F_{calc}||)/\Sigma_{hkl}|F_{obs}|$; $wR2 = [\Sigma_{hkl}w(|F_{obs}| - |F_{calc}|)^2/\Sigma_{hkl}wF^2_{obs}]^{1/2}$; $w = 1/\sigma^2(F_{obs})$; $GOF = [\Sigma_{hkl}w(|F_{obs}| - |F_{calc}|)^2/(n_{data} - n_{vari})]^{1/2}$.

Table 5.3. Crystallographic Data for Compounds **5.8 - 5.10**[a].

Compound	**5.8**	**5.9**	**5.10**
Empirical formula	$Ir_5Bi_1P_2O_9C_{39}H_{24}$	$Ir_3Bi_1Ru_4O_{18}C_{18}$	$Ir_3Bi_1Ru_3O_{15}C_{15}$
Formula weight	1868.50	1694.0	1508.94
Crystal system	Monoclinic	Orthorhombic	Monoclinic
Lattice parameters			
a (Å)	14.4576 (6)	11.9089(5)	9.5471 (2)
b (Å)	16.9071(7)	15.2262(7)	12.0688(2)
c (Å)	17.5453 (7)	15.8791(7)	21.7419 (5)
α (deg)	90	90	90
β (deg)	100.245(1)	90	95.53
γ (deg)	90	90	90
V ($Å^3$)	4220.3(3)	2879.3(2)	2493.50 (9)
Space group	$P2_1$/c	Pnma	$P2_1$/c
Z value	4	4	4
ρ_{calc} (g / cm^3)	2.941	3.908	4.020
μ (Mo Kα) (mm^{-1})	19.987	22.012	24.813
Temperature (K)	294(2)	294(2)	294(2)
$2\Theta_{max}$ (°)	50.06	50.04	50.06
No. Obs. (I > 2σ(I))	7454	2639	4411
No. Parameters	505	211	334
Goodness of fit (GOF)	1.025	1.215	1.063
Max. shift in cycle	0.001	0.001	0.001
Residuals*: R1; wR2	0.0435; 0.0924	0.0525 ;0.1191	0.0264 ; 0.0606
Absorption Corr.Max/min	Multi-scan 1.000 / 0.511	Multi-scan 1.000/0.452	Multi-scan 1.000/0.543

166

Largest peak in Final Diff. Map (e⁻ / Å³)	4.066	1.681	0.901

* R1 $= \Sigma_{hkl}(||F_{obs}| - |F_{calc}||)/\Sigma_{hkl}|F_{obs}|$; wR2 $= [\Sigma_{hkl}w(|F_{obs}| - |F_{calc}|)^2/\Sigma_{hkl}wF^2_{obs}]^{1/2}$; $w = 1/\sigma^2(F_{obs})$; GOF $= [\Sigma_{hkl}w(|F_{obs}| - |F_{calc}|)^2/(n_{data} - n_{vari})]^{1/2}$.

167

Table 5.4 Selected intermolecular angles and bond distances for **5.2** [a]

Atom	Atom	Distance	Atom	Atom	Atom	Angle
Ir1	Ir3	2.6533(7)	Ir3	Ir2	Ir1	58.145(18)
Ir1	Ir4	2.6632(7)	Ir3	Ir2	Ir1	58.145(18)
Ir1	Ir2	2.7317(7)	Ir3	Ir2	Ir4	60.113(17)
Ir2	Ir3	2.7286(7)	Ir1	Ir2	Ir4	58.315(18)
Ir2	Ir4	2.7345(7)	Ir3	Ir2	Bi2	117.94(2)
Ir2	Bi2	2.7803(7)	Ir1	Ir2	Bi2	175.81(2)
Ir2	Ir6	2.7883(7)	Ir3	Ir2	Ir6	90.72(2)
Ir2	Ir5	2.7996(7)	Bi2	Ir2	Ir6	58.16(2)
Ir3	Ir4	2.7362(7)				
Ir3	Ir5	2.7644(7)				
Ir3	Bi1	2.8116(7)				
Ir4	Bi1	2.7800(7)				
Ir4	Ir6	2.7979(7)				

[a] Estimated standard deviations in the least significant figure are given in parenthesis.

Table 5.5 Selected intermolecular angles and bond distances for **5.3** [a]

Atom	Atom	Distance	Atom	Atom	Atom	Angle
Ir1	Ir2	2.7722(7)	Bi1	Ir1	Ir2	59.773(17)
Ir1	Ir3	2.7916(6)	Ir2	Ir1	Ir3	59.641(17)
Ir2	Ir3	2.7668(6)	Bi1	Ir2	Ir3	59.179 (17)
Ir1	Bi1	2.7304(6)	Bi1	Ir2	Ir1	59.356(17)
Ir3	P1	2.320(3)	Ir3	Ir2	Ir1	60.528(17)
Ir3	Bi1	2.7203(6)	Ir2	Ir3	Ir1	59.831(17)
			Ir3	Bi1	Ir1	61.614(16)

[a] Estimated standard deviations in the least significant figure are given in parenthesis.

Table 5.6 Selected intermolecular angles and bond distances for **5.4** [a]

Atom	Atom	Distance	Atom	Atom	Atom	Angle
Ir1	Bi1	2.7295(5)	Ir3	Bi1	Ir1	61.650(11)
Ir2	Bi1	2.7312(5)	Ir3	Bi1	Ir2	61.546(11)
Ir3	Bi1	2.7211(5)	Ir1	Bi1	Ir2	61.026(11)
Ir1	Ir2	2.7725(4)	Ir2	Ir1	Ir3	60.161(10)
Ir1	Ir3	2.7930(4)	Ir3	Ir2	Ir3	60.283(10)
Ir2	Ir3	2.7896(4)	Ir2	Ir3	Ir1	59.556(11)
Ir1	P1	2.3249(18)				
Ir2	P2	2.3270(18)				

[a] Estimated standard deviations in the least significant figure are given in parenthesis

Table 5.7 Selected intermolecular angles and bond distances for **5.5** [a]

Atom	Atom	Distance	Atom	Atom	Atom	Angle
Ir1	Bi1	2.7204(6)	Ir3	Bi1	Ir3	61.990(16)
Ir2	Bi1	2.7306(6)	Ir3	Bi1	Ir2	61.725(16)
Ir3	Bi1	2.7224(6)	Ir1	Bi1	Ir2	61.587(16)
Ir1	Ir2	2.7907(6)	Ir2	Ir1	Ir3	60.012(15)
Ir1	Ir3	2.8029(6)	Ir3	Ir2	Ir3	60.283(10)
Ir2	Ir3	2.7973(6)	Ir1	Ir2	Ir3	60.211(15)
Ir1	P1	2.325(3)	Ir2	Ir3	Ir1	59.777(15)
Ir2	P2	2.315(3)				
Ir3	P3	2.321(3)				

[a] Estimated standard deviations in the least significant figure are given in parenthesis.

171

Table 5.8 Selected intermolecular angles and bond distances for **5.6** [a]

Atom	Atom	Distance	Atom	Atom	Atom	Angle
Ir6	Bi2	2.6997(8)	Ir3	Bi1	Ir6	89.06(2)
Ir5	Bi2	2.7100(8)	Ir3	Bi1	Ir4	58.239(17)
Ir3	Bi1	2.7903(7)	Ir4	Bi1	Ir5	88.60(2)
Ir2	Bi2	2.7768(8)	Ir6	Bi6	Ir5	62.47(2)
Ir1	Ir2	2.7550(8)	Ir3	Ir4	Ir2	60.680(18)
Ir1	Ir4	2.6854(7)	Ir1	Ir4	Ir6	121.51(2)
Ir3	Ir4	2.7293(7)	Bi2	Ir6	Ir4	119.45(2)
Ir6	Bi1	2.7941(8)				
Ir4	Bi1	2.8181(7)				
Ir5	Bi1	2.8217(7)				
Ir2	Ir4	2.7406(7)				
Ir4	Ir6	2.7965(8)				

[a] Estimated standard deviations in the least significant figure are given in parenthesis.

Table 5.9 Selected intermolecular angles and bond distances for **5.7** [a]

Atom	Atom	Distance	Atom	Atom	Atom	Angle
Bi1	Ir2	2.7127(6)	Ir2	Bi1	Ir3	60.163(15)
Bi1	Ir3	2.7295(6)	Ir2	Bi1	Ir1	64.219(15)
Bi1	Ir1	2.7898(6)	Ir3	Bi1	Ir1	60.417(15)
Ir1	P1	2.336(3)				
Ir1	Ir3	2.7775(6)				
Ir1	Ir2	2.9255(6)				
Ir1	H1	1.82(13)				
Ir2	Ir3	2.7278(6)				
Ir2	H1	1.53(12)				
Ir3	P2	2.288(3)				

[a] Estimated standard deviations in the least significant figure are given in parenthesis.

Table 5.10 Selected intermolecular angles and bond distances for **5.8** [a]

Atom	Atom	Distance	Atom	Atom	Atom	Angle
Bi1	Ir1	2.8294(8)	Ir1	Bi1	Ir4	89.04(2)
Bi1	Ir4	2.8342(7)	Ir1	Bi1	Ir2	60.37(2)
Bi1	Ir2	2.8411(7)	Ir4	Bi1	Ir2	59.412(18)
Bi1	Ir5	2.8817(7)	Ir1	Bi1	Ir5	57.875(18)
Ir1	Ir5	2.7637(8)	Ir4	Bi1	Ir5	58.318(17)
Ir1	Ir3	2.7642(7)	Ir2	Bi1	Ir5	87.45(2)
Ir1	Ir2	2.8510(8)	Ir5	Ir1	Ir3	60.129(19)
Ir2	Ir3	2.7309(7)				
Ir2	Ir4	2.8124(7)				
Ir3	Ir5	2.7694(8)				
Ir2	P1	2.331(4)				
Ir3	P1	2.238(4)				
Ir4	P2	2.285(3)				
Ir5	P2	2.272(3)				
Ir1	C53	2.077(14)				
Ir3	C58	2.091(14)				

[a] Estimated standard deviations in the least significant figure are given in parenthesis

Table 5.11 Selected intermolecular angles and bond distances for **5.9** [a]

Atom	Atom	Distance	Atom	Atom	Atom	Angle
Bi1	Ir1	2.7319(14)	Ir1	Bi1	Ru1[i]	63.08(4)
Bi1	Ru1[i]	2.7514(17)	Ir1	Bi1	Ru1	63.08(4)
Bi1	Ru1	2.7514(17),	Ru1[i]	Bi1	Ru1	62.54(6)
Ir1	Ir2[i]	2.7308(10)				
Ir1	Ir2	2.7308(10)				
Ir1	Ru3	2.757(2)				
Ir1	Ru1	2.8684(15)				
Ir2	Ru3	2.6718(17)				
Ir2	Ir2[i]	2.7428(13)				
Ir2	Ru2	2.8304(17)				

[a] Estimated standard deviations in the least significant figure are given in parenthesis.

Table 5.12 Selected intermolecular angles and bond distances for **5.10** [a]

Atom	Atom	Distance	Atom	Atom	Atom	Angle
Bi1	Ir1	2.7898(4)	Ir1	Bi1	Ir2	60.093(11)
Bi1	Ir2	2.7918(5)	Ir1	Bi1	Ru1	58.935(16)
Bi1	Ru1	2.8220(7)	Ir2	Bi1	Ru1	89.932(17)
Bi1	Ru2	2.8337(7)	Ir1	Bi1	Ru2	89.352(17)
Ru3	Ir2	2.6804(7)	Ir2	Bi1	Ru2	59.039(16)
Ir1	Ru3	2.6811(7)	Ru1	Bi1	Ru2	61.098(19)
Ru3	Ir3	2.6844(7)				
Ru1	Ir1	2.7607(7)				
Ru2	Ir2	2.7721(7)				
Ir2	Ir3	2.7617(4)				

[a] Estimated standard deviations in the least significant figure are given in parenthesis.

R<small>EFERENCES</small>

1. (a) Grasselli, R. K. *Catal. Today* **2014**, *238*, 10–27. (b) Grasselli, R. K., *Topics in Catal.* **2002**, *21*, 79 – 88. (c) Grasselli, R.K. *Handbook of Heterogeneous Catalysis*, Ertl, G., Knozinger, H., Weitkamp, J., VCH Publishers, Weinheim, vol. 5, **1997**, pp 2302-2326. (d) Grasselli, R.K., *Catal. Today*, **2005**, *99*, 23-31. (e) Goddard III, W. A.; Chenoweth, K.; Pudar, S.; van Duin, A. C. T.; Cheng, M.-J. *Top Catal*. **2008**, *50*, 2–18. (f) Jang, Y. H.; Goddard III, W. A. *J. Phys. Chem. B* **2002**, *106,* 5997-6013.

2. (a) Raja, R.; Adams, R. D.; Blom, D. A.; Pearl, W. C. Jr.; Gianotti, E.; Thomas, J. M.; *Langmuir* **2009**, *25*, 7200–7204. (b) Gianotti, E.; Shetti, V. N.; Manzoli, M.; Blaine, J. A. L.; Pearl, W. C. Jr.; Adams, R. D.; Coluccia, S.; Raja, R.; *Chem Eur. J.* **2010**,*16*, 8202-8209.

3. Kruppa, W.; Blaeser, D.; Boese, R.; Schmid, G., *Organisch. Chem.*, **1982**, *37B*, 209-213.

4. Adams, R. D.; Chen, M.; Elpitiya, G.; Potter, M. E.; Raja, R., *ACS Catal.*, **2013**, *3*, 3106−3110.

5. Adams, R. D.; Chen, M., Elpitiya, G.; Zhang, Q., *Organometallics*, **2012**, *31*, 7264 - 7271.

6. Garlaschelli, L.; Della Pergola, R.; Martinengo, S., *Inorg. Synth*. **1990**, 28, 211-215.

7. Foulds, G. A.; Johnson, B. F. G.; Lewis, J.; *J. Organomet. Chem.,* **1985,** *296*, 147-153

8. SAINT+, version 6.2a, Bruker Analytical X-ray Systems, Inc., Madison, WI, 2001.

9. Sheldrick, G. M. SHELXTL, version 6.1, Bruker Analytical X-ray Systems, Inc., Madison, WI, 1997.

10. Mingos, D. M. P.; *Acc. Chem. Res* .**1984**, *17* , 311-319

11. (a) Bau, R.; Drabnis, M. H.; *Inorg. Chim. Acta* **1997**, *259*, 27 - 50. (b) Teller, R. G. ; Bau, R.; *Struc. Bonding* **1981**, *41*, 1 – 82.

12. Adams, R. D.; Pearl, W. C. Jr.; *Inorg. Chem.* **2010,** *49*, 7170 - 7175.

13. Adams, R. D.; Kan, Y.; Zhang, Q.; *J. Organomet. Chem.,* **2014***, 751,* 475 – 481.

14. Johnson, B. F. G.; Lewis, J. ; Raithby, P. R.; Whitton, A. J.; *J. Chem. Soc., Chem. Commun.* **1988**, 401 – 402.

15. Hay, C. M.; Johnson, B. F. G.; Lewis, J. ; Raithby, P. R.; Whitton, A. J.; *J. Chem. Soc. Dalton Trans.* **1988**, 2091 – 2097.

16. Adams, R. D.; *The Chemistry of Metal Cluster Complexes*, Shriver, D. F. ; Kaesz, H. D. ; Adams, R. D.; Ed., VCH Publishers, New York, **1990**, Ch. 3.

17. Adams, R. D.; Dawoodi, Z. D.; Segmueller, F. Foust, B.; *J. Am. Chem. Soc.* **1983**, *105*, 831-838.

18. Adams, R. D.; Babin, J. E. ; Wolfe, T. A.; *Polyhedron* **1989**, *8,* 1123 – 1134.

19. Adams, R. D.; Chen, G. ; Tanner, J. T. ; Yin, J. ; *Organometallics.* **1990**, 1240 - 1245.

CHAPTER 6

SYNTHESIS AND CHARACTERIZATION OF AN IRIDIUM-BISMUTH METALLAHETEROCYCLE

Introduction

The synthesis and chemistry of heavy atom metallaheterocycles is an important and an interesting field in chemistry which has remained largely unexplored until recently. Some recent studies done by Adams[1,2,3] et al. and W. K. Leong[4,5] have unveiled several unusual new metallaheterocycles by linking heavy transition metal groupings with heavy atom bridging ligands, such as diphenylbismuth and diphenylantimony. (Figure 6.1 and 6.2). The three membered heterocycle $Re_2(CO)_8(\mu\text{-}SbPh_2)(\mu\text{-}H)$ synthesized by Adams et al. has been shown to react with $Pt(P\text{-}t\text{-}Bu_3)$ by a reversible ring opening insertion of a $Pt(P\text{-}t\text{-}Bu_3)$ group into one of its Re-Sb bonds to yield the compound $Re_2Pt[P\text{-}(t\text{-}Bu_3)]$ $(CO)_8(\mu\text{-}SbPh_2)_2(\mu\text{-}H)$. (Scheme 6.1). Furthermore, they have discovered an interesting process reminiscent of host-guest behavior related to a tetrarhena-heterocycle, $Re_4(CO)_{16}(\mu\text{-}SbPh_2)_2(\mu\text{-}H)_2$ formed from the palladium-catalyzed dimerization of $Re_2(CO)_8(\mu\text{-}SbPh_2)(\mu\text{-}H)$ further highlighting the importance of this new class of compounds[6]. The compound shown in Figure 6.2 synthesized by Leong et al. is an example of an Osmium analog of the tetrarhena-heterocycle synthesized by Adams et al. The osmium compound, $[Os_3(CO)_{10}(\mu\text{-}SbPh_2)(\mu\text{-}H)]_2$ can be regarded as a dimeric form of $Os_3(CO)_{10}(\mu\text{-}SbPh_2)(\mu\text{-}H)$ which was also isolated and characterized by a crystal

179

structure analysis. Herein we are reporting the newest addition to this metellaheterocycles class of compounds which has been synthesized by reaction of the heavy transition metal iridium and heavy main group metal bismuth by using the reagents $[HIr_4(CO)_{11}]^-$ and Ph_2BiCl.

Experimental Details

General Data.

Reagent grade solvents were dried by the standard procedures and were freshly distilled prior to use. Infrared spectra were recorded on a Thermo Nicolet Avatar 360 FT-IR spectrophotometer. Room temperature ^1H NMR spectra were recorded on a Varian Mercury 300 spectrometer operating at 300.1 MHz. Mass spectrometric (MS) measurements performed by a direct-exposure probe using electrospray ionization (ESI) using a Micromass Q-TOF instrument. $Ir_4(CO)_{12}$ and Ph_3Bi were obtained from STREM and were used without further purification. $[PPN][HIr_4(CO)_{11}]$, PPN = $[Ph_3PNPPh_3]^+$ was prepared according to a previously reported procedure[7]. Ph_2BiCl was prepared from a previous report by using PhLi instead of MeLi[8]. All product separations were performed by TLC in air on Analtech 0.25mm silica gel 60 Å F254 glass plates.

Synthesis of $[Ir_4(CO)_{10}(\mu\text{-}BiPh_2)(\mu\text{-}H)]_2$, 6.1.

A 22.0 mg (0.014 mmol) portion of $[HIr_4(CO)_{11}]PPN$ was dissolved in 15 mL of methylene chloride and the reaction flask was placed in an ice bath. A 22.0 mg (0.055 mmol) portion of Ph_2BiCl was stirred in to the reaction mixture and a rapid color change from yellow to dark red was observed. The reaction was stirred for 10 minutes and then the solvent was removed *in vacuo*, and the product was isolated by TLC with a 6/1

180

hexane/methylene chloride solvent ratio as the eluent. This gave 2.0 mg (0.0007 mmol) of dark red $[Ir_4(CO)_{10}(\mu\text{-}BiPh_2)(\mu\text{-}H)]_2$, **6.1** in   (10 % yield) and trace amounts of previously known compounds: yellow $Ir_3(CO)_9(\mu_3\text{-}Bi)$[9], **6.2**, green $Ir_6(CO)_{13}(\mu_3\text{-}Bi)(\mu_4\text{-}Bi)$, **6.3**, and red $Ir_5(CO)_{10}(\mu_3\text{-}Bi)_2(\mu_4\text{-}Bi)$[10], **6.4**. Spectral data for **6.1**: IR υ_{CO} (cm^{-1} in CH$_2$Cl$_2$) 2080(s), 2061(vs) .^{1}H NMR (CDCl$_3$, in ppm) δ = -17.149 (s, Ir-H, 2H), ES (positive) /MS for **6.1**: m/z = 2826 (M$^{+\cdot}$). The isotope distribution pattern is consistent with the presence of eight iridium atoms and two bismuth atoms.

Crystallographic Analyses:

Red crystals of **6.1** suitable for x-ray diffraction analyses were obtained by slow evaporation of solvent from a solution of the compound in pure benzene at room temperature. The data crystal was glued onto the end of a thin glass fiber. X-ray intensity data were measured by using a Bruker SMART APEX CCD-based diffractometer using Mo Kα radiation (λ = 0.71073 Å).   The raw data frames were integrated with the SAINT+ program by using a narrow-frame integration algorithm[11]. Correction for Lorentz and polarization effects was also applied with SAINT+. An empirical absorption correction based on the multiple measurement of equivalent reflections was applied using the program SADABS. The structure was solved by a combination of direct methods and difference Fourier syntheses, and refined by full-matrix least-squares on F^2 by using the SHELXTL software package [12]. All non-hydrogen atoms were refined with anisotropic displacement parameters. Hydrogen atoms on the phenyl rings and on the solvent were placed in geometrically idealized positions and included as standard riding atoms during the final cycles of least-squares refinements. The hydride ligands were located and

181

refined during the final cycles of least squares refinements. Crystal data, data collection parameters, and results of the analysis are listed in Table 6.1.

Compound **6.1** crystallized in the monoclinic crystal system. The space group $P2_1$/c was indicated by the systematic absences in the data. The structure was confirmed by the successful solution and refinement of the analysis. One molecule of benzene co-crystallized with the asymmetric crystal unit of compound **6.1** from the crystallization solvent. The hydrido ligand in **6.1** was located in a difference Fourier map as a bridge across the Ir(1) – Ir(2) bond, and was refined with a isotropic thermal parameter. For compound **6.1** there is only half of a symmetry-independent molecule in the asymmetric crystal unit.

Results and Discussion

The new compound $[Ir_4(CO)_{10}(\mu\text{-}BiPh_2)(\mu\text{-}H)]_2$, **6.1** was obtained in 10 % yield by a simple salt elimination and a self-dimerization of the monomeric counterpart $[Ir_4(CO)_{11}(\mu\text{-}BiPh_2)(\mu\text{-}H)]$ with CO elimination. Compound **6.1** was characterized by IR and mass spectral analysis and by a single crystal X-ray diffraction analysis. An ORTEP drawing of the molecular structure of **6.1** as it is found in the solid state is shown in Figure 6.3. The molecule of compound **6.1** is located on a crystallographic two-fold rotation axis and there are two Ph_2Bi ligands bridging the two $Ir_4(CO)_{10}$ tetrahedra on opposite sides. The compound **6.1** could be considered as a 6 membered ring with the $Ir_2(BiPh_2)Ir_2(BiPh_2)$ atom arrangement. Interestingly the two bridging hydride ligands between the Ir1 - Ir3 bond and Ir1[i] - Ir3[i] bond are positioned inside the ring. The ring is planar and the monomeric cluster unit $Ir_4(CO)_{10}(\mu\text{-}BiPh_2)(\mu\text{-}H)$ contains 60 valence

electrons which is consistent for a tetrahedron according to electron counting rules. Each BiPh$_2$ ligand donates 3 electrons to the overall structure and each Ir atom attains an 18 electron configuration. The Ir-Ir bond distances in the iridium tetrahedron have an average bond distance of 2.6963 (7) Å, Ir(1)-Ir(2) = 2.7065(7) Å, Ir(1) - Ir(4) = 2.6897(6) Å, Ir(2) - Ir(4) = 2.6854(7) Å, Ir(2) - Ir(3) = 2.7078(6) Å, Ir(3) - Ir(4) = 2.6925(7) Å except for the hydride bridging Ir(1)- Ir(3) bond distance which is 2.834 (7) Å . The longer bond distance of the Ir1-Ir3 and Ir1^i -Ir3^i bonds could be attributed to the presence of the bridging hydride ligands. The previously known IrBi compound, Ir$_3$(CO)$_9$(μ_3-Bi) synthesized by Schmid et al.[9] has an average Ir-Ir bond distance of 2.759(2) Å which is longer than the average Ir-Ir bond distance in **6.1** which could be due to the steric strain imposed by the 6 membered ring. The hydride bridged Ir-Ir bond distance reported for the compound, Ir$_3$(CO)$_6$(GePh$_3$)$_3$(μ_3-Bi)(μ-H)$_3$ [13] is 3.0079(8) Å which is much longer than in **6.1** which could again be attributed to the steric strain imposed by the 6 membered ring. The Ir-Bi bond distance in **6.1**, Ir(1) - Bi(1) = 2.7597(6) Å and Ir(3) - Bi(1) = 2.7610(6) Å is very similar to the Ir-Bi bond distance observed in Ir$_3$(CO)$_9$(μ_3-Bi) which is, 2.759(2) Å. The ring angle around the Bi(1)- Ir(1)- Ir(3) is 112.96(2)° while the angle around the bismuth atom, Ir(1) - Bi(1) - Ir(3) is 135.86(2)°. The angle around bismuth, although tetra coordinated is very much larger than the expected value of 109.5 may be due to several factors such as the lone pair on bismuth and the bulky iridium tetrahedron. A similar bond angle is observed in the compound [Re(CO)$_4$(μ-BiPh$_2$)]$_3$, for the Re-Bi-Re angle which is 134.895(18)°. [1]

183

Summary and Conclusions

A summary of the results of this work is presented in Scheme 6.2. Compound **6.1** is readily synthesized by the loss of two CO ligands and salt formation during the reaction of $[HIr_4(CO)_{11}]^-$ anion with Ph_2BiCl at 0 ºC. $[HIr_4(CO)_{11}]^-$ has a tetrahedron of four Ir atoms in solid state and it preserves this tetrahedral arrangment during the course of the reaction presumably forming a electron rich monomer $Ir_4(CO)_{11}(\mu\text{-}BiPh_2)(\mu\text{-}H)$ (62 valence electrons) which undergoes CO elimination and self dimerization to produce the new compound $[Ir_4(CO)_{10}(\mu\text{-}BiPh_2)(\mu\text{-}H)]_2$, **6.1**. No mechanistic studies have been performed to prove the mechanism of the formation of **6.1** due to low yields of the product. This compound is the first IrBi metallaheterocycle with a six membered ring although Adams et al. and Leong et al. have synthesized several new and unusual metallaheterocycles in the recent years with Rhenium and Osmium.[1,3]
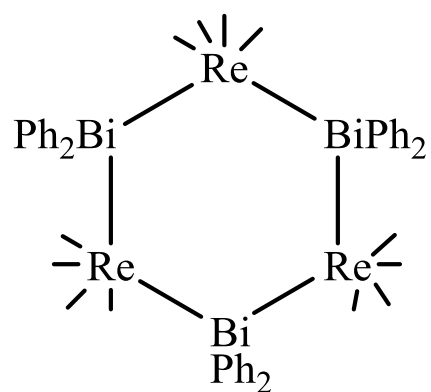
Figure 6.1. $Re_3(CO)_{12}(\mu\text{-}BiPh_2)_3$
synthesized by Adams et al.
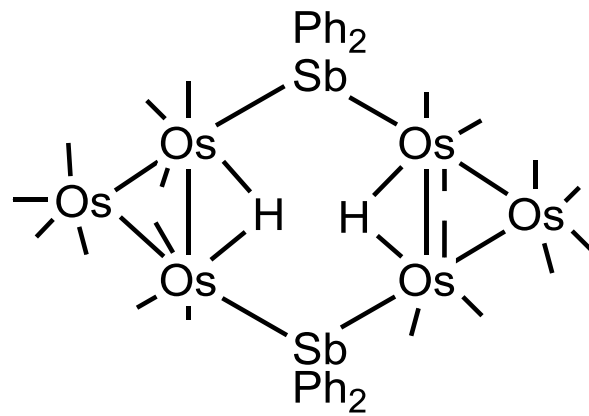
Figure 6.2. $[Os_3(\mu\text{-}SbPh_2)_2(\mu\text{-}H)]_2$ synthesized by Leong et al.
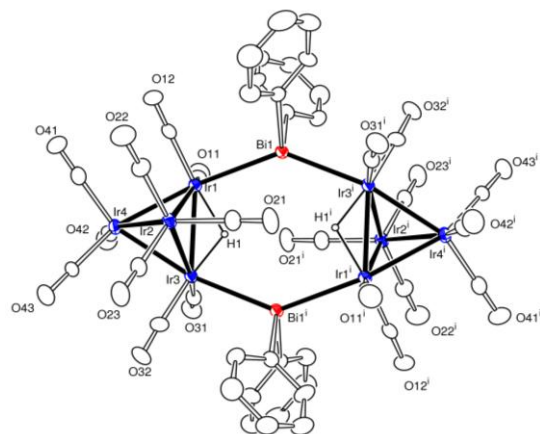
Figure 6.3. An ORTEP diagram of the molecular structure of $[Ir_4(CO)_{10}(\mu\text{-}BiPh_2)(\mu\text{-}H)]_2$, 6.1 showing 20% thermal ellipsoid probability.
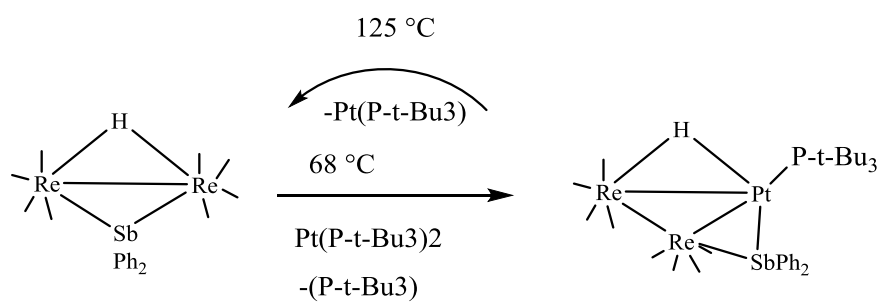
Scheme 6.1. Reversible Conversion of $Re_2(CO)_8(\mu\text{-SbPh}_2)(\mu\text{-H})$ into $Re_2Pt[P\text{-}(t\text{-Bu}_3)](CO)_8(\mu\text{-SbPh}_2)_2(\mu\text{-H})$.
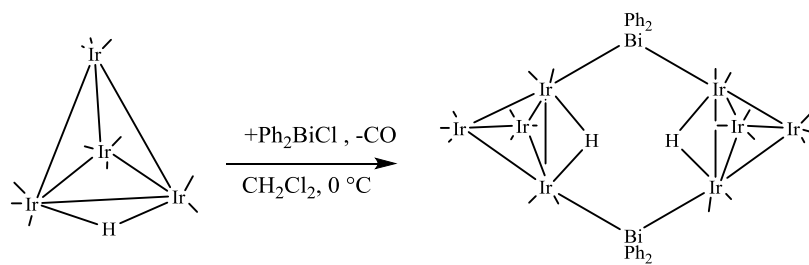
Scheme 6.2. Synthesis of compound [Ir$_4$(CO)$_{10}$(µ-BiPh$_2$)(µ-H)]$_2$, 6.1.

Table 6.1. Crystallographic data for **6.1**.[a]

Compound	**6.1**
Empirical formula	$Ir_4BiC_{25}O_{10}H_{14}$
Formula weight	1452.14
Crystal system	Monoclinic
Lattice parameters	
a (Å)	13.5982(9)
b (Å)	12.6815(8)
c (Å)	18.7194(12)
α (deg)	90.00
β (deg)	104.8640(10)
γ (deg)	90.00
V ($Å^3$)	3120.1(3)
Space group	$P2_1/c$
Z value	4
ρ_{calc} (g / cm^3)	3.091
μ (Mo Kα) (mm^{-1})	22.669
Temperature (K)	294(2)
$2\Theta_{max}$ (°)	50.06
No. Obs. (I > 2σ(I))	5508
No. Parameters	350
Goodness of fit (GOF)[a]	1.024
Max. shift in cycle	0.001
Residuals:[*] R1; wR2	0.0371; 0.1041
Absorption Correction, Max/min	Multi-scan 1.000 / 0.438
Largest peak in Final Diff. Map ($e^-/Å^3$)	1.549

[*] $R1 = \Sigma_{hkl}(||F_{obs}| - |F_{calc}||)/\Sigma_{hkl}|F_{obs}|$; $wR_2 = [\Sigma_{hkl}w(|F_{obs}| - |F_{calc}|)^2/\Sigma_{hkl}wF^2_{obs}]^{1/2}$; $w = 1/\sigma^2(F_{obs})$; $GOF = [\Sigma_{hkl}w(|F_{obs}| - |F_{calc}|)^2/(n_{data} - n_{vari})]^{1/2}$.

Table 6.2. Selected intermolecular angles and bond distances for **6.1.**[a]

Atom	Atom	Distance	Atom	Atom	Atom	Angle
Ir1	Ir2	2.7065(7)	Bi1	Ir1	Ir3	112.96(2)
Ir1	Ir3	2.8339(7)	Ir1	Bi1	Ir3	135.86(2)
Ir1	Ir4	2.6897(6)	Bi1	Ir3	Ir1	111.177(19)
Ir2	Ir4	2.6854(7)				
Ir2	Ir3	2.7078(6)				
Ir3	Ir4	2.6925(7)				
Ir1	Bi1	2.7597(6)				
Ir3	Bi1	2.7610(6)				
Ir1	H1	1.75(11)				
Ir3	H1	1.67(11)				

[a]Estimated standard deviations in the least significant figure are given in parenthesis.

(1)   Adams, R. D. ; Pearl, W. C. *Inorg. Chem.* **2009**, *48* (19), 9519–9525.

(2)   Adams, R. D. ; Pearl, W. C.. *Organometallics* **2010**, *29* (17), 3887–3895.

(3)   Adams, R. D.; Pearl, Jr., W. C., Wong, Y. O., Hall, M. B.; Walensky, J. R., *Inorg. Chem.*   **2015**, *54*, 3536−3544.

(4)   Leong, W. K.; Chen, G. *J. Chem. Soc. Dalton Trans.* **2000**, No. 23, 4442–4445.

(5)   Li, Y.-Z.; Ganguly, R.; Leong, W. K. *Organometallics* **2014**, *33* (14), 3867–3876.

(6)   Adams, R. D. ; Pearl, W. C. *J. Am. Chem. Soc.* **2011**, *133* (33), 12994–12997.

(7)   Garlaschelli, L.; Martinengo, S.; Chini, P.; Canziani, F.; Bau, R. *J. Organomet. Chem.*   **1981**, *213* (1), 379–388.

(8)   Benjamin, S. L.; Levason, W.; Reid, G.; Rogers, M. C.; Warr, R. P. *J. Organomet. Chem.* **2012**, *708*, 106–111.

(9)   Kruppa, W.; Blaeser, D.; Boese, R.; Schmid, G., *Organisch. Chem.*, **1982**, *37B*, 209-213.

 (10)   Adams, R. D.; Chen, M.; Elpitiya, G.; Potter, M. E.; Raja, R. *Acs Catal.* **2013**, *3* (12), 3106–3110.

(11)   SAINT+, version 6.2a, Bruker Analytical X-ray Systems, Inc., Madison, WI, 2001.

(12)   Sheldrick, G. M. SHELXTL, version 6.1, Bruker Analytical X-ray Systems, Inc., Madison, WI, 1997.

(13)   Adams, R. D.; Chen, M., Elpitiya, G.; Zhang, Q., *Organometallics*, **2012**, *31*, 7264 - 7271.

APPENDIX A - COPYRIGHT RELEASES

193

www.manaraa.com

ACS Publications
Most Trusted. Most Cited. Most Read.

Title: Synthesis and Characterizations of Bismuth-Bridged Triiridium Carbonyl Complexes Containing Germyl/Germylene and Stannyl/Stannylene Ligands

Author: Richard D. Adams, Mingwei Chen, Gaya Elpitiya, et al

Publication: Organometallics

Publisher: American Chemical Society

Date: Oct 1, 2012

Copyright © 2012, American Chemical Society

Logged in as:
Gaya Elpitiya

LOGOUT

194

www.manaraa.com